Mechanisms operating during plastic deformation of metals under concurrent production of cascades and dislocations

Trinkaus, H.; Singh, Bachu Narain

Publication date:
2008

Document Version
Publisher's PDF, also known as Version of record

Risø-R-Report

Mechanisms Operating during Plastic Deformation of Metals under Concurrent Production of Cascades and Dislocations

H. Trinkaus and B.N. Singh

Risø-R-1610(EN)

Risø National Laboratory
Technical University of Denmark
Roskilde, Denmark
April 2008

Author: H. Trinkaus[1)] and B.N. Singh[2)]

Title: Mechanisms Operating during Plastic Deformation of Metals under Concurrent Production of Cascades and Dislocations

Department: Materials Research Department

[1)] Institut für Festkörperforschung, Forschungszentrum Jülich, D-52425 Jülich, Germany
[2)] Materials Research Department, Risø National Laboratory, Technical University of Denmark, DK-4000 Roskilde, Denmark

Risø-R-1610(EN)
April 2008

Abstract

Recent in-reactor tensile tests (IRTs) on pure copper have revealed a deformation behaviour which is significantly different from that observed in post-irradiation tensile tests (PITs). In IRTs, the material deforms uniformly and homogeneously without yield drop and plastic instability as commonly observed in PITs. An increase in the pre-yield dose results in an increase in the level of hardening over the whole test periods and a decrease in the uniform elongation suggesting that the materials "remember" the impact of the pre-yield damage level.

These features are modelled in terms of the decoration of dislocations with glissile dislocation loops. During pre-yield irradiation, dislocation decoration is due to the one-dimensional (1D) diffusion of cascade induced self-interstitial (SIA) clusters and their trapping in the stress field of the static grown-in dislocations. During post-yield irradiation and deformation, moving dislocations are decorated by the sweeping of matrix loops.

The interaction of dislocations with loops and between loops is discussed as a function of the relevant parameters. On this basis, the kinetics of decoration is treated in terms of fluxes of loops to and reactions with each other in a conceived 2D space of decoration. In this space, loop coalescence, alignment and mutual blocking reactions are characterised by appropriate reaction cross sections. In the kinetic equations for "dynamic decoration" under deformation, the evolution of the dislocation density is taken into account. Simple solutions of the kinetic equations are discussed. The apparent memory of the system for the pre-yield dose is identified as the result of simultaneous and closely parallel transient evolutions of the cascade damage and the dislocations up to the end of the IRTs.

The contributions of dislocation decoration to yield and flow stresses are attributed to the interaction of dislocations with aligned loops temporarily or permanently immobilized by other loops or SFTs ("decoration enhanced obstacle hardening"). On this basis, the yield and flow stresses are discussed as a function of pre-yield dose, post-yield dose and strain. Assuming physically reasonable values for the parameters involved we are able to reproduce the general trends and the right orders of magnitude of the yield and flow stresses measured in the IRTs on Cu.

ISSN 0106-2840
ISBN 978-87-550-3608-6

Contract no.:
Underlying Technology Programme

Group's own reg. no.:
1610003-00

Sponsorship: EU – Fusion Technology Programme

Cover :

Pages: 67
Tables: 1
References: 21

Information Service Department
Risø National Laboratory
Technical University of Denmark
P.O.Box 49
DK-4000 Roskilde
Denmark
Telephone +45 46774004
bibl@risoe.dk
Fax +45 46774013
www.risoe.dtu.dk

Quantities and Symbols

A: area vector of loop; $A_0 \approx b^2$ atomic unit area

B, b: Burgers vector of dislocation, loop, of magnitude B, b

c: atomic concentration

c_g: atomic concentration of glissile loops

$c_{i,v}^{(ml,SFT)}$: atomic concentrations of SIAs, vacancies accumulated in the matrix loops, SFTs

c_i^{dc}: atomic SIA concentration involved in decoration

D_g: diffusion coefficient of primary glissile SIA clusters (= $10^{-8}m^2/s$)

D: NRT displacement dose (= $G_{NRT}t$)

D_0: dose at transition from dislocation to matrix cluster dominance

D_y: pre-yield dose (10^{-3} to 10^{-2} dpa)

d_l, d_{ml} , d_{SFT}: average diameter of decorating loop, matrix loop, SFT

d_{dl}, d_{ll}: dislocation-loop, loop-loop distance

d_{tr}: "trapping range" ($d_{tr} < 200b < 50$ nm)

d_{dc}: width of the decorated region (during deformation $\approx 80b \approx 20$ nm)

$d_{i,v}^{(sw)}$: width for absorption of SIAs and vacancies by dislocation sweeping ($\approx$ 20b $\approx$ 5 nm)

E_{dl}, E_{ll}: dislocation- loop, loop-loop interaction energy

$\mathbf{F}_{dl}$, $\mathbf{F}_{ll}$: dislocation-loop, loop-loop force vector

f : strength factor for loop interaction with dislocations

f_r: fractions of SIAs recombining, (= 0.9)

f_r, $f_i^{g,s}$: fractions of SIAs clustered in glissile, sessile loops, ($f_i^{g,s}$ = 0.1, 0.4)

G: normal vector on glide plane

g : unit vector in loop glide direction

G: defect generation rate, $G = (1-f_r)G_{NRT}$; G_{NRT}: NRT displacement rate (= $5x10^{-8}$/s)

$G_i^{g,s} = f_i^{g,s}G$: generation rate of SIAs in glissile, sessile loops

$G_{ik}(\mathbf{r})$: elastic Green's function

$J_{l,SFT}$: apparent flux density of matrix loops, SFTs to moving dislocation

$j_{i,v,}$: apparent flux density of SIAs and vacancies in matrix clusters to moving dislocation

k^2, k_g^2: sink strength, for glissile loops.

kT_m: thermal energy at melting point T_m

L: unit vector along dislocation line

M_F: mobility of loops in force field

$M_{l,SFT}$: Number density of matrix loops, SFTs

$m_{l,SFT}$: average number of SIAs, vacancies in matrix loops, SFTs (100 to 200, 30 to 100)

N: 2D number density of decorating loops, N_+ of aligned loops

n: average number of SIAs in decorating loops, n_+ in aligned loops

p: fraction of differing loop orientations, p = 5/6 and 1/2 for edge and screw dislocations

Q: eigen-strain tensor of loops, components Q_{ij}

$q^{l,SFT}, q^{l,SFT} = (s_{tr}^{l,SFT} / s_{geom}^{l,SFT})$: ratio of trapping to geometrical cross sections (2 to 5)

$\mathbf{r}_{dl}$: separation vector between dislocation and loop

s: cross section

s^*: cross section of strong interaction ($s^* \approx 4m^{1/2} br_{dl}$)

s_{co}, s_{al}, s_{bl}, s_{an}: cross sections for loop coalescence, alignment, blocking annihilation

s_{geom}: geometrical cross section of loop ($\approx mb^2$)

$s_{tr}^{l,SFT}$: trapping cross section of loops and SFTs

s: coordinate of loop along glide path; origin at point of closest approach to other defect

T: temperature

T_m: melting temperature

t: time

v_d: dislocation velocity

x, y, z: coordinates in the glide direction, normal to the glide plane, along the dislocation line

α: "coverage", fraction of decorated plane covered with SIAs ($0 \le \alpha \le 1$)

α_+: coverage by aligned loops (5% to 30% for "moderate decoration")

β: rate constant for dislocation evolution (0.1 to 0.5)

δ: effective "stand-off" distance of blocked loops from dislocation ($\approx 10b \approx 2.5$ nm)

ε: plastic strain

$\varepsilon_{i,v}^{(sw)}$: characteristic strains for matrix defect reduction by dislocation sweeping (≈ 10 to 20%)

$\dot{\varepsilon}$: strain rate = 10^{-7}/s

$\eta_{i,v}$: fraction of NRT SIAs/ vacancies accumulating in matrix loops/ SFTs (≈ 0.5 to 2%)

κ: reciprocal mean free path;

$\kappa_{d,l,SFT}$: contributions of dislocations, sessile SIA loops, SFTs to κ

μ: shear modulus (= 55 GPa for Cu)

ν: Poisson's ratio (= 1/3 for Cu)

ρ: dislocation density; initial value $\rho_0 \approx 10^{12}/m^2$; saturated value $\rho_s \approx$ (2 to 5)x$10^{14}/m^2$

σ: stress field**;** $\boldsymbol{\sigma}^{\mathbf{d}}$: stress field of dislocation

$\tilde{\sigma}$: resolved shear stress;

$\tilde{\sigma}_y$: shear yield stress; σ_y: tensile yield stress $\approx 3\tilde{\sigma}_y$

$\tilde{\sigma}_f$: flow shear stress; σ_f: tensile flow stress $\approx 3\tilde{\sigma}_f$

τ: time to quasi-steady-state of primary glissile clusters

$\phi_{i,v}$: fractions of SIAs and vacancies which can be absorbed and annihilated: $\phi_i \le$ ½, $\phi_v << 1$

χ_+, χ_-: fraction of aligned, non-aligned loops (averages over dislocation types: $\chi_+ = ¼$, $\chi_- = ¾$)

Ω: matrix atom volume ($\Omega = b^3/\sqrt{2}$ for FCC)

Contents

1. Introduction

Effects of irradiation with energetic particles such as fission and fusion neutrons on the mechanical properties of metals and alloys, particularly at temperatures below recovery stage V, have been recognized and studied since the beginning of the 1960s [1-3]. Post-irradiation tensile tests (PITs) have shown that (i) the yield strength of metallic materials increases with increasing displacement dose, (ii) materials irradiated to a dose beyond a certain level exhibit the phenomenon of yield drop and the deformation is found to occur in a localized fashion, (iii) the irradiation causes an almost complete loss of work hardening and a drastic decrease in uniform elongation, i.e. ductility (see Ref [3] for review).

It is scientifically as well as technologically of great interest to examine the relevance of PITs by studying the response of materials to a more realistic simultaneous exposure to neutron irradiation and deformation in a real reactor environment. Such in-reactor tensile tests (IRTs) have been performed recently on pure Cu and a CuCrZr alloy [4]. The deformation behaviour observed in these tests is indeed qualitatively different from that observed in post-irradiation tensile tests (PITs). The IRTs show, for example: (a) the materials deform homogeneously and do not exhibit yield drop and plastic instability as commonly observed in PITs, and (b) an increase in the pre-yield dose results in an increase in the yield stress, a decrease in the post-yield hardening rate, an increase in the maximum hardening level and a decrease in the uniform elongation (see figs. 1 and 2). The effect of pre-yield dose on the hardening rate and the level of maximum hardening suggest that the materials "remember" the impact of the pre-yield damage level over the whole test period.

Modelling of radiation hardening is based on two classical hardening theories designed for two extreme microstructural situations: (1) Orowan's "Dispersed Barrier Hardening (DBH) model" where dislocation glide is assumed to be hindered by a random distribution of (immobile and indestructible) obstacles such as precipitate particles [5,6]; in this case, the yield stress is defined by the resolved shear stress necessary for dislocations to overcome the obstacles by bowing out between them, and the yielding process is necessarily associated with dislocation generation; (2) Cottrell's "atmosphere hardening" where impurities accumulated in the strain field of dislocations are assumed to block the dislocations [7]; in this case, the yield stress is defined by the resolved shear stress required to pull the dislocations away from the impurity "atmosphere", and yielding is followed by a yield drop without generation of new dislocations.

Most previous attempts to model radiation hardening are based on the DBH-model assuming that irradiation produces (immobile and indestructible) obstacles against dislocation glide such as stacking fault tetrahedra (SFTs) and dislocation loops (see for instance [8]). Striking features in radiation hardening under cascade damage conditions such as the increase of the yield stress without dislocation generation, the yield drop, the tendency to plastic instability and flow localization in narrow bands can, however, not be rationalized in terms of any DBH-type model. These features have been treated in terms of "Cascade Induced Source Hardening" (CISH) model [9] where the defect structure locking the dislocations are assumed to originate from the glide and trapping of glissile clusters of self-interstitial atoms (SIAs) in the form of small dislocation loops produced in displacement cascades [10,11].

It is important to recognize that in the past the treatment of radiation hardening has been strictly limited to the consideration of the effect of irradiation only on the yield stress. Both from

scientific and technological points of view, it is of interest, however, to understand the effect of irradiation not only on the yield stress but also on the evolution of the plastic flow and strain hardening beyond the yield point as a function of strain and displacement dose. Note that it is this evolution which may determine the life time of materials employed in different components of fission and fusion reactors.

In the present paper, we make an attempt to model the concurrent production of displacement cascades and dislocations under irradiation and deformation as occurring in IRTs. Under IRT conditions, the decoration of dislocations with dislocations loops is assumed to develop continuously during pre- as well as during post-yield irradiation; during pre-yield irradiation by the one-dimensional (1D) diffusion and trapping of newly produced glissile clusters, during post yield irradiation mainly by the sweeping of matrix loops. We sketch a "decoration hardening" model where the yield stress as well as the post-yield flow stress is considered to be controlled by the degree of decoration. Our emphasis will be on identifying the necessary conditions and mechanisms.

In section 2, we first describe the main experimental results of the recent in-reactor tensile tests (IRTs) and the main theoretical ideas of the physical processes considered to be relevant for the experimental observations. Section 3 is devoted to the elastic interaction between dislocations and small dislocation loops and between such loops which is considered to form the energetic basis for the evolution of dislocation decoration with loops. The kinetics of dislocation decoration under pre-yield as well as post-yield conditions is treated in section 4. The effect of dislocation decoration on the yield and the flow stress is discussed in section 5. In section 6, the main results are summarised and their implications for other irradiation and deformation conditions and other materials are discussed. Conclusions are presented in section 7.

2. Physical Basis for the Present Theoretical Considerations

2.1 Experimental observations

The theoretical considerations of this paper are based on the results of recent in-reactor tensile tests (IRTs) and microstructural investigations of pure Cu samples studied in these tests [4]. The stress response of pure Cu samples as a function of test time is shown in fig. 2.1 for 3 different pre-yield doses when the deformation was started (increasing in the sequence of test numbers 3, 1, 2). These results form the basis for figs. 2.2a and 2.2b where the increases in the yield stress and post-yield flow stress relative to unirradiated reference samples are plotted vs. dose and strain, respectively. Figures 2.1, 2.2a and 2.2b show that the samples deform uniformly without yield drop. A prominent feature of the stress response observed in the IRTs is that an increase in the pre-yield dose results in an increase in the level of hardening in its whole evolution from the yield stress to the on-set of fracture - as if the materials "remembered" the impact of the pre-yield damage level over the whole test period, i.e. over a dose range of more than 2 orders of magnitude.

As illustrated by the example shown in fig. 2.3, microstructures observed after IRTs are characterized by a relatively homogeneous spatial distribution of substantially decorated dislocations, without indication of segregation in the form of walls and cells as observed in unirradiated and deformed pure Cu samples. These features indicate that deformation proceeds in a rather homogeneous fashion.

The mechanical behaviour revealed by figs. 2.1 and 2.2 is fundamentally different from what would be expected from the point of view of the conventional picture of radiation hardening which assumes that radiation induced immobile and indestructible obstacles such as SFTs and dislocation loops (determined by the total dose) control the mechanical response of materials. In such a model it is not understandable at all why the stress response, say at $2x10^{-2}$ dpa, should significantly depend on the much lower pre-yield dose in the range $< 10^{-2}$ dpa.

We conclude from this surprising dependence of the stress response on pre-yield dose that, under IRT conditions, the hardening cannot be explained in terms of radiation induced obstacle hardening alone. Instead, the stress response in IRTs seems to originate from the structure of the dislocation and their immediate environment, i.e. from the dislocations coupled to the loops decorating them. Therefore, we will focus in the following on modelling the evolution of dislocation decoration under static as well as dynamic conditions and its effect on the stress response.

2.2 Physical processes

In the present paper, we attribute hardening under IRT conditions primarily to the decoration of dislocations with cascade induced dislocation loops. Naturally, the direct contact of dislocations with obstacles such as loops and SFTs will also contribute to hardening. The details of the microscopic processes involved in dislocation decoration are very complicated. It appears therefore useful to start the discussion with a qualitative description of these processes.

In displacement cascades, efficient recombination and clustering of both vacancies and self-interstitial atoms (SIAs) take place. Certain fractions of the surviving SIAs form glissile and sessile clusters, respectively. Glissile SIA clusters in the form of small dislocation loops perform a very fast and far ranging one-dimensional (1D) diffusion along close packed directions of the lattice [12]. During the early stages of irradiation (pre-yield irradiation), particularly of pure metals, such clusters are mainly trapped in the long range strain/stress fields of grown-in dislocations and accumulate there because of the limitation of their diffusion to 1D (provided they are able to change their direction of motion or to climb transversally to their 1D diffusion directions). Thus, the 1D diffusion of SIA clusters and their interaction with dislocations is the origin of the decoration of static dislocations with SIA loops [10, 11].

Loops with different, though crystallographically equivalent, Burgers vectors approach a dislocation from different diffusion directions and are repulsed at one side and attracted at the opposite side of the dislocation as schematically illustrated in fig. 2.4. For edge dislocations, the interaction is strongest when the Burgers vectors of the dislocation and the loop have the same direction (“aligned loop”). During the evolution of dislocation decoration process, loops themselves interact and react with each other. The following main reactions are conceivable: coalescence of two aligned or two “non-aligned loops” and coalescence of a non-aligned with an aligned loop with subsequent alignment.

While dislocations at rest are decorated by the 1D diffusion and trapping of primary cascade induced SIA clusters, dislocations moving during deformation are considered here to get decorated with loops mainly by sweeping the matrix during their glide. The experimental findings that dislocations formed during deformation are significantly decorated with loops [4] provide evidence that these dislocations have indeed swept and dragged matrix loops.

As schematically illustrated in fig. 2.5, dislocations moving during deformation “see” an apparent drift flux of matrix clusters (loops and SFTs) with whom they interact and react via the cloud of aligned loops accompanying them. The fate of matrix loops swept by a moving dislocation depends on their glide direction relative to the glide plane of the dislocation. Matrix loops gliding

parallel to the glide plane (aligned loops) can join the loop cloud accompanying a dislocation. Upon close contact, one aligned loop may agglomerate with another aligned loop or with a non-aligned loop with subsequent alignment forming thereby a larger aligned loop. A member of the aligned loop ensemble may be immobilised and left behind the moving dislocation by a close interaction without direct contact with a matrix cluster.

A Matrix loop gliding transversely to the glide plane can approach the dislocation and can get incorporated in its core, provided its motion to the dislocation has not been blocked by a close interaction with another matrix cluster. The preferential absorption of (non-aligned) loops (compared to vacancy absorption) would cause edge segments to climb and render screw segments helical[1)]. A contact between a member of the loop ensemble and a SFT will result in partial recombination of SIAs and vacancies contained in both. Growth of the loop ensemble, absorption of loops by the dislocation and partial recombination of SIAs in loops and vacancies in SFTs will reduce the fraction of defects accumulated in the matrix.

Decoration is expected to reduce the effective mobility of the dislocations which are being continuously produced during deformation. Because "younger" (i.e. a newly generated) dislocation segments are less decorated, they are more mobile and faster than "older" segments and, consequently, sweep faster, such that their degree of decoration soon becomes comparable to that of "older" segments. Dislocations once decorated will remain decorated during deformation, i.e. they will not get separated from their loop cloud.

Because of the reduction of the effective mobility of dislocations upon decoration, the stress required to move them with a certain velocity increases with increasing degree of decoration. In the stress response to deformation, this manifests itself in an increase in the yield and the post-yield flow stress. An important point to be discussed in hardening due to dislocation decoration is the origin of the force between a moving dislocation and the dragged loop ensemble responsible for the reduction of the dislocation mobility. Two main contributions to this force have to be considered: (1) the finite mobility of the loops, and (2) the mutual interaction between members of the loop ensemble and between the latter and matrix clusters.

In the following, we make an attempt to quantify the qualitative picture of dislocation decoration and its relation to hardening as described in the present section. A central question in our considerations will be as to whether or not the mechanisms introduced here are efficient enough to be relevant for the observed defect accumulation and the associated mechanical response.

[1)] It is not clear, however, whether screw dislocation segments are able to incorporate loops completely or partially in their cores as they do incorporate single SIAs and vacancies.

3. Energetics of Dislocation Decoration with Loops

The strong long-range elastic interaction between dislocations and SIA clusters moving one-dimensionally in form of a small glissile dislocation loops forms the basis of dislocation decoration under static as well as dynamic conditions. With progressing decoration, also the interaction between members of the loop ensembles decorating dislocations becomes increasingly important. The relative strength of the loop-dislocation and loop-loop interaction may be expected to be essential for the evolution of decoration and the related mechanical response. It is clear that already the energetics of dislocation decoration represents a very complicated multi-particle problem which can not be treated rigorously. For the discussion of the kinetics of decoration, at least some basic elements of its energetics are needed which we present in this section.

Details of the loop-dislocation and loop-loop interaction depend on the crystallography of the dislocations and loops involved. Considering a FCC crystal structure (e.g. of Cu), we assume for both dislocations and loops, Burgers vectors (BVs) of <110>/2-type, for the former glide planes of {111}-type, and for the latter, according to computer simulations for Cu [14], {110}-type habit planes (differently from the {111}-type habit planes assumed in [11]), i.e. totally 6 loop configurations. For a given edge dislocation, for instance, 3 of the 6 loop configurations are able to glide parallel to the glide plane of the dislocation, (1 of them with BV *b* aligned with the BV *B* of the dislocation, and the other 2 with glide components in the dislocation line direction, allowing a distribution of such loops over a gliding dislocation); and the other 3 of the 6 configurations glide obliquely to the glide plane of the dislocation and can thus be absorbed when the latter moves.

If a loop glides parallel to the glide plane of a (moving) dislocation it can reach this only by climb or by changing its direction, i.e. its Burgers vector [15] (which we ignore here). If a loop glides obliquely to the glide plane of a moving dislocation, both can meet each other by glide at the intersection of the loop path with the glide plane.

3.1 Interaction of dislocations with single loops

We use the isotropic elastic continuum approach to estimate the magnitude of the elastic interaction between a single dislocation and a single loop as a function of the spatial separation vector, $\boldsymbol{r}_{dl}$, i.e. the distance and relative orientation between the dislocation and the loop. For loop-dislocation distances large compared to the loop diameter, $d_{dl} >> d_l$, the loop may be considered to represent an elastic dipole of eigen-strain tensor $\mathbf{Q}$. In this small (or "infinitesimal") loop approximation, the interaction energy of the loop, E_{dl}, in the stress field of the dislocation, $\boldsymbol{\sigma}^{\mathbf{d}}(d_{dl})$, may be written as [16, 17]

$$E_{dl}(\boldsymbol{r}_{dl}) = -\mathbf{Q}\cdot\boldsymbol{\sigma}^{\mathbf{d}}(\boldsymbol{r}_{dl}) = -Q_{ij}\,\sigma^{d}_{ij}(\boldsymbol{r}_{dl})\,. \tag{3.1}$$

Einstein's summation convention for summing up over repeated indices (denoting components of vectors and tensors) is to be used in eq. (3.1) and, when appropriate, later. The force between the dislocation and the loop is given by the gradient of the interaction energy

$$\mathbf{F}_{dl}(\boldsymbol{r}_{dl}) = -\nabla E_{dl}(\boldsymbol{r}_{dl}). \tag{3.2}$$

For a well developed loop of area vector $\mathbf{A}$ and Burgers vector $\mathbf{b}$

$$\mathbf{Q} = (\mathbf{A}\,\mathbf{b} + \mathbf{b}\,\mathbf{A})/2 \rightarrow (A_i b_j + A_j b_i)/2\,, \text{ with } \mathbf{A}\cdot\mathbf{b} = A_i b_i \approx n\Omega\,, \tag{3.3}$$

where n is the number of SIAs contained in the loop and $\Omega \approx b^3$ ($\Omega = b^3/\sqrt{2}$ for FCC) is the volume of matrix atoms. For isotropic **Q**, as for instance for SFTs, $Q_{ij} = n\Omega\delta_{ij}/3$, $Q_{ii} = n\Omega$.

In the small loop approximation where the radius of curvature of the dislocation has to be large compared to the diameter d_l of the loop, we may approximate the stress field in eq. (3.1) by that of a straight dislocation. According to eq. (3.1), the spatial dependence of the interaction energy is determined by that of the stress field of the dislocation. Thus, for a straight dislocation segment, the dependence of the interaction energy on $\boldsymbol{r}_{dl}$ has the symmetry corresponding to $\boldsymbol{\sigma}^{\mathbf{d}}(-\boldsymbol{r}_{dl}) = -\boldsymbol{\sigma}^{\mathbf{d}}(\boldsymbol{r}_{dl})$, i.e.

$$E_{dl}(-\boldsymbol{r}_{dl}) = -E_{dl}(\boldsymbol{r}_{dl}) \; . \tag{3.4}$$

According to eq. (3.4), the directional dependence of the interaction energy is characterised by attractive and repulsive directions. If a loop is attracted at one side of the dislocation, it is repulsed at the opposite side; it is, for instance, attracted at the side of dilatation and repulsed at the side of compression of an edge dislocation. As a result, the directional average of the interaction energy vanishes.

Simple estimates of the magnitude of the interaction energy and the force between dislocations and loops are obtained by ignoring the vector and tensor characters of the quantities in eq, (3.1). Setting $\mathbf{Q} \rightarrow n\Omega$, $\boldsymbol{\sigma}^{\mathbf{d}}(\boldsymbol{r}_{dl}) \rightarrow \mu b/2\pi r_{dl}$ we write

$$|E_{dl}(r_{dl})| \sim n\mu\Omega^2 b/2\pi r_{dl} \text{ and } |F_{dl}(r_{dl})| \sim n\mu\Omega^2 b/2\pi r_{dl}^2, \tag{3.5}$$

where μ is the shear modulus of the matrix.

According to eq. (3.5), the energy and the force $E_{dl}(r_{dl})$ and $F_{dl}(r_{dl})$ increase linearly with the number n of SIAs contained in the loop and decrease inversely with the distance and the square of the distance, respectively. Equation (3.5) suggests using $n\mu\Omega^2/2\pi$, $n\mu\Omega^2/b2\pi$, and r_{dl}/b as natural energy, force and length units, respectively. We will use eq. (3.5) for SFTs as well as for loops.

The dependence of the interaction energy on the direction of the spatial separation vector, $\boldsymbol{r}_{dl}$, i.e. the angular dependence, is much more complicated than the distance dependence and varies considerably with the configuration of the loop relative to that of the dislocation (a relatively simple expression can be derived for pure screw dislocations, see appendix A1). For the derivation of explicit expressions for interaction energies and forces, the coordinate system is chosen such that the expressions for the stress fields of straight dislocations given in text books [17, 18] can be directly used: x, y and z coordinates in the glide direction, perpendicular to the glide plane (normal vector **G**) and along the dislocation line (unit vector **L**), respectively (suffices 1,2 and 3 for vector and tensor components).

To illustrate the dependence of the interaction energy on the direction, lines of equal interaction energy, "equipotential lines", in appropriate planes as plotted in fig. (3.1) have been calculated (see appendix A1). The equipotential lines are kidney shaped for the interaction of a loop with an edge dislocation (except for loops with BV perpendicular to BV of the edge dislocation), and circular for the interaction of a loop with a screw dislocation.

The calculations show that the interaction is strongest for **b** ∥ **B**(edge), vanishes for **b** ∥ and ⊥ **B**(screw), and is comparable in magnitude for the remaining 9 combinations of configurations listed in table A1, including the 4 remaining combinations of loop configurations with a screw type dislocation (in variance to the common assumption, that screw dislocations do not interact with loops).

For edge dislocations, the interaction is attractive, $E_{dl}(\boldsymbol{r}_{dl}) < 0$, and repulsive, $E_{dl}(\boldsymbol{r}_{dl}) > 0$, at the side of dilatation, and compression, respectively. At one side of a screw dislocation, the

interaction is attractive for one loop configuration gliding parallel to the glide plane of the dislocation and repulsive for the other. Analogous relationships hold for loops gliding obliquely to the glide plane of a screw dislocation. Accordingly, under irradiation without deformation, decoration will develop only at one side of edge type but around screw type dislocations. Note that upon cross slip of a screw dislocation segment non-aligned loops would become aligned and visa versa.

A 1D diffusing glissile loop arriving at an attractive side of a dislocation at rest will be trapped in a local energy minimum, in a "valley", defined by the tangent of the 1D diffusion direction to the corresponding equipotential line. In the case of an edge dislocation, two "valleys" separated by a "mountain ridge" exist for kidney shaped equipotential lines. The relative strengths of the interactions of loops of different configurations with a dislocation are expected to manifest themselves in the frequency distributions of the loops decorating the dislocation.

An important quantity in dislocation decoration is the width of the decorated region, d_{tr}. The pre-yield decoration of dislocations at rest is most likely spatially limited by the thermally activated de-trapping of small primary 1D diffusing loops at the boundary of decoration which determines an upper bound of d_{tr}. For estimating the range of efficient trapping as a function of temperature, for the time being without regard to the degree of decoration, we introduce in eq. (3.5) $\mu\Omega \approx 35kT_m$ as a homologous elastic energy unit where kT_m is the thermal energy at the melting point T_m of the metal:

$$|E_{dl}| \approx 6nkT_m b/r_{dl} . \qquad (3.6)$$

Trapping of loops by dislocations at rest is expected to be efficient within the "trapping range", $r_{dl} < d_{tr}$, where the magnitude of the attractive interaction energy is larger than the thermal energy, $|E_{dl}| > kT$. In this range, the probability for detrapping decreases steeply with decreasing r_{dl}. Neglecting detrapping and using $|E_{dl}| > kT$ in eq. (3.6), we obtain an upper bound estimate of the trapping range scaling as

$$d_{tr} \approx 6nbT_m/T . \qquad (3.7)$$

For the temperatures around 380K of the IRTs considered here, we find $d_{tr} \approx 20nb$, meaning that, for instance, for primary loops with $n = 10$ SIAs per loop the width of the decorated region would be as large as $d_{tr} \approx 200b \approx 50$ nm[2)]. For loops having grown far beyond the size of primary loops, $n >> 10$, the trapping range would be significantly larger. Thermally activated de-trapping from dislocations is, however, negligible for such loop sizes, i.e. it does not play any role in the sweeping of matrix loops by dislocations moving under deformation. Under such dynamic conditions, the spatial width of decoration is not limited by the loop-dislocation interaction energy relative to the thermal energy but most likely by the mutual immobilisation of dragged loops by matrix clusters as considered below.

3.2 Interaction between two loops

So far, we have considered the interaction between a single dislocation and a single loop. During the evolution of a loop cloud around a dislocation, the probability of members of the loop cloud to interact with each other more strongly than with the dislocation increases with increasing density of loops in the decorated region. Two loops will react with each other if their glide cylinders intersect each other. But even if their glide cylinders do not intersect, the elastic

[2)] A more rigorously derived estimate of a representative interaction energy [19] yields a smaller factor of about 3.5 instead of 6 in eqs. (3.6), resulting in correspondingly lower values for d_{tr}.

interaction between 2 loops can be stronger than their interactions with the dislocation if their distance is small compared to their distance to the dislocation.

For loop-loop distances larger than the loop diameters, $d_{ll} >> d_l$, we may again use the small loop approximation to estimate the loop-loop interaction energy. In this approximation, the interaction energy of two loops, (1) and (2), E_{12}, is given by an expression analogous to eq. (3.1), except that the strain tensor is now that of one of the loops and the stress tensor that of the other loop. By use of the elastic Greens function, the complicated stress field of a loop may be related to its eigen-strain tensor as shown in the appendix A1.

The dependence of the interaction energy of 2 loops with non-intersecting glide cylinders on their distances from their positions of closest approach is illustrated in fig. (3.2) for different combinations of loop configurations. For all combinations, the interaction energy has an absolute minimum at the closest approach positions of the loops.

As done in eq. (3.5) for the interaction of a single loop with a dislocation, we may introduce simple estimates for the interaction energy and the corresponding force between two loops containing m and n SIAs, respectively, by ignoring the vector and tensor character of the quantities involved. Accordingly, we write for two loops containing *m* and *n* SIAs

$$|E_{ll}(r_{ll})| \sim mn\mu\Omega^2/4\pi r_{ll}^3 \text{ and } |F_{ll}(r_{ll})| \sim 3mn\mu\Omega^2/4\pi r_{ll}^4. \qquad (3.8)$$

Equation (3.8) is also a reasonable estimate for the interaction of a loop with a well relaxed large SFT and represents an upper bound estimate for the small SFTs developing under cascade damage conditions.

As for the trapping of a loop in the field of a dislocation, mutual trapping of two small loops is expected to be efficient within the "trapping range", $r_{ll} < r_{tr}$, where the magnitude of the attractive interaction energy is $|E_{ll}| > kT_m$. With eq. (3.8), this yields for the trapping range, r_{tr}, and the corresponding trapping cross section, s_{tr}, respectively

$$r_{tr} \sim 1.5\,(mnT_m/T)^{1/3}\,b, \quad s_{tr} = \pi r_{tr}^2 \sim 7(mnT_m/T)^{2/3}b^2, \qquad (3.9)$$

in agreement with the estimate given in ref. [19]. The trapping cross section given in eq. (3.9) can be significantly larger (say by 1 order of magnitude) than the geometrical cross section of the bigger of the two loops, $s_g \approx mb^2$.

3.3 Interaction between two loops in the field of a dislocation

In a loop cloud decorating a dislocation, loops interact with each other as well as with the stress field of the dislocation. In fact, it is the strength of loop-loop interaction relative to the loop-dislocation interaction which will be assumed later to limit the evolution of dislocation decoration and to determine the associated yield and flow stresses. For example, an "aligned" loop accompanying a moving dislocation will be removed from the loop cloud by a close interaction with a "non-aligned" loop if the maximum attractive force between both is larger than that between the "aligned" loop and the dislocation, and when, in addition, no physical contact with subsequent alignment takes place.

Assuming $r_{ll} << r_{dl}$, we find an estimate of the effective cross section for strong interaction, s^*, by equating the loop-dislocation and loop-loop forces as given by eqs. (3.5) and (3.8)[3)]

$$s^* = \pi r_{ll}^2 \approx 4m^{1/2}\,br_{dl}, \qquad (3.10)$$

[3)] we choose the letter *s* for cross section to avoid confusion with the letter σ for stress

According to eq. (3.10), the cross section for strong loop-loop interaction increases linearly with the distance of the blocked loop from the dislocation r_{dl}. Since strong interaction may result in mutual blocking of loops of different glide direction ("blocking cross section"), s* represents a key quantity in the evolution of dislocation decoration and the associated yield and flow stresses as will be shown below. Equation (3.10) is confirmed by a more quantitative derivation in the framework of the small loop approximation given in the appendix A1. Even though this approximation is doubtful for small loop distances, it is considered here to reproduce the main trends.

The interaction of more than two loops in the field of a dislocation is analytically intractable. For estimating effects of loop-loop interaction in dense loop ensembles it is useful to focus on 1 loop or two loops, and to approximate the surrounding loops, in the sense of a mean field approximation, by a continuous distribution beyond an appropriately chosen distance from the loops considered.

4. Kinetics of Decoration of Dislocations with SIA Loops

Dislocation decoration is the result of the capture of cascade induced loops and a variety of reactions between such loops in the distorted lattice region close to the dislocation. An analytical treatment of this complicated inhomogeneous defect reaction kinetics is not possible without substantial simplifications. We describe the kinetics occurring in the real 3D region of decoration by an equivalent kinetics occurring in an imaginary 2D space defined by a conceived projection of the real loop distribution on a plane containing the dislocation and the normal to its glide plane. In this description, a useful measure for the local degree of decoration is the fraction of that plane covered with SIAs, the "coverage" α, given by the projected (2D) number density of loops times the average number of SIAs per loop (with a limiting value $\alpha = 1$ for one additional atomic layer).

4.1 Kinetics of decoration in the absence of plastic deformation

In displacement cascades, efficient recombination and clustering of both vacancies and self-interstitial atoms (SIAs) take place. SIA clusters are produced in the form of small dislocation loops which are glissile or sessile on the time scale of computer simulations (for reviews see [12]). The relations between the NRT-displacement rate, G_{NRT}, and the generation rates of SIAs surviving intra-cascade recombination, G, consisting of partial fractions surviving in glissile and sessile loops, $G_{\mathrm{i}}^{\mathrm{g,s}}$, may be written as

$$G = (1 - f_r) G_{NRT}\,, \quad G_i^{g,s} = f_i^{g,s} G \ , \tag{4.1}$$

where f_{r} (≥ 80%) and $f_{\mathrm{i}}^{\mathrm{g,s}}$ ($f_{\mathrm{i}}^{\mathrm{g}} + f_{\mathrm{i}}^{\mathrm{s}} \approx 50\%$) are the fractions of SIAs recombining in cascades and clustered in glissile or sessile loops, respectively[4)]. The formation of stable SIA clusters and the 1D diffusion of a fraction of them forms the basis of the extended "production bias model" (PBM) [12, 13].

The temporal evolution of the concentration of glissile loops (per matrix atom), c_{g}, is determined by their generation rate, G_{g}, and their rate of trapping and/or absorption by sinks

[4)] to avoid confusion with the strain denoted by the letter ε, we use here the letter f for the fractions, in stead of ε as used in our previous work [12]

$$\dot{c}_g = G_g - D_g c_g k_g^2 \ . \tag{4.2}$$

Here $G_g = f_i^g \, G_i^g / n_i^g$ is the generation rate (n_i^g: average number of SIAs in glissile loops), D_g is the diffusion coefficient for 1D diffusion and k_g^2 is the total strength for reactions of the glissile loops with sinks. This sink strength k_g^2 is determined by the reciprocal mean free path κ of the 1D diffusing loops in the sink structure [12, 15]

$$k_g^2 = 6\kappa(\kappa_d + \kappa_l + \kappa_{SFT}) \, , \tag{4.3}$$

which consists of partial contributions from dislocations, existing sessile SIA loops and stacking fault tetrahedra (SFTs), respectively:

$$\kappa_d = \pi d_{tr} \rho / 4, \quad \kappa_{l,SFT} = s_{l,SFT} N_{l,SFT} \, , \quad \kappa = \kappa_d + \kappa_l + \kappa_{SFT} \tag{4.4}$$

Here d_{tr} is the diameter of the trapping range and ρ the density of dislocations; $s_{l,SFT}^{tr}$ and $N_{l,SFT}$ are the trapping cross sections and number densities of loops and stacking fault tetrahedra, respectively.

For the very fast diffusing glissile loops the transient to quasi-steady-state occurs at a very early stage where (in pure metals) the dislocations form the dominant sinks and thus determine the characteristic time to quasi-steady-state, τ, defined by eq. (4.2) as

$$\tau = 1 / D_g k_g^2 \approx 1 / D_g k_{g,d}^2 \, . \tag{4.5}$$

With $D_g \approx 10^{-8}$m^2/s, an initial dislocation density $\rho_0 \approx 10^{12}$/m^2 and $d_{tr} \approx 50$nm, we obtain $\tau \approx 0.1$s, corresponding to about $5\text{x}10^{-9}$dpa for $G_{NRT} = 5\text{x}10^{-8}$/s. In the stage following this very short transient, the glissile loops are simply partitioned over the existing sinks, first predominantly over the existing dislocations, later predominantly over sessile loops and SFTs evolving between the dislocations.

The basis for dislocation decoration during pre-yield irradiation is that a 1D diffusing glissile loop once trapped in the strain field of a dislocation can not reach the dislocation core and get absorbed there, unless it climbs or changes its glide direction, which are unlikely processes for the temperature range considered here. In describing dislocations decoration, defect accumulation within the trapping range of dislocations has to be coupled with that in the matrix between the dislocations. The latter has been treated in some detail within the framework of the so called "production bias model" (PBM) [12, 13]. For the purpose of the present paper, aimed primarily at identifying mechanisms and conditions for dislocation decoration, it is sufficient to use appropriate approximations allowing an analytical treatment of the features of the matrix evolution relevant for decoration. For estimating defect accumulation during pre-yield irradiation in its early build-up stage, we make the following approximations:

(1) certain constant fractions, $\eta_{i,v}$ (0.5 to 2%), of the SIAs and vacancies generated by NRT displacements are accumulating in loops and SFTs, implying that the total concentrations of SIAs and vacancies accumulated in loops and SFTs, $c_{i,v}^{l,SFT}$, increase linearly with increasing dose which is a reasonable assumption for low pre-yield irradiation dose < 10^{-2} dpa, and

(2) the trapping cross sections $s_{tr}^{l,SFT}$ in $\kappa_{l,SFT}$ are proportional to (even though larger than) the corresponding geometrical cross sections, $s_{l,SFT}^{geom}$.

Using these approximations we may write

$$\kappa_{l,SFT} \approx q^{l,SFT}\, c_{i,v}^{l,SFT}/b \approx q^{l,SFT}\, \eta_{i,v} G t/b \qquad (4.6)$$

where $q^{l,SFT} = (s_{tr}^{l,SFT}/s_{geom}^{l,SFT})$ is the ratio of the trapping and the geometrical cross sections.

A measure for the **global** degree of decoration is the volume averaged atomic SIA concentration involved in decoration, c_i^{dc}. In quasi-steady-state of the glissile loop concentration within the matrix, we may write the temporal rate of change of this quantity according to eqs. (4.1) to (4.4) as

$$\dot{c}_i^{dc} = f_i^g G \kappa_d(t)/\kappa(t)\,. \qquad (4.7)$$

A useful measure for the **local** degree of decoration is the atomic "coverage", α, of the conceived plane of decoration as introduced above. Its average value is obtained by taking the total SIA concentration involved in decoration, c_i^{dc}, to be distributed over the volume defined by the total dislocation length, ρV, the width of decoration, d_{dc}, and the thickness of an atomic layer, b. This yields the relation

$$c_i^{dc} = d_{dc} b \rho \alpha\,. \qquad (4.8)$$

Using the approximation given by eq. (4.6), the analytical integration of eq. (4.7) yields a logarithmic dose dependence of c_i^{dc}, and, according to eq. (4.8), analogously of α. Assuming $\eta_i = \eta_v = \eta$ and $q^l = q^{SFT} = q$, we may write the solution for α in the form

$$\alpha = (\alpha_0/q)\ln(1+qt/t_0) \text{ with } \alpha_0 = (\pi/8) f_i^g/\eta \text{ and } t_0 = \pi b d_{tr}\rho_0/(8\eta G)\,, \qquad (4.9)$$

where α_0 and t_0 are the values of coverage and time characterising the transition from dislocation to matrix cluster dominance in the sink strength. Order of magnitude values of the parameters are $\alpha_0 \approx 0.1$ and $D_0 = G_{NRT} t_0 \approx 10^{-4}$ to 10^{-3} dpa.

The dose dependence of α according to eq. (4.9) is plotted in fig. (4.1) for $\alpha_0 = 0.2$ and different values of q and D_0. In the stage where the strain fields of the dislocations form the dominant sink for primary glissile loops, $qt << t_0$, the dependence of the coverage on pre-yield dose is first linear, independently of η and q, and flattens later, for $qt > t_0$, to a slower logarithmic increase, when the flux of these loops is being increasingly screened by the loops and SFTs evolving between the dislocations. With increasing dose, the uncertainty in α becomes increasingly larger due to the increasing uncertainty in the evolution of the matrix clusters. The dependence of α on dose will manifest itself in the dependence of the yield stress as we will show in section 5.

Already at a minimum pre-yield dose of $5\text{x}10^{-4}$ dpa (corresponding to an elastic strain of 10^{-3}) we find significant dislocation decoration with values of the coverage α between 2% and 10%. The reduction of the mobility of dislocations by such well developed loop clouds already at low pre-yield dose may well be expected to prevent them from segregating in cell walls. This is consistent with the experimental observation that no cell walls are formed in the Cu samples treated in IRT with a pre-yield dose of $7.5\ 10^{-4}$ dpa [4].

4.2 Kinetics of decoration during plastic deformation

While dislocations at rest are decorated by the 1D diffusion and trapping of primary cascade induced SIA clusters, dislocations moving during deformation are considered here to acquire loops mainly from sweeping the matrix. The experimental findings that dislocations formed during deformation are significantly decorated with loops provide evidence that such loops, even though apparently sessile in the matrix, are indeed able to move in the strong stress fields of

dislocations. We may refer in this context to the well known phenomenon that apparently sessile loops move to and disappear at free surfaces due to attractive image forces [20].

Decoration is expected to reduce the mobility of the dislocations which are being continuously produced during deformation. Because "younger" dislocation segments are less decorated, they are more mobile and faster than "older" segments and, consequently, sweep faster, such that their degree of decoration soon becomes comparable to that of "older" segments, depending on the instantaneous levels of dislocation density and stress. Because of this state dependent spectrum of dislocation decoration and velocity, the evolution of decoration and stress would be necessarily coupled from the very beginning. Under the condition of strain rate controlled deformation, the treatment of these interconnected evolutions can be separated into two parts, first the treatment of dislocation decoration, then the analysis of the related stress response, by assuming that all dislocations move with the same (the average) velocity determined by the dislocation density and the strain rate.

We will use this simplification in the following treatment. One has to keep in mind, therefore, that within this approach only the evolution of some representative average degree of dislocation decoration can be studied.

The relation between the plastic strain rate, $\dot{\varepsilon} = \mathrm{d}\varepsilon/\mathrm{d}t$, (or the total plastic strain, ε) and the average velocity of mobile dislocations v_d (or average dislocation displacement Δx) is given by the Orowan equation in its differential or integral form

$$\dot{\varepsilon} = \rho b v_d , \quad \varepsilon = b\rho\Delta x . \tag{4.10}$$

For a strain rate of 10^{-7}/s and dislocation densities $\rho > \rho_0 = 10^{12}/\mathrm{m}^2$, typical for the IRTs considered here, we find a rather low upper bound estimate for the dislocation velocities, $v_\mathrm{d} < 0.5$ nm/s and values decreasing from there with increasing ρ during deformation. This range of velocities is more than 12 orders of magnitude lower than the ones used in computer simulations for dislocations dragging primary cascade induced SIA clusters [21]. This means, in turn, that the loops having been formed in the matrix would be able to follow the dislocation even if they were by 12 orders of magnitude less mobile than the primary cascade induced SIA clusters, i.e. virtually sessile relative to the latter on the scales of simulations.

A necessary condition for the continuous dragging of a loop of a given mobility, M_l, at a distance $r_\mathrm{dl} = y$ from the glide plane of a dislocation moving with velocity v_d is that the force exerted by the dislocation on the loop, F_dl, is sufficiently strong to allow the loop to follow the dislocation with the same velocity, $v_\mathrm{l} = v_\mathrm{d}$, meaning that the maximum force for that distance $F_{dl}^{\max}(y)$ is equal to or larger than the necessary force, $M_\mathrm{F} F_\mathrm{dl} = v_\mathrm{l} = v_\mathrm{d}$. i.e.

$$M_F F_{dl}^{\max}(y) \geq M_F F_{dl} = v_d . \tag{4.11}$$

According to this, loops developed in the matrix would be able to follow the dislocation even if they were by 12 orders of magnitude less mobile than the primary cascade induced SIA clusters, i.e. virtually sessile relative to the latter.

From this we can draw a conclusion on the role of the loop mobility in dislocation decoration under dynamic conditions. Let us assume that the width of the decorated region is limited at $y = d_\mathrm{dc}$ by the mobility of the dragged loops and consider the consequences of this assumption. Using in eq. (4.11) for $F_{dl}^{\max}(y)$ the (not specified) estimate of the level of F_dl as given by eq. (3.5) and for v_d eq. (4.10) we find that decoration would be limited to the range

$$y \leq d_{dc} \approx (n\mu\Omega M_F \rho b^2 / 2\pi\dot{\varepsilon})^{1/2} . \tag{4.12}$$

According to eq. (4.12), d_{dc} would depend on two parameters, M_F and ρ, which must be considered to vary by several orders of magnitude during irradiation and deformation. Thus, on the one hand, ρ increases during deformation by more than 2 orders of magnitude which, at a constant M_F, would result in an increase in d_{dc} by more than 1 orders of magnitude; on the other hand, a steep decrease of the M_F (say by 12 orders of magnitude) with increasing loop size in the matrix at a constant ρ would manifest itself in a steep decrease of d_{dc} (by 6 orders of magnitude). Such strong variations in d_{dc} to be considered on the basis of eq. (4.12) contrast with real variations of d_{dc} apparently limited to a range of a few tens of nm during IRTs which are very unlikely to be consistent with eq. (4.12).

We therefore conclude that dislocation decoration is most likely not controlled by the loop mobility, at least not in most parts of the parameter ranges of the IRTs considered here. This means that the loop mobility is most likely far above the limit defined by eq. (4.11). Below, we will argue that the spatial limitation of decoration (to a few tens of nm) is due to the mutual blocking of loops of different Burgers vectors the probability of which increases with increasing distance from the dislocation.

A dislocation moving with a velocity v_d through the matrix containing SIA and vacancy clusters in the form of loops and SFT, respectively, "sees" continuous apparent drift fluxes of matrix loops and SFTs, $J_{l,SFT}$, and the corresponding fluxes of SIAs and vacancies contained in them, $j_{i,v}$, which may be related to the dislocation velocity and the strain rate as

$$J_{l,SFT} = v_d M_{l,SFT}, \quad j_{i,v} = v_d c_{i,v}^{(m)} / \Omega \text{ with } v_d = \dot{\varepsilon} / b\rho. \tag{4.13}$$

Matrix loops gliding parallel to the glide plane of a dislocation, "aligned loops" (fraction χ_+ of all loops), can follow the dislocation, pulled and pushed at the side of attractive and repulsive interaction with the dislocation, respectively. Differently from the decoration of dislocations at rest with loops during pre-yield irradiation, moving dislocations are decorated at both the sides of attractive and repulsive interaction. Loops gliding obliquely to the glide plane, "non-aligned loops" (fraction χ_- of all loops), can reach the dislocation and get absorbed by it provided they are not blocked by the interaction with loops with different Burgers vector, particularly with aligned members of the dragged loop ensemble. Vacancies in the form of SFTs may interact with dragged aligned loops which may result in (partial) annihilation.

Absorption of non-aligned loops by moving dislocations and the partial annihilation of SFTs with aligned loops results in reductions of the concentrations of SIAs and vacancies accumulated in the matrix, $c_{i,v}^{(m)}$. Using eq. (4.13), we may describe this reduction by

$$\dot{c}_{i,v}^{(m)}\Big|_{sw} = -\phi_{i,v} j_{i,v} d_{dc} \rho \Omega = -\phi_{i,v} (\dot{\varepsilon} d_{dc} / b) c_{i,v}^{(m)}, \tag{4.14a}$$

or alternatively, by using $d/dt = \dot{\varepsilon} d/d\varepsilon$,

$$dc_{i,v}^{(m)}/d\varepsilon\Big|_{sw} = -\varepsilon / \varepsilon_{i.v}^{(sw)} \text{ with } \varepsilon_{i,v}^{(sw)} = (b/d_{i,v}^{(sw)})/\phi_{i,v}, \tag{4.14b}$$

where $\phi_{i,v}$ are fractions $\phi_{i,v}$ of SIAs and vacancies which can be absorbed and annihilated, respectively, when encountered by a decorated dislocation within ranges of widths $d_{i,v}^{(sw)}$, where $\varepsilon_{i,v}^{(sw)}$ is the characteristic strains for the reduction of $c_{i,v}^{(m)}$ by dislocation sweeping. (Note that the total volume fractions swept by all dislocations is given by $\varepsilon d_{i,v}^{(sw)}/b$). It is emphasised here, that by the Orowan equation (4.10), the strain rate has dropped out in eq. (4.14b).

The effects of dislocation sweeping on SIA and vacancy accumulation in the matrix are qualitatively different and the meaning of the parameters is correspondingly different. Since at

most all non-aligned, i.e. half of all matrix loops, can get absorbed by the dislocation, the fraction ϕ_i is limited to $\phi_i \leq ½$. The fraction ϕ_v of vacancies in SFTs partially annihilated by dragged aligned loops will increase with increasing degree of decoration. However, because of the necessity of direct contacts between SFTs and loops for (partial) annihilation, ϕ_v and with this the sweeping effect on vacancy accumulation in the matrix SFTs, may be expected to remain negligible during deformation. The width for the sweeping and absorption of non-aligned loops, $d_i^{(sw)}$, will decrease with increasing degree of decoration because of the increasing probability for blocking of non-aligned matrix loops by aligned loops accompanying the dislocations.

An interesting question in this context is as to whether sweeping of matrix loops by moving decorated dislocations can significantly affect the SIA concentration in the matrix. Assuming for the characteristic strain $\varepsilon_{i,v}^{(sw)}$ in eq. (4.14b) $\phi_i \leq ½$ and $d_i^{(sw)} \approx 20\text{b} \approx 5$ nm, we find a rough lower bound estimate $\varepsilon_i^{(sw)} \geq 10\%$ (see discussion below). This means that for the IRTs discussed here a reduction in the SIA concentration in the matrix by dislocation sweeping should indeed not be ignored. Incorporation of SIA loops into the core of dislocations (with edge component) would lead to jog formation and by this reduce the mobility of the dislocations. Preferential absorption of SIAs would result in climb of the moving dislocations and an accumulation of an excess of vacancies in the matrix. Since these are second order effects of dislocation sweeping we will neglect them in the following.

The moving system constituted by a dislocation and its associated loop ensemble will encounter matrix clusters with whom it interacts and reacts as described qualitatively in section 2.2. With respect to the evolution of the dragged loop ensemble, gain and loss processes may be distinguished. An "aligned loop" (fraction χ_+ of all loops) gliding parallel to the glide plane of a dislocation will be incorporated into the dragged cloud which thus represents a gain process. Coalescence between two aligned loops may occur. This process does not change the coverage but reduces the number of aligned loops by one. A "non-aligned loop" (fraction χ_- of all loops) gliding obliquely to the glide plane can get absorbed by the dislocation unless it does not significantly interact with members of the dragged cloud; in the latter case, it either gets aligned and consequently incorporated into the dragged cloud, or it blocks an "aligned loop" and stays back together with the latter behind the moving dislocation. Reaction and (partial) annihilation of "aligned loop" with SFTs will result in a reduction of the degree of decoration. These gain and loss processes may be described in terms of effective cross sections for loop coalescence and alignment, mutual loop blocking and (partial) annihilation, s_{co}, s_{al}, s_{bl}, and s_{an}, respectively.

On the basis of these considerations, rate equations for the temporal evolution of the coverage of the decorated area with SIAs, α_+, and for the 2D number density of aligned loops N_+ may be derived. We illustrate the main features of the derivation by discussing the effect of matrix loop incorporation into decoration and refer to Appendix A2 for the complete derivation. According to eq. (4.13) in conjunction with eq. (4.10), the apparent drift flux of matrix loops aligned with respect to the Burgers vector of the dislocation (fraction χ_+ of all loops) to a atomic unit area $A_0 \approx b^2$ in the decorated area results in a local increase of α_+ described by

$$d\alpha_+/dt\big|_{in} = \chi_+ j_i^{(ml)} b^2 = \chi_+ \dot{\varepsilon} c_i^{(ml)} / (b^2 \rho) \tag{4.15a}$$

or alternatively, using $d/dt = \dot{\varepsilon} d/d\varepsilon$,

$$d\alpha_+/d\varepsilon\big|_{in} = \chi_+ c_i^{(ml)} / (\rho b^2) \tag{4.15b}$$

As in eq. (4.14b), the strain rate has dropped out in eq. (4.15b) upon using the Orowan equation (4.10).

In the description of decoration during deformation, the expansion of the whole decorated space (i.e. the increase in the product of the total dislocation length and the width of the decorated area) when the dislocation density increases has to be taken into account. This can be achieved by introducing an effective loss term $-\alpha_+(d\rho/dt)/\rho$ in eq. (4.15b) where $(d\rho/dt)/\rho$ describes the relative volume increase of the decorated space due to the increase in the dislocation density. This term can be included in the rate of change term at the right hand side of eq. (4.15b) which thus may be written in the form

$$d(\alpha_+\rho b^2)/d\,\varepsilon\big|_{in} = \chi_+ c_i^{(ml)} \tag{4.16}$$

Including alignment, blocking and annihilation reactions as described above, we may write the complete rate equation for the temporal evolution of the coverage, α_+, in the form (for more details see appendix A2)

$$\begin{aligned} d(\alpha_+\rho b^2)/d\varepsilon = &\left\{\chi_+ + \chi_-(s_{al}/n_+ - s_{bl}^{(ml)}/m_i^{(ml)})\alpha_+/b^2\right\}c_i^{(ml)} \\ &-\left\{s_{bl}^{(SFT)}/m_v^{(SFT)} + s_{an}/n_+\right\}\alpha_+ c_v^{(SFT)}/b^2 \end{aligned} \tag{4.17}$$

In eq. (4.17), n_+ and m are the average numbers of SIAs per aligned loop in the dragged cloud and per SIA loop in the matrix, respectively, $c_i^{(ml)}$ and $c_v^{(SFT)}$ are the concentrations of SIAs and vacancies clustered in the matrix loops and SFTs, respectively.

For the temporal evolution of the 2D number density of aligned loops, a rate equation analogous to eq. (4.15) may be derived (with coalescence of 2 aligned loops as an additional loss term, without alignment as a gain term). From the solutions of the rate equations for the coverage and the density, the average size of the aligned loops may be deduced (see Appendix A2). In our following discussion of the main features in the evolution of decoration and its effect on the mechanical response, where we consider the loop size as a parameter, consideration of the temporal evolution of the coverage as determined by eq. (4.17) is, however, sufficient.

To complete eq. (4.17), we have to consider the temporal increase of the dislocation density during deformation. In the early stage, i.e. in the absence of recovery, the dislocation density may be assumed to increase as

$$\dot\rho = \beta v_d \rho^{3/2} = \beta\dot\varepsilon\rho^{1/2}/b; \quad d\rho/d\varepsilon = \beta\rho^{1/2}/b\,, \tag{4.18a}$$

where $0.1 < \beta < 1$ is a numerical rate constant. Limiting this multiplication rate by a factor accounting for saturation of the dislocation density by recovery at some saturation level ρ_s, we may describe the evolution of the dislocation density parametrically as

$$d\rho/d\varepsilon = \beta\rho^{1/2}[1-(\rho/\rho_s)^{1/2}]/b\,. \tag{4.18b}$$

Equation (4.17), describing the evolution of dislocation decoration during deformation, is the central equation of this section. Without deriving solutions, we can draw an important conclusion from the terms appearing in eq. (4.17): the instantaneous rate of decoration evolution depends on the instantaneous values of the dislocation density ρ and the defect densities accumulated in the matrix $c_{i,v}^{(m)}$, and, via the evolution of ρ and $c_{i,v}^{(m)}$, on the levels of strain and dose reached (and other parameters involved), but it does not explicitly depend on strain and dose rates.

From the mathematical point of view, eq. (4.17) represents an inhomogeneous, linear 1st order differential equation for α_+ as a function of the main variable, strain or dose, and parameters

including the distance from the dislocation, y, contained in the distance dependence of the critical cross section for mutual loop blocking, $s^* \approx 4m^{1/2}by$. Its solution, subject to an appropriate initial condition, can be obtained by standard methods. Assuming transient build-up behaviour for defect accumulation in the matrix as well as for the dislocation evolution, more precisely, linear increase of $c_{i,v}^{(ml,SFT)}$ with dose and validity of eq. (4.18.a), respectively, this solution can be expressed in terms of incomplete gamma functions of the main variable and the parameters as detailed in Appendix 2.

For understanding the main trends, it is sufficient to discuss certain characteristic limiting cases which we do here for negligible recombination of loops with SFTs (last term in eq. (4.17)). The two main limiting cases are

(1) "weak decoration" (exactly valid at the "medium distance" where the terms for loop gain by alignment and loss by blocking in eq. (4.17) just cancel each other):

$$d(\alpha_+ \rho b^2)/d\varepsilon = \chi_+ c_i^{(ml)}; \tag{4.19a}$$

(2) quasi-steady state ($d\alpha_+/d\varepsilon \to 0$):

$$\alpha_+ = \chi_+ c_i^{(ml)} / \left\{ d(\rho b^2)/d\varepsilon + \chi_- (s_{bl}^{(ml)}/m_i^{(ml)} - s_{al}/n_+) c_i^{(ml)}/b^2 + (s_{bl}^{(SFT)}/m_v^{(SFT)}) c_v^{(SFT)}/b^2 \right\}. \tag{4.19b}$$

The choice of values for the fractions of "aligned loops" and "non-aligned loops", χ_+ and χ_-, ($\chi_+ + \chi_- = 1$) deserve a brief discussion here. As already discussed in section 3 for FCC crystals, 3 of the 6, i.e. half of the loop configurations glide parallel to the {111}-type glide plane of a dislocation, suggesting to use $\chi_+ = \chi_- = ½$. For an edge dislocation, the loop configuration with the same Burgers vector as the dislocation ("fully aligned loop") is energetically most favourable and is expected to align other loops upon direct contact. The other two configurations gliding parallel to the glide plane have opposite glide components in the dislocation line direction. Therefore, these loops immobilise and remove themselves efficiently, even at relatively low densities within the planes of attractive or repulsive interaction in which they are pulled or pushed by the moving dislocation, respectively. For edge dislocations, we therefore consider only fully aligned loops to contribute significantly to decoration and, accordingly, assume χ_+(edge) = 1/6, χ_-(edge) = 5/6.

A screw dislocation, on the other hand, does not interact with loops having the same Burgers vector. The other two configurations gliding parallel to the glide plane move well separated from each other, one pushed ahead, the other pulled behind the moving dislocation at one side, and the opposite at the other side of the dislocation, respectively. Accordingly we assume χ_+(screw) = 1/3, χ_-(screw) = 2/3 for screw dislocations. Averaging simply over the values for edge and screw dislocation, we assume in the following $\chi_+ = ¼$ and $\chi_- = ¾$.

Other important parameters are the cross sections for coalescence, alignment, blocking and annihilation reactions, s_{co}, s_{al}, s_{bl}, and s_{an}, for which quantitative values are also not known with certainty. For alignment of non-aligned matrix loops by aligned dragged loops, it is reasonable to assume that the glide cylinders of such loops will have at least to touch each other, meaning that $n_+ b^2 < s_{al} \approx 4n_+ b^2$ (coalescence + alignment, $s_{co} = s_{al}$). As described in section 3 and appendix A2, mutual blocking occurs when the interaction of an aligned loop with a non-aligned loop is stronger than with the dislocation which applies within an area $s^* \approx 4m^{1/2}by$ around each of the loops, where y (= r_{dl}) is the distance of the centre of the bound di-loop complex from the glide plane of the dislocation, and when, in addition, no direct contact with subsequent alignment takes

place. Accordingly the blocking cross section is defined by $s_{bl} = s^* - s_{al}$. A loop line has probably to cut a SFT to yield significant annihilation, which even then will be most likely not complete as computer simulations indicate. We therefore neglect s_{an} in our parametric study of the dynamic evolution of decoration.

Equation (4.19a) is most suited to illustrate the conditions for the maintenance of "moderate decoration" during deformation. The global sweeping rate represented by the right hand side of eq. (4.19a) must be sufficiently large to keep α_+ at the left hand side of eq. (4.19a) during dislocation evolution at a "significant but moderate" level, say between 5% and 30%. Setting α_+ in eq. (4.19a) constant, using there eq. (4.18a) for $d\rho/d\varepsilon$, and assuming $\chi_+ = 1/4$ and $\beta = 0.15$, we estimate that "significant but moderate decoration" should occur in the range of the damage to dislocation density ratio, $c_i^{(ml)}/b\rho^{1/2}$,

$$0.03 < c_i^{(ml)}/b\rho^{1/2} < 0.2 \qquad (4.20)$$

Assuming for the concentration of SIAs accumulating in the matrix during the transient $c_i^{(ml)} \approx$ 1% of the dose, and for the initial and final dislocation density $10^{12}/m^2$ and $2x10^{14}/m^2$, respectively, we find that the ratio $c_i^{(ml)}/b\rho^{1/2}$ in eq. (4.20) increases for a low pre-yield dose of 10^{-3} dpa upon irradiation to $2x10^{-2}$ dpa (and straining to 4%) from about 0.04 to 0.06, and decreases for a high pre-yield dose of 10^{-2} dpa from about 0.3 to 0.07, i.e. in the first case it moves up from close to the lower boundary to the middle of the range, whereas in the second it moves down from the upper boundary to the middle.

This is illustrated in fig. (4.2), where the range of "moderate decoration" in the $c_i^{(ml)}$-ρ parameter plane is shown together with the values of $c_i^{(ml)}$ and ρ expected for low and high pre-yield dose at the beginning and towards the end of deformation in the IRT experiments, respectively. Above the upper boundary, realised by even longer pre-irradiation, heavy decoration as in PITs is expected to occur, whereas below the lower boundary, realised for higher strain rates and/or lower SIA accumulation than in the IRTs considered here, decoration is expected to be insignificant. Also a substantial increase of the dislocation density by pre-irradiation work hardening would tend to reduce decoration according to eq. (4.20). Note again that decoration depends on strain and dose but not explicitly on strain and dose rate.

The relatively small variation of the damage to dislocation build-up ratio defined by eq. (4.20) provides also an explanation for the apparent memory of the deforming material concerning the impact of the pre-yield damage level on the degree of decoration and the related flow stress during the whole IRT period. Under the concurrent production of cascade damage and dislocations, the supply of SIAs from the increasing storage in the matrix to the growing dislocation population seems to be just sufficient to maintain "moderate decoration" during the whole test periods – even though the ratio $c_i^{(ml)}/b\rho^{1/2}$ varies somewhat, depending on the initial damage accumulated during pre-yield irradiation as illustrated in fig. (4.2).[5)]

A more detailed discussion of the evolution of the degree of decoration as a function of pre-yield-dose and post-yield dose or strain confirms this interesting maintenance of moderate decoration. In order to illustrate this feature, we employ the "weak decoration"/"medium distance" approximation given by eq. (4.19a) assuming for the SIA concentration in the matrix linear dose increase, $c_i^{(ml)} = \eta_i D$, and for ρ the validity of eq. (4.18a). In fig. 4.3, the degree of decoration α_+ resulting from these approximations is plotted vs. strain for low and high pre-yield doses pre-

[5)] The apparent memory may be illustrated by the following simple picture: two cars (cascade damage and dislocations) starting at different times from a certain starting point on a road will approximately keep their initial distance if they move approximately with the same velocity.

yield doses D_y. For the low pre-yield dose, α_+ does not depend significantly on dose/strain since the effects of the increasing loop supply and the increasing dislocation population almost balance each other; for the high pre-yield dose, on the other hand, α_+ is first high, or even increases initially, due to the high level of loop supply, which is subsequently, however, not sufficiently high to maintain the high level of α_+ for the increasing density of dislocations.

It is important to emphasise here that the strong initial variation of α_+ for high pre-yield dose is an artefact of our assumption that all dislocations start to move at the same time and continue to move with the same (the average) velocity (determined by the dislocation density and the strain rate) and with the same degree of decoration during deformation. Such an artefact may be removed by averaging α_+ over strain increments characteristic for the evolution of the dislocations (< 1%). Fortunately, however, the behaviour of α_+ briefly after yielding and thus the artefact do not significantly affect the later evolution of decoration. This is due to the fact that α_+ tends to approach quasi-steady state independent of its initial value, as demonstrated by the dashed lines in fig. 4.3 for which, in addition to "weak decoration" approximation given by eq. (4.19a), the quasi-steady state approximation given by eq. (4.19b) is used.

So far, unlimited transient behaviour for both defect accumulation in the matrix and dislocation multiplication was assumed. It has been mentioned above that, at a few % of strain, sweeping by dislocations moving under deformation must be considered to be associated with a significant reduction of defect accumulation in the matrix. Here, we add a brief parametric discussion of this effect. Assuming a source term corresponding to a transient linear defect accumulation in the matrix in the absence of deformation, $c_{i,v}^{(m)} = \eta_{i,v} D$, and a loss term according to eq. (4.14b), $-c_{i,v}^{(m)} / \varepsilon_{i,v}^{(sw)}$, describing the effect of sweeping on the evolution of defect concentrations during deformation, we introduce the following simple rate equation

$$dc_{i,v}^{(m)}/d\varepsilon = \eta_{i,v}/\varepsilon' - c_{i,v}^{(m)}/\varepsilon_{i,v}^{(sw)} \quad , \tag{4.21}$$

where $\varepsilon' \equiv d\varepsilon/dD$ (= 2). Assuming for the time being that the characteristic strains for the sweeping effect, $\varepsilon_{i,v}^{(sw)} = (b/d_{i,v}^{(sw)})/\phi_{i,v}$, is a rate constant (independent of strain) and taking the initial condition $c_{i,v}^{(m)}(\varepsilon = 0) = \eta_{i,v} D_y$, we may write the solution of eq. (4.21) in the form

$$c_{i,v}^{(m)}(\varepsilon) = \eta_{i,v}(\varepsilon_{i,v}^{(sw)}/\varepsilon')\left\{1 - (1 - D_0\varepsilon'/\varepsilon_{i,v}^{(sw)})\exp(-\varepsilon/\varepsilon_{i,v}^{(sw)})\right\} \tag{4.22}$$

As mentioned above, $\varepsilon_{i,v}^{(sw)}$ depends, via $d_{i.v}^{(sw)}$ and $\phi_{i,v}$, on the degree of decoration (and via this on strain).

For the sweeping and absorption of non-aligned loops, we may estimate the dependence of $d_i^{(sw)}$ on α_+ in the following way: On its way to the moving dislocation, a non-aligned loop may be blocked by an aligned loop. The probability for this blocking increases with increasing distance from the dislocation. The value of $d_i^{(sw)}$ may be considered the distance where the probability for finding within the cross section of strong interaction an aligned loop reaches the order of 1, meaning $s^* N_+ \approx 1$. Using $s^* \approx 4m^{1/2} b\, d_i^{(sw)}$ and $N_+ = \alpha_+/(nb^2)$ we find $d_i^{(sw)} = m^{1/2} b/(4\alpha_+)$ and $\varepsilon_i^{(sw)} = 4\alpha_+/(\phi_i m^{1/2})$. According to this, $\varepsilon_i^{(sw)}$ is of the order of α_+. We have used eq. (4.22) to illustrate the effect of dislocation sweeping on decoration assuming 10% and 20% for $\varepsilon_{i,v}^{(sw)}$ for the low and high pre-yield doses, respectively. According to fig. 4.3, dislocation sweeping results in a significant reduction of the degree of decoration in the strain range of a few %. On a relative scale, this reduction is stronger for low than for high pre-yield doses. It should,

however, be noticed here that, in this strain range, saturation of the dislocation density by recovery is also expected to occur. Dislocation saturation would result in a trend opposite to that induced by sweeping, i.e. it would increase the degree of decoration.

An important feature of decoration under deformation is its dependence on the distance $|y|$ from the dislocation which is determined by the distance dependence of the blocking cross sections, $s_{bl}^{(ml)}$, $s_{bl}^{(SFT)} \propto |y|$. Using the latter dependences in eq. (4.19b), we find that α_+ decreases for large $|y|$ asymptotically as $\alpha_+ \sim 1/|y|$. The transition occurs around the "medium distance", y_{tr}, where the terms for loop gain by alignment and loss by blocking in eq. (4.19b) counterbalance each other. Using there χ_- =3/4, $s_{bl}/s_{al} = y\sqrt{m}/b$ and $c_i^{(ml)} = c_v^{(SFT)}$, we may write y_{tr} as

$$y_{tr} \approx (3/2)/(3/4b\sqrt{m_i^{(ml)}} + 1/b\sqrt{m_v^{(SFT)}}) \approx (3/2)/(3/4d_{ml} + 1/d_{SFT}), \qquad (4.23)$$

where d_{ml} and d_{SFT} are average matrix loop and SFT diameters, respectively. Since the decrease of α_+ with $|y|$ is relatively moderate, $\alpha_+ \sim 1/|y|$, decoration may be expected to affect the flow stress significantly even for $y > y_{tr}$. The effective range of decoration at one side of a dislocation may therefore be estimated to be some multiple, say between 2 to 5, of y_{tr}, and the effective total width of decoration, d_{dc}, twice of this multiple of y_{tr}. Assuming in eq. (4.23) loop and SFT sizes of 5nm and 2.5nm, respectively, we estimate the values of d_{dc} to range from 10 to 25 nm which is consistent with TEM observations after the IRTs considered here. Independent of quantitative values, eq. (4.23) shows that the spatial scale of dislocation decoration under deformation is controlled by the average sizes of the matrix clusters.

5. The Role of Dislocation Decoration in Hardening

In crystalline materials, plastic deformation is due to the generation and motion of dislocations. Accordingly, the stress response to deformation depends on the resistance of such dislocations to motion, defined by their intrinsic mobility, their interaction with other dislocations (increasing during plastic deformation) and their interaction with other lattice defects such as impurities, precipitate particles and, during or after irradiation, irradiation induced self-defects such as SIA clusters and SFTs (increasing during irradiation). An increase in the density of the defects interacting with dislocations increases the stress required to start them moving and multiplying.

In general, several of these types of interactions must be considered to concurrently contribute to an increase in the yield and the flow stress (hardening) [5,7]. Each contribution to hardening is characterised by some typical length scale: "strain (or work) hardening" resulting from the mutual interaction of dislocations, for instance, by the spacing in Frank-Read sources; "particle (obstacle) hardening" by the distance between the obstacles in glide planes of the dislocation. Generally, each contribution increases with decreasing length scale, as for instance in strain and obstacle hardening.

In the case of plastic deformation under concurrent production of cascades and dislocations in pure Cu, treated in the present work, "strain hardening" and "radiation hardening" by SIA clusters and SFTs must be considered to contribute to total hardening. Self-defects such as SIA clusters and SFTs indeed represent obstacles against dislocation glide. They do not represent, however, indestructible and in the case of loops even not immobile obstacles as considered in the DBH model, but can move in the field of dislocations and can get incorporated and annihilated in the dislocation core. In fact, contributions of SIA clusters and SFTs to hardening may originate

from the interaction of these types of defects with dislocations at three fundamentally different spatial levels:

(1) Clusters incorporated into the core of a dislocation (with an edge component) form super-jogs there and reduce by this the intrinsic dislocation mobility.[6)]

(2) Clusters encountered by dislocations act as (temporary) obstacles against glide.

(3) Decoration of dislocations with clusters is associated with forces contributing to hardening.

We consider the latter effect which we call "decoration hardening" to be particularly relevant under the IRT conditions considered here and focus therefore our attention on this contribution. In this mechanism, again two fundamentally different types of contributions have to be distinguished:

(a) the contribution due to the limited intrinsic mobility of loops,

(b) the contribution due to the temporary or permanent immobilisation of members of a loop cloud by their mutual interaction and their interaction with matrix clusters.

The locking of dislocations by a completely blocked cloud of loops as considered in the cascade induced source hardening (CISH) model [9] is a limiting case of the latter mechanism. For members of a loop ensemble dragged by a moving dislocation, matrix clusters represent obstacles. The contribution of the interaction of a loop cloud with matrix clusters and the transfer of the corresponding forces to the dislocation may therefore be considered to be an indirect obstacle hardening enhanced by the accumulation of loops ("decoration enhanced indirect obstacle hardening").

We start here with discussing mechanism (3a), i.e. the possible role of the finite intrinsic loop mobility.

5.1 Possible role of the finite intrinsic loop mobility in decoration hardening

In order to keep our discussion of the role of the intrinsic mobility of loops decorating dislocations transparent, we ignore their mutual interaction and their interaction with matrix clusters and assume in addition that all members of the loop ensemble are aligned ($\alpha = \alpha_+$) and have the same mobility, and that, at and after yielding, all dislocations are equally and homogeneously decorated and move with the same velocity determined by the Orowan equation (4.10). In this case, the forces between the moving dislocations and the loops accompanying them are, according to eq. (4.11), independent of the loop-dislocation distance up to the boundary of the decorated region, d_{dc}, defined by eq. (4.12). During the motion of a dislocation, the force on its segments due to a resolved shear stress, $\tilde{\sigma}$, is balanced by the total force of all loops on these segments. Using for the maximum force at $y = d_{dc}$ the estimate given by eq. (3.5) and multiplying this with the aerial density of the loops and the area covered by loops we obtain

$$\tilde{\sigma}_{y,f} = \alpha\mu b / 2\pi d_{dc} \qquad (5.1)$$

In this mechanism, the width of the decorated region is the characteristic length scale. If decoration hardening were controlled by the intrinsic loop mobility, eq. (5.1) would apply to both yielding and post-yielding plastic flow. Values of $\tilde{\sigma}$ around 30 MPa corresponding to tensile yield and flow stresses of the order of 100 MPa as observed in PITs on copper (μ = 55Gpa)

[6)] Note that this contribution to hardening is enhanced due to the fact that loops are collected within a relatively broad range around the dislocations (sweeping range).

would be consistent with $\alpha \approx 0.2$ and $d_{dc}/b \approx 60$ (15 nm) which appears reasonable. The problem is, however, that, according to eq. (4.12), d_{dc} depends on ρ and M_F according to $d_{dc} \propto (M_F \rho)^{1/2}$ which must thus be considered to vary significantly during irradiation and deformation. An increase in ρ during deformation by two orders of magnitude, at constant M_F, for instance, would result in an increase of both d_{dc} according eq. (4.12) and a corresponding decrease of $\tilde{\sigma}$ according to eq. (5.1), by 1 order of magnitude. It would be an extraordinary coincidence if this wrong tendency (decrease of $\tilde{\sigma}$ with increasing strain) were just compensated in the required way by an opposite trend in M_F. We conclude that decoration hardening is most likely not controlled by the intrinsic loop mobility, at least not in most parts of the parameter range used in the IRTs considered here.

5.2 Contribution of cluster-cluster interactions to decoration hardening

The temporary or permanent immobilisation of members of a loop cloud by their mutual interaction and their interaction with matrix clusters is associated with forces on the dislocation dragging (pulling or pushing) them which contribute to hardening. This indirect hardening can dominate the direct obstacle hardening by matrix clusters because of the high degree of accumulation associated with decoration ("decoration enhanced indirect obstacle hardening").

The dynamic behaviour of a decorated dislocation is a complicated multi-particle problem. All members of the loop ensemble do not only interact with the dislocation but also with each other. The relative importance of an interaction between two members of the interacting ensemble compared to the other interactions depends on their mutual distance in relation to their distance to other loops and the dislocation as described in section 3. Thus, even though the interaction between 2 loops is generally smaller than their interaction with the dislocation, the former can become larger than the latter for loop-distances much smaller than the loop-dislocation distances. Below the critical distance where the change over from loop-dislocation to loop-loop dominance occurs, 2 loops with different Burgers vectors will block each other in their motion relative to the dislocation. This mutual blocking does not only limit the evolution of decoration during deformation but the interaction of blocked pairs or complexes of loops with dislocations can also contribute significantly to decoration hardening, as will be discussed in the following.

5.2.1 Contribution of blocked loops to the yield stress

We first consider the extreme limiting case of complete immobilisation of loop clouds by mutual loop blocking used previously to estimate source hardening in PITs [11]. In this case, the (upper) yield stress was interpreted as the stress necessary to unlock the dislocations from their loop clouds. Two idealised arrangements of immobile loops were considered: a row of loops, and a broad continuous distribution of loops of width d_{dc}, both separated from the leading dislocation by a "stand-off" distance, δ. In the latter case which is more suited as an introductory example for our subsequent discussion, the loop distribution was assumed to form a sessile edge dislocation dipole of effective Burgers vector b' and width d_{dc} (see fig. 5.1). The shear stress, $\tilde{\sigma}_y$, necessary to unlock an edge dislocations from such a dipoles is given by the maximum opposite shear stress exerted by the immobile dipole on the dislocation which yields for $d_{dc} >> \delta$ [11]

$$\tilde{\sigma}_y = \alpha\mu b / 8\pi(1-\nu)\delta, \qquad (5.2)$$

where we have introduced the effective coverage $\alpha = b'/b$. The formal similarity of eqs. (5.1) and (5.2) is striking but the difference in the length scales in the denominator, d_{dc} in eq. (5.1) and δ in eq. (5.2), is essential for the difference in the corresponding stress levels.

Using $\alpha = 1$, $\delta = 10b \approx 2.5$ nm in eq. (5.2),[7] a yield stress as high as $\tilde{\sigma} \approx 300$ MPa was estimated for Cu ($\mu \approx 55$GPa, $\nu \approx 1/3$) [11]. Half of this value, i.e. 150 MPa, would be obtained for a more reasonable value of $\alpha = 0.5$. We emphasise here that the tensile yield stress is about 3 times the shear yield stress, $\sigma_y \approx 3\tilde{\sigma}_y$, i.e. for $\tilde{\sigma}_y \approx 300$ (150) MPa, $\sigma_y \approx 900$ (450) which is 3 (1.5) times higher than the value of $\sigma_y \approx 300$ MPa measured in PITs after irradiation to about 0.1dpa (with values in parenthesis for $\alpha = 0.5$).[8] It was concluded that such seriously decorated dislocations are completely locked by their cluster clouds and new dislocations can be generated only locally at heterogeneities in the lattice where the stress is substantially intensified. This would initiate inhomogeneous deformation along channels associated with a sudden yield drop.

Apart of possible overestimates of the yield stress due to an overestimate of α (= 1) and/or an underestimate of δ ($\approx$ 2.5 nm) in our previous discussion of hardening in PITs, there are the following additional reasons for overestimating the yield stress by using eq. (5.2) without the required caution: The leading dislocation as well as the dislocation dipole are assumed in eq. (5.2) to be of pure edge type for which the interaction between both is maximum. On the one hand, screw components of more general than pure edge dislocations would reduce their interaction with a loop ensemble. On the other hand, a pure edge type dislocation dipole, which would represent an ensemble of aligned loops, would not be immobile as assumed in eq. (5.2) but would easily follow the leading dislocation. Hence, non-aligned loops are not only likely to occur within the loop ensemble but even necessary to immobilise it. Thus, in an adequate estimate of the yield stress, both the limited probability of blocking of aligned by non-aligned loops and the reduction in the total interaction between the loop ensemble and the leading dislocation have to be considered. In the following, all of these factors mentioned here will be taken into account.

In the case of moderate decoration with coverage, say $\alpha < 0.3$, as occurring in IRTs at relatively low pre-yield doses < 10^{-2} dpa, most of the loops in the cloud are well separated. Aligned loops not blocked by non-aligned ones can follow the dislocation; non-aligned loops are absorbed or left behind as long as they are not blocked by other loops on their way to or away from the dislocation, respectively. The fraction of loop pairs blocking each other (without direct contact) is small close to the dislocation. Assuming the contribution of this inner region to hardening to be not significant, we have to expect that the yield stress at low doses does no longer depend sensitively on the "stand-off distance", δ.

With increasing distance y from the dislocation, the blocking cross section introduced in section 4.2, $s_{bl} = s^*(y) - s_{al} \approx 4n^{1/2}by - s_{al}$, (where n is the average number of SIAs per loop) increases such that, above a certain critical distance, $y > \delta^*$, the blocked fraction will exceed a limit where virtually all members of the loop ensemble are interconnected and blocked by mutual interaction. Around the transition point, $y = \delta^*$, the probability for finding, within the blocking cross section of a certain loop, another loop of different configuration (i.e. the probability for mutual blocking) reaches the order of 1, meaning $s_{bl}N' \approx 1$, where N' is the 2D number density of loops with orientations differing from the one considered to be blocked ($N'/N = p = 5/6$ and 1/2 for edge and screw dislocations, respectively). Using $s_{bl} \approx s^{*\prime}n^{1/2}b\delta^* - s_{al}'nb^2$ and $nNb^2 \approx \alpha$ in the condition sblN' $\approx$ 1, where s*'$\approx$ 4 and sal' $\approx$ 1 to 4 are numerical factors of the relevant cross sections, we find for the critical distance δ*

$$(s^{*\prime}\delta^*/\sqrt{n}b - s_{al}')\,p\alpha \approx 1 \quad \rightarrow \quad \delta^*/b \approx \{\sqrt{n}/(s^{*\prime}p\alpha)\}(1 + s_{al}'\,p\alpha) \qquad (5.3)$$

[7] Misprint in ref. [11], p. 184, 2nd column, 1st sentence after eq. (25): incorrectly printed "25 nm" instead of correctly "2.5 nm".

[8] This is not mentioned in ref. [11].

According to eq. (5.3), the critical distance δ^* decreases, via an increase in α, with increasing dose. Assuming that the main contribution to an increase in the yield stress comes from the outer region, $y > \delta^*$, where the existing loops block themselves effectively, we obtain an estimate of the yield stress as a function of pre-yield dose by schematically dividing the region of decoration in an inner region adjacent to the dislocation, $y < \delta^*$, where mutual loop blocking is neglected, and an outer region, $y > \delta^*$, where virtually all loops are assumed to block each other (see fig. 5.2). Substituting, according to this scheme, δ in eq. (5.2) by δ^* as given by eq. (5.3) we obtain

$$\tilde{\sigma}_y = \tilde{k}_y^{(1)} \mu \alpha^2 (s^{*\prime}/\sqrt{n})/(1 + ps_{al}{}'\alpha) \tag{5.4a}$$

with $$\tilde{k}_y^{(1)} = pf/8\pi(1-\nu), \tag{5.4b}$$

where f is a factor accounting for the reduction of the average strength of the interaction between a general dislocation with a screw component compared to an edge dislocation and a loop ensemble containing non-aligned loops. For a random distribution of all loop configurations, averages of f and pf are estimated to $\langle f \rangle \approx 0.5$, $\langle pf \rangle \approx 0.35$ (see appendix A3), meaning $\tilde{k}_y^{(1)} \approx 0.02$ for $\nu = 1/3$.

In equation (5.4a), the characteristic length scale associated with the yield stress is the average size of the loops, $d_l \approx \sqrt{n}b$, which may be assumed to be of similar magnitude as the "stand-off" distance δ in eq. (5.2). On the other hand, the dependence of the yield stress on α as described by eq. (5.4) is no longer linear as in eq. (5.2) but (for small α) quadratic, except for the correction factor in the denominator of eq. (5.4). This **quadratic** dependence corresponds to our assumption that the yield stress is determined by the **pair-wise** mutual blocking of loops. Only in the (unphysical) limiting case of $\alpha \to \infty$, eq. (5.4) would formally become linearly dependent upon α and converge to eq. (5.2) if $f = 1$ (pure edge type dislocation and dislocation dipole) and $\delta \approx d_l \approx \sqrt{n}b$ is assumed.

For given dislocation type and given probability distribution of loop configurations in the loop ensemble (i.e. given pf), eq. (5.4) most likely represents a lower bound estimate of the yield stress since the contributions of the decreasing number density of blocked pairs in the inner region, $y < \delta^*$, is completely neglected even though the weight of each contribution increases with decreasing distance from the dislocation due to the increasing magnitude of the interaction.

An upper bound estimate of the yield stress is obtained by considering a finite probability for mutual loop blocking increasing continuously with increasing distance from the dislocation (without a step at some critical distance) and by assuming, in addition, that each loop pair contributes with the maximum possible force on the dislocation attainable at the corresponding distance between the dislocation and the loop pair. In fact, when a dislocation is displaced by the action of a stress field, loop pairs closer to the dislocation reach their maximum force earlier than loop pairs further away. As shown in appendix A3, such an upper bound estimate can be derived more rigorously than eq. (5.4), i.e. without using a schematic division of the decorated region as in deriving eq. (5.4).

The steps in deriving such an upper bound for the yield stress as detailed in appendix A3 may be summarised here in the following way: multiply the maximum force between **one** loop and the dislocation with the loop density at that position and with the probability to find at least 1 blocking other loop within the blocking cross section around the first loop and integrate the resulting **local** force density over the whole decorated area. At yielding, the resulting maximum

total force between the loop **ensemble** and the dislocation is balanced by the force on the dislocation due to the shear stress $\tilde{\sigma}$ acting on it.

This procedure yields an expression of similar form as that given by eq. (5.4), except that the value of the pre-factor $\tilde{k}_y^{(2)} \approx 0.13pf \approx 0.05$ is about 2.5 times higher than $\tilde{k}_y^{(1)}$ given by eq. (5.4b), and that the correction term $1/(1+ps_{al}'\alpha)$ in eq. (5.4) has now the form of an exponential integral which has, however, exactly the same asymptotic behaviour as the correction term. In our following discussion, we use the simpler form given by eq. (5.4a), and for the pre-factor of the tensile yield stress $k_y \approx 3\tilde{k}_y \approx 0.1$, corresponding to a value of $\tilde{k}_y$ between the lower and upper bound estimates, $\tilde{k}_y^{(1)}$ and $\tilde{k}_y^{(2)}$.

In fig. (5.3), the tensile yield stress according to eq. (5.4a) is plotted vs. dose for $\tilde{k}_y^{(1)} \rightarrow k_y = 0.1$, $s^{*\prime} \approx 4$, $s_{al}' \approx 3$, $p = 0.7$, $n = 100$ (corresponding to a loop size of $d_l \approx 2.5$ nm) and the values used in fig. (4.1) for characterising the evolution of the coverage α as a function of pre-yield dose. For comparison, the available experimental points for the three IRTs considered here and for one PIT are included. The uncertainty in the model curves increases with increasing pre-yield dose due to the increasing uncertainty in the evolution of α which is related the increasing uncertainty in the evolution of the matrix clusters. Nevertheless, the experimental trend is rather well reproduced by the model curves. Note that all experimental points are located in the range of the weak logarithmic increase of α where the increasing concentration of defects accumulating in the matrix form the dominant sink for cascade induced primary glissile loops as discussed in section 4.1 in conjunction with eq. (4.9).

Upon yielding, a significant fraction of the loops blocked in the outer region, $y > \delta^*$, will be left behind the moving dislocation, but a certain fraction of the aligned loops will follow the dislocation, particularly when, before yielding, the aligned loops in the cloud prevailed in density and size compared with the non-aligned ones as may be expected. This remaining fraction will affect the subsequent evolution of decoration during deformation.

5.2.2 Contribution of blocked loops to the flow stress

During deformation, aligned loops are able to glide with dislocations while non-aligned loops are either absorbed by or left behind the dislocations. In this case, decoration hardening is no longer expected to be due to the mutual interaction of members of the decorating loop ensembles as in yielding but will result from their interaction with matrix clusters encountered by them during their motion with their parent dislocation ("decoration enhanced indirect obstacle hardening"). Members of loop ensembles will be temporarily or permanently displaced by matrix clusters. By this "head wind" of clusters against the decorated dislocations, energy is dissipated which manifests itself in a resistance of the dislocations against the forces resulting from the applied shear stress.

According to this picture, the rate of energy transfer from the matrix clusters to the loops accompanying the dislocations has to be estimated in order to obtain an estimate of the flow stress. The energy transferred by **one** matrix cluster, a dislocation loop or a SFT, on **one** member of the loop ensemble, $\Delta E_{mc,l}$, generally depends on their mutual distance and their position in the decorated area. To calculate the **total** rate of energy transfer from the matrix cluster wind on the loop ensemble dE/dt, the pair wise energy transfer $\Delta E_{mc,l}$ multiplied with the apparent flux of matrix clusters, $J_{mc} = M_{mc}v_d$ (where M_{mc} is their matrix number density) and with the 2D number

density of loops in the decorated area, N_l, has to be integrated over the distance coordinates and the position coordinate in the 2D area of decoration.

The procedure simplifies substantially by making the reasonable assumption that the main contribution to the flow stress is due to permanent blocking of members of the loop ensemble by matrix clusters, occurring for cluster-loop distances within the blocking cross section, $s^*(y)$. In this case, the energy transferred from a matrix cluster to a certain loop decorating the dislocation is close to the extreme value of the energy change along the path of that loop in the stress field of the dislocation, $\Delta E_{mc,l} \approx \left| E_{dl}^{ext}(y) \right|$. We use this approximation in equating the rate of energy transfer from matrix clusters to the loops in a decorated area of width d_{dc} and length increment Δl with the rate of work done by the shear stress on the dislocation, $\tilde{\sigma} b v_d \Delta l$, obtaining by this for the shear flow stress

$$\tilde{\sigma}_f = M_{mc} \int_0^{d_{dc}} \left| E_{dl}^{ext}(y) \right| N_l s^*(y) dy / b \qquad (5.5)$$

Since $\left| E_{dl}^{ext}(y) \right| \propto 1/y$ and $s^*(y) \propto y$, the integrand in eq. (5.5) becomes constant and the integration correspondingly trivial. Quantitative extreme values of $\left| E_{dl}^{ext}(y) \right|$ in units of $n\mu b^3/2\pi$ are 1.70 b/y and 0.86 b/y for edge and screw dislocations, respectively (see table A1). Taking into account that also temporary displacement contribute to the flow stress, even though less than permanent ones, we estimate the average energy transferred per matrix cluster as $\left| E_{dl}^{ext}(y) \right| \approx 1.5 n\mu b^4 / 2\pi y$. Assuming further $s^*(y) \approx 4m^{1/2}by$, and expressing the 3D number densities of matrix clusters by the corresponding concentrations of SIAs and vacancies accumulated in the clusters, $M_{l,SFT} \approx v_d c_{i,v}^{(ml,SFT)} / (m_{l,SFT} b^3)$, and the 2D density of loops as $N_l \approx \alpha_+ / nb^2$, we may write eq. (5.5) as

$$\tilde{\sigma}_f \approx \mu \alpha_+ \left\{ c_i^{(ml)} / m_l^{1/2} + c_v^{(SFT)} / m_{SFT}^{1/2} \right\} (d_{dc}/b) . \qquad (5.6)$$

According to eq. (5.6), the flow stress is, analogous to the yield stress, a bi-linear functions of the degrees of defect accumulation in the decorated region and in the matrix, α_+ and $c_{i,v}^{(ml,SFT)}$. This is due to our assumption that $\tilde{\sigma}_f$ is controlled by the (two-body) interaction of members of the loop ensemble with matrix clusters. Differently from the yield stress (and other contributions to hardening), the flow stress given in the form of eq. (5.6) depends on 2 (instead of 1) meso-scopic length scales: it is directly proportional to the width of the decorated region, d_{dc}, and, similar as in eq. (5.4a) for the yield stress, inversely proportional to the size of the matrix clusters $m_{l,SFT}b$.

According to eq. (5.6) in conjunction with eq. (4.15), α_+ controls the dependence of $\tilde{\sigma}_f$ on the pre-yield dose and on the evolution of the dislocation density. Both α_+ and $\tilde{\sigma}_f$ depend on dose and strain as well as on the dislocation density, but not separately on dose rate and strain rate. These two rates and their ratio control, however, as to whether or not a moderate degree of decoration is maintained during IRTs which is able to control a continuous flow stress.

In figure (5.4), we have used eq. (5.6) in conjunction with eq. (4.19a) for α_+ to plot the tensile flow stress, $\sigma_f = 3\tilde{\sigma}_f$, as a function of plastic strain for three different values of the pre-yield dose, assuming a transient linear increase of $c_{i,v}^{(ml,SFT)}$ with dose. The parameters assumed for the evolution of the coverage α_+ are the same as used in fig. (4.3); for the other parameters contained

in eq. (5.6) we have assumed $d_{dc} = 80b \approx 20$ nm, $m_l = 150$, $m_{SFT} = 70$ (corresponding to average loop and SFT sizes of about 5 and 2.5 nm, respectively).

Also included in fig. (5.4) are curves illustrating the dislocation sweeping on the flow stress. For the characteristic strain of the sweeping effect, the same values as in fig. 4.4 are assumed. According to fig. (5.5), saturation of the SIA concentration in the matrix results in a significant reduction of the flow stresses increasing with increasing strain. It should, however, be noticed here that, at high strains, also saturation of the dislocation density by recovery is expected to occur. Dislocation saturation would result in a trend opposite to that induced by sweeping, i.e. it would increase the level of the flow stress.

According to fig. (5.4), the level of the flow stress is significantly lower for the low than for the high pre-yield dose, but the rate of hardening is larger in the former than in the latter case, i.e. the distance between the curves decreases with increasing strain. These trends shown by the curves, particularly the effect of the pre-yield dose on the flow stress are consistent with the trends found in the IRTs considered here. At large strain, however, the hardening rate appears to be too strong. The incl,usion of the effect of dislocation sweeping seems to bring the shapes of the flow stress curves closer to the experimental ones shown in fig. (2.2). As for the coverage, the apparent memory concerning the impact of the pre-yield damage level on the flow stress during the whole IRT period is due to the simultaneous and parallel evolution of dislocations and defects accumulating in the matrix during their build-up phases, with differences in the flow stress increasing with increasing pre-yield dose.

At low total doses (pre-yield + post-yield dose), the model curves shown in fig. (5.4) deviate systematically from the experimentally observed trends. In this dose range, the estimated contribution of decoration hardening to the flow stress is obviously too small to explain the experimentally observed steep increase in the flow stress. This indicates that another contribution is dominating in this range. We think that this contribution may be attributed to irradiation induced obstacle hardening, most likely due to SFTs.

In view of the simple nature of the approximations used in this work, the experimentally observed trends, particularly the pronounced effect of the pre-yield dose on the flow stress, may be considered to be roughly reproduced by our approach.

6. Summary and Discussion

In the present work, an analytical study of the plastic deformation of metals under concurrent production of cascades and dislocations as observed in recent in-reactor tensile tests (IRTs) on pure copper is presented. In these tests, two surprising features were observed: (i) the material deforms uniformly and rather homogeneously without yield drop as commonly observed in post-irradiation tensile tests (PITs), and (ii) an increase in the pre-yield dose results in an increase in the level of hardening over the whole test period.

These features were modelled in terms of the decoration of dislocations with small dislocation loops which are assumed to restrain the dislocations when starting and continuing to move upon yielding and deformation. During pre-yield irradiation, dislocation decoration results from the one-dimensional (1D) diffusion of cascade induced self-interstitial (SIA) clusters and their trapping in the stress field of the static grown-in dislocations. In this initial phase, loops accumulate at the side of the dislocation where the interaction is attractive. A loop once trapped near a dislocation can not reach the dislocation core and get absorbed there, unless it climbs or changes its glide direction. We have assumed that such processes are negligible in Cu in the temperature range considered here.

During concurrent post-yield irradiation and deformation, a moving dislocation sweeps by its stress field loops accumulated in the matrix. The assumption that loops are able to move in the strain field of dislocations contrasts with the assumption of immobile (and indestructible) radiation induced obstacles in conventional models of radiation hardening. Loops with Burgers vector parallel to the glide plane of a dislocation (i.e. “aligned loops”) were assumed here to follow the dislocation, pushed at the repulsive and pulled at the attractive side of the interaction, while non-aligned loops were assumed to approach the moving dislocation and get absorbed by this. Aligned loops temporarily or permanently immobilized by other loops or stacking fault tedrahedra (SFTs) exert restraining forces on dislocations which manifest themselves in contributions of dislocation decoration to yield and flow stresses. We expect that this new mechanism of decoration enhanced indirect obstacle hardening may even dominate common obstacle hardening by direct physical contact of dislocations with irradiation induced clusters as well as hardening by enhanced jog formation, provided the degree of accumulation of loops in the decorated region is sufficiently high.

According to this qualitative picture, a detailed knowledge of the interactions of dislocations with loops and between loops is required as a basis for a quantitative treatment of the kinetics and dynamics of dislocation decoration. In the present work, we have employed the isotropic linear elastic continuum approach to discuss these interactions occurring within the dislocation-loop system as functions of dislocation type (edge and screw), Burgers vectors of loops (aligned and non-aligned), relative to the dislocation-loop orientations and distances. The interactions of loops with screw dislocations have been found to be not significantly smaller than with edge dislocations.

Dislocation decoration during pre-yield irradiation is the result of very complicated inhomogeneous defect reaction kinetics in the distorted lattice near the dislocations which are embedded into a matrix where displacement damage accumulates. This complex problem can not be treated analytically without substantial simplifications. We have therefore substituted the complicated kinetics occurring in the real 3D region of decoration by an equivalent kinetics occurring in an imaginary 2D space and introduced the local “coverage” of this plane with SIAs

as a measure of the local degree of decoration. The quality of this approach should be checked by appropriate computer simulations, for instance of Monte Carlo type.

Defect accumulation within the space of decoration around the dislocations is due to cluster fluxes arriving from the matrix and is thus coupled to the defect accumulation there. This problem may be treated separately, for instance within the framework of the so called "production bias model". For the purpose of the present paper, aimed primarily at identifying mechanisms and conditions for dislocation decoration, we have introduced simple approximations allowing an analytical treatment of the main features of the defect evolution in the matrix relevant for decoration. Using these approximations (which may be expected to be good for low doses) we have found non-negligible dislocation decoration even at the lowest pre-yield dose applied in the IRTs considered which we consider to be sufficient for preventing segregating of dislocations in the form of walls during deformation and for rendering deformation uniform and homogeneous.

An adequate treatment of dislocation decoration under plastic deformation must include an adequate consideration of the dislocation evolution. In a fully consistent treatment of the concurrent evolution of dislocations and the associated evolution of their decoration with loops, coupled spectra of the degree of dislocation decoration and dislocation velocities, with "younger" dislocation segments being less decorated and faster than "older" ones, would have to be considered. We have substantially simplified this complicated problem by assuming that all dislocations move with a given average velocity determined by the dislocation density and the strain rate, and, consequently, that the local and instantaneous degree of decoration has the same average value for all dislocations depending on total dose and strain but not on their "age".

Within the framework of this "average dislocation approach" and the "2D decoration approach", already used in treating pre-yield decoration, we have formulated kinetic rate equations for the evolution of decoration under deformation which contain gain terms due to sweeping and loss term due to loop blocking as well as reaction terms for loop coalescence and alignment characterized by appropriate reaction cross sections. The form of these equations shows that the instantaneous rate of decoration evolution depends on the instantaneous densities of dislocations and defects accumulated in the matrix, and, via these quantities, on the levels of strain and dose reached (and other parameters involved), but it does not explicitly depend on strain and dose rates.

In our model, loop clouds accompanying dislocations during deformation form open dissipative sub-systems incorporating matrix loops and excreting (pairs of) clusters back into the matrix. Dislocations once decorated remain decorated during deformation, meaning that they do not get completely separated from their loop clouds. Thus bunches of loops would stay back only when dislocations unlock from part of their loop clouds during yielding but not when they move during plastic flow after yielding. On the other hand, we have shown that, even at a strain of only a few percent, the sweeping and absorption of matrix defects by moving dislocations results in a significant reduction in the degree of decoration. This effect was found to be stronger for low than for high pre-yield doses.

On the basis of approximate solutions for the evolution of decoration, the contributions of dislocation decoration to yield and flow stresses were estimated as a function of pre-yield dose and plastic strain (or total dose). Postulating that the restraining forces on the moving dislocation are due to the interaction of loops decorating dislocations with matrix loops and SFTs, we were able to reproduce the experimentally observed general trends: the increase of the yield stress with dose is faster than that of the flow stress; an increase in the pre-yield dose results in an increase in the level of hardening over the whole dose/strain ranges studied. The qualitative agreement in the

flow stress was found to improve when the reduction of defects accumulated in the matrix by dislocation sweeping was taken into account. Assuming physically reasonable values for the parameters involved we even obtained the right orders of magnitude of the yield and flow stresses found in the IRTs, except for low total dose.

These encouraging results indicate that, in the IRTs of Cu considered here, decoration enhanced indirect obstacle hardening is the dominant hardening mechanisms at high total doses. At low pre-yield and total dose, however, other hardening mechanisms such as conventional radiation hardening by direct contact of dislocations with radiation induced obstacles or hardening by enhanced jog formation must be considered to provide larger contributions to the total hardening than decoration enhanced hardening discussed in the present work.

The apparent memory concerning the impact of the pre-yield damage level on the flow stress during the whole IRT period was identified in our study as the result of the simultaneous and closely parallel transient evolution of dislocations and displacement damage in the matrix up to the end of the IRTs. We have found that the increasing supply of SIAs from the increasing storage in the matrix required to decorate the growing dislocation population is sufficiently large on the one hand and sufficiently limited on the other to maintain "significant but moderate" levels of the degree of decoration and of the associated flow stress during the whole test period.

The limitation of the features discussed in the present work to a relatively narrow band in the parameter plane defined by the accumulated defect density and the dislocation density implies that our conclusions must be expected to be rather sensitive to changes in the rates of dislocation generation or damage accumulation in the matrix when changing from pure Cu considered here to an alloy or to another metal of different crystal structure (e.g. BCC). A decrease or increase in the rate of defect accumulation relative to the rate of dislocation generation is expected to result in an insignificant decoration associated with an insignificant contribution to hardening.

Also the assumption concerning the properties of cascade induced SIA clusters, for instance their intrinsic resistance to direction changes, can not be expected to be justified for other materials. An increase in the probability for changes in the glide direction would reduce the degree of decoration on the one hand but increase the absorption of clusters from the matrix and the associated disturbance of the dislocation cores on the other. These considerations underline the necessity for performing IRTs on other materials and for extending our analytical modelling to different materials and different irradiation and deformation conditions.

7. Conclusions

In the past, experimental and theoretical studies of radiation hardening were restricted to the determination and interpretation of the yield stress observed in post-irradiation tensile tests (PITs). In recent in-reactor tensile tests (IRTs) both the yielding behaviour and the evolution of plastic flow were studied in detail under the conditions of constant damage rate and constant strain rate. In these tests, the material has been found to deform uniformly and rather homogeneously without yield drop as commonly observed in PITs. Another interesting observation is that an increase in the pre-yield dose results in an increase in the flow stress over the whole test period.

In the present work, this surprisingly different deformation behaviour of metals in IRTs was attributed to the decoration of dislocations with small dislocation loops developing during the concurrent production of cascades and dislocations as revealed by micrographs. During pre-yield irradiation, dislocation decoration was considered to result from the one-dimensional diffusion of cascade induced self-interstitial (SIA) clusters and their trapping in the stress field of the static

grown-in dislocations. During post-yield irradiation and deformation, moving dislocations were supposed to get decorated by sweeping with their stress fields loops accumulated in the matrix. Decoration was considered to restrain the dislocations from moving under an applied stress.

According to this qualitative model description, a quantitative analytical treatment of the deformation behaviour during the concurrent production of cascades and dislocations would consist of appropriately combined considerations of the three main problem complexes: (i) the interaction of dislocations with loops and loop ensembles, (ii) the kinetics of decoration under pre-yield irradiation as well as post yield irradiation and deformation, and (iii) the dynamics controlling the contribution of decoration to yield and flow stresses. Since the primary aim of the present work was, to identify the main mechanisms and to describe the general trends properly, the treatment was substantially simplified. It should be recognised, however, that a considerable amount of work is necessary to extend the present model to describe the problem of IRT deformation behaviour comprehensively and qualitatively.

Linear elasticity theory was employed to study the fundamental interactions occurring within the open defect systems of decorated dislocations as a function of the dislocation and loop characteristics and their relative orientations and distances. The interactions were found to be strong enough for significant decoration of both edge as well as screw dislocation segments.

The very complicated kinetics of decoration was simplified by substituting the real 3D region of decoration by a 2D space. In addition, for decoration under deformation where dislocations are continuously generated, the complicated coupled distributions of ages, degrees of decoration and velocities of dislocations was represented by a system of “average dislocations” moving with the same instantaneous average degree of decoration and average velocity determined by the dislocation density and the strain rate.

Within the framework of these approximations, kinetic rate equations for the evolution of decoration under pre-yield irradiation as well as post-yield irradiation and deformation were formulated. Approximate solutions of these rate equations were derived and used in discussing the general trends in the evolution of decoration. More rigorous solutions of the rate equations are expected to provide more details.

On the basis of the derived approximate solutions for the evolution of decoration, the contributions of dislocation decoration to yield and flow stresses were discussed in terms of the interactions of dislocations with “aligned” loops immobilized by the interaction with other loops and stacking fault tetrahedra. Most of the experimentally observed general trends, particularly of the dependence of the flow stress on both strain and total dose, can be rationalised by this new “decoration hardening” indicating that this is the dominant hardening mechanism in the IRTs of Cu considered here.

The apparent memory of the system for the pre-yield damage level was identified as the result of simultaneous and closely parallel transient evolutions of displacement damage and dislocations up to the end of the IRTs. It is found that the specific features discussed in the present work are limited to a relatively narrow band in the parameter space of accumulated defect density and dislocation density. Any significant change in the ratio of both, for instance by straining copper samples before irradiation or by changing to another material with different dislocation and cascade defect properties, must be considered to be associated with a qualitative change in the significance of decoration hardening.

Acknowledgements

The present work was partly funded by the European Fusion Technology Program. The authors are very grateful to Niels Jørgen Pedersen for his valuable help in for preparing the figures and the manuscript.

HT would like to thank Materials Research Department at Risø DTU for very kind hospitality during his visits to Risø.

References

[1] T.H. Blewitt, R.R. Coltman, R.E. Jamison, J.K. Redman, J. Nucl. Mater. 2 (1960) 277.
[2] M.J. Makin, Radiation Effects 37 (1966) 627.
[3] J. Diehl, in: "Vacancies and Interstitials in Metals", Proc. Int. Conf., KFA Jülich, 1968 (North-Holland, Amsterdam, 1969).
[4] B. N. Singh, D. J. Edwards, S. Tähtinen, P. Moilanen, P. Jacquet and J. Dekeyser, Risø Report No. Risø-R-1481 (EN), October (2004), 47 p.
[5] E. Orowan, Nature 149 (1942) 643.
[6] A. Seeger, Proc. 2nd UN Int. Conf. on Peaceful Uses of Atomic Energy, Geneva, Sept. 1958, Vol. 6, p. 250.
[7] A.H. Cottrell, Dislocations and Plastic Flow in Crystals (Clarendon Press, Oxford, 1953).
[8] G.E. Lucas, J. Nucl. Mater. 206 (1993) 287.
[9] B.N. Singh, A.J.E. Foreman, H. Trinkaus, J. Nucl. Mater. 249 (1997) 103.
[10] H. Trinkaus, B.N. Singh, A.J.E. Foreman, J. Nucl. Mater. 249 (1997) 91.
[11] H. Trinkaus, B.N. Singh, A.J.E. Foreman, J. Nucl. Mater. 251 (1997) 172.
[12] B.N. Singh, H. Trinkaus, S.I. Golubov, Encyclopaedia of Materials: Science and Technology, Eds. K.H.J. Buschow, R.W.Cahn, M.C. Flemings, B. Ilschner, E.J. Kyamer and S. Mahajan, Elsevier Science Ltd, (2001) 7957
[13] S.I. Golubov, B.N. Singh, H. Trinkaus, Phil. Mag. A 81 (2001) 2131.
[14] Y.N. Osetsky, A. Serra, B.N. Singh, S.I. Golubov, Phil. Mag. A 80 (2000) 2131.
[15] H. Trinkaus, H.L. Heinisch, A.V. Barashev, S.I. Golubov and B.N. Singh, Phys. Rev. B 66, (2002) 060105(R).
[16] F. Kroupa, in: Theory of Crystal Defects, ed. Gruber (Academic Press, New York, 1966)
[17] T. Mura, Micromechanics of Defects in Solids (Nijhoff, the Hague, 1982).
[18] J.P. Hirth and J. Lothe, Theory of Dislocations (McGrawhill, New York, 1968)
[19] H. Trinkaus, B.N. Singh, A.J.E. Foreman, J. Nucl. Mater. 206 (1993) 200.
[20] W. Jäger, W. Frank, K. Urban, Radiation Effects 46 (1980) 47.
[21] Y.N. Osetsky, D.J. Bacon, Z. Rong, B.N. Singh, Phil. Mag. Lett. 84 (2004) 745.

Appendix

A1. Energetics of Dislocation Decoration with Loops

A1.1 Interaction of dislocations with single loops

In this work, disturbances of the crystal lattice induced by dislocations and small dislocation loops are treated in terms of the isotropic linear elastic continuum approach. For loops, the small ("infinitesimal") loop approximation is used which is valid when the loop diameter is small compared to the other spatial scales involved. In this approximation, a SIA cluster of ideal loop shape is completely determined by its eigen-strain tensor **Q** which may be represented by its area vector **A** and its Burgers vector **b [**17**]**

$$\mathbf{Q} = (\mathbf{A}\,\mathbf{b} + \mathbf{b}\,\mathbf{A})/2 \rightarrow (A_i b_j + A_j b_i)/2\ , \text{ with } \mathbf{A}\cdot\mathbf{b} = A_i b_i \approx n\Omega \qquad \text{(A1.1)}$$

Einstein's summation convention for summing up over repeated indices (denoting components of vectors and tensors) is employed here and later, when appropriate. In eq. (A1.1), $n\Omega$ is the eigen-volume of the loop, n is the number of point defects (SIAs) contained in it and $\Omega \approx b^3$ is the volume of matrix atoms. For isotropic **Q** as for instance for SFTs, $Q_{ij} = Q_{kk}\,\delta_{ij}/3$ with $Q_{kk} = n\Omega$ where δ_{ij} is Kronecker's unit matrix.

The elastic interaction energy and the corresponding force between a loop and a dislocation, inducing at the distance vector of the loop, $\mathbf{r}_{dl}$, a stress field $\boldsymbol{\sigma}^{\mathbf{d}}(\mathbf{r}_{dl})$, are given, respectively, by

$$E_{dl}(\mathbf{r}_{dl}) = -\,\mathbf{Q}\,\boldsymbol{\sigma}^{\mathbf{d}}(\mathbf{r}_{dl}) = -\,A_i b_j\,\sigma^{d}_{ij}(\mathbf{r}_{dl})\ , \qquad \text{(A1.2a)}$$

$$\mathbf{F}_{dl}(\boldsymbol{r}_{dl}) = -\nabla E_{dl}(\boldsymbol{r}_{dl}) = \nabla A_i b_j\,\sigma^{d}_{ij}(\mathbf{r}_{dl}). \qquad \text{(A1.2b)}$$

Because of the inversion symmetry of the stress field, $\boldsymbol{\sigma}^{\mathbf{d}}(-\mathbf{r}_{dl}) = -\boldsymbol{\sigma}^{\mathbf{d}}(\mathbf{r}_{dl})$, the interaction energy of a loop close to a straight dislocation segment is characterised by attractive and repulsive directions and, consequently, its directional average vanishes:

$$E_{dl}(-\mathbf{r}_{dl}) = -E_{ll}(+\mathbf{r}_{dl}), \quad \left\langle E_{dl}(\mathbf{r}_{dl})\right\rangle = 0 \qquad \text{(A1.3)}$$

Quantitative details depend on the crystallography of dislocations and loops. In the following, a FCC crystal structure is assumed with dislocations characterised by Burgers vectors of <110>/2-type and glide planes of {111}-type, and loops characterised by <110>/2-type Burgers vectors and {110}-type habit planes (differently from the {111}-type habit planes assumed in [11]), i.e. totally 6 equivalent loop configurations.

For the derivation of explicit expressions for interaction energies and forces, the coordinate system is chosen such that the expressions for the stress fields of straight dislocations given in text books [17, 18] can be directly used: x, y and z coordinates in the glide direction, perpendicular to the glide plane (normal vector **G**) and along the dislocation line (unit vector **L**), respectively (suffices 1,2 and 3 for vector and tensor components). With this, eq. (A1.2) becomes

$$E_{dl}(\mathbf{r}_{dl}) = -[(\mathbf{A}\cdot\mathbf{V}^i)(\mathbf{b}\cdot\mathbf{V}^j) + (\mathbf{b}\cdot\mathbf{V}^i)(\mathbf{A}\cdot\mathbf{V}^j)]\sigma^d_{ij}(\mathbf{r}_{dl})/2\ . \qquad \text{(A1.4)}$$

Here, $\mathbf{V}^{1,2,3}$ are the 3 unit vectors in the directions of the coordinates of the dislocation representing the matrix for the transformation of the loop vectors into the coordinate system of the dislocation.

Ignoring the vector and tensor characters of the quantities in eqs. (A1.2a) and by setting $\mathbf{Q} \rightarrow n\Omega$, $\boldsymbol{\sigma}^{\mathbf{d}}(\boldsymbol{r}_{dl}) \rightarrow \mu b/2\pi r_{dl}$ simple estimates of the magnitude of the interaction energy and the corresponding force (without directional dependence) are obtained

$$|E_{dl}(r_{dl})| \sim n\mu\Omega b/2\pi r_{dl} \text{ and } |F_{dl}(r_{dl})| \sim n\mu\Omega b/2\pi r_{dl}^2, \qquad \text{(A1.5)}$$

where μ is the shear modulus of the metal. According eq. (A1.5), the natural energy, force and length units are $n\mu\Omega/2\pi$, $n\mu\Omega/2\pi b$, and r_{dl}/b, respectively, which are therefore used in the results presented below.

The dependence of the interaction energy on the direction of the spatial separation vector, $\boldsymbol{r}_{dl}$, i.e. the angular dependence, is much more complicated than the distance dependence and varies considerably with the configuration of the loop relative to that of the dislocation. Only for pure screw dislocation segments, a relatively simple expression is obtained:

$$E_{dl}(r_{dl}) = (n\mu\Omega b/\pi)(\mathbf{g}\cdot\mathbf{L})[\mathbf{g}\cdot(\mathbf{L}\times\mathbf{r}_{dl})]/(\mathbf{L}\times\mathbf{r}_{dl})^2, \qquad \text{(A1.6)}$$

where $\mathbf{g} = \mathbf{b}/b$ is the unit vector in the glide direction of the loop.

For calculating interaction energy profiles in certain planes perpendicular to a straight dislocation line (lines of equal interaction energy, "equipotential lines"), defined by assuming a certain constant values for $E_{dl}(\mathbf{r}_{dl})$ we have used polar coordinates for $\sigma^d_{ij}(\mathbf{r}_{dl})$. For calculating the interaction energy felt by a loop passing a dislocation on a straight line in direction $\mathbf{g}$, it is better to use Cartesian coordinates and to introduce the loop path in vector form as

$$\mathbf{r}_{dl} = \mathbf{r}_0 + s\mathbf{g}\ , \text{ with } \mathbf{r}_0 = r_0\,\mathbf{n}\ , \qquad \text{(A1.7)}$$

where $\mathbf{r}_0$ is the minimum distance vector between the dislocation and the loop with a unit vector in its direction $\mathbf{n} = \mathbf{r}_0/r_0 = (\mathbf{g}\times\mathbf{L})/|\mathbf{g}\times\mathbf{L}|$, and s is the coordinate of the loop on its path measured from the point of closest approach.

In figure (A1.1), lines of equal energy (equipotential lines) in appropriate planes are plotted for all combinations of dislocation-loop configurations introduced. For the same configurations, interaction energies and the corresponding forces acting on a loop passing a dislocation are plotted as a function of the loop coordinate s in figure (A1.2). The extreme values of these energies and forces are obtained by setting $\partial E_{dl}/\partial s = 0$ and $\partial F_{dl}/\partial s = -\partial^2 E_{dl}/\partial s^2 = 0$. In table (A1), extrema data (positions and values) are listed (in the figures and the table, a value of 1/3 is assumed for Poisson's ratio ν).

According to table (A1), the interaction is strongest for $\mathbf{b} \parallel \mathbf{B}$(edge). It vanishes for $\mathbf{b} \parallel$ and $\perp \mathbf{B}$(screw) for which the scalar and cross vector products in eq. (A1.6) vanish. The strength generally decreases with increasing angle between the loop direction and the glide plane. The values confirm the usefulness of the crude estimate given by eq. (A1.5).

Dislocation	Edge $[110]/[1\bar{1}1]/[1\bar{1}\bar{2}]$				Screw $[110]/[1\bar{1}1]/[110]$			
Loop	E(extreme)		F(extreme)		E(extreme)		F(extreme)	
	site	strength	site	strength	site	strength	site	strength
$[110]$	0.58	1.70	1.22	0.83		0		0
$[011]/[10\bar{1}]$	0	1.12	1.73	0.29	0	0.87	0.67	0.49
$[1\bar{1}0]$	2.55	0.37	0	0.54		0		0
$[101]/[01\bar{1}]$	1.14	0.83	0.98	0.65	0	0.87	0.67	0.49

Table A1: Data for the extreme values for the interaction of a dislocation with a loop passing the dislocation at unit minimum distance: loop coordinate *s* in units of b, energies and forces in units of $n\mu\Omega/2\pi$, $n\mu\Omega/2\pi b$, respectively (Poisson's ratio $\nu = 1/3$). The dislocations are characterised by their Burgers vector, glide plane normal and line vector directions, the loops by their Burgers vector directions.

A1.2 Interaction between two loops

The interaction energy of two loops as a function of their relative positions and orientations may be also estimated within the framework of isotropic elastic continuum approach using the small loop approximation, which becomes reasonable for loop-loop distances larger than the loop diameters, $r_{ll} > (>) d_l$. With these approximations, the interaction energy of two loops, (1) and (2), $E_{ll}^{(12)}$, may be represented by [17]

$$E_{ll}^{(12)} = P_{ij}^{(1)} G_{ik,jl} P_{kl}^{(2)} \tag{A1.8}$$

Here the tensors $\mathbf{P}^{(1,2)}$ are elastic dipole-force tensors related to the eigen-strain tensors $\mathbf{Q}^{(1,2)}$ of the loops according to

$$P_{ij}^{(1,2)} = C_{ijkl} Q_{kl}^{(1,2)}, \tag{A1.9}$$

where C_{ijkl} are the components of the 4th order elastic tensor, and G_{ik} is the elastic Green's function which reads for elastically isotropic materials

$$G_{ik} = \frac{1}{8\pi C_{11} C_{44}} \left\{ (C_{11} + C_{44}) \delta_{ik} / r_{ll} + (C_{11} - C_{44}) x_i x_k / r_{ll}^3 \right\}, \tag{A1.10}$$

where C_{11} and C_{44} are 2 independent elastic constants of an elastically isotropic material in the Voigt notation. In $G_{ik,jl}$, the subscript combination (,jl) means 2nd order partial differentiation of G_{ik} with respect to the coordinates (jl). Because of the inversion symmetry of $G_{ik,jl}$, $E_{ll}^{(12)}$ is symmetric and its directional average vanishes:

$$E_{ll}^{(12)}(-\mathbf{r}_{ll}) = -E_{ll}^{(12)}(+\mathbf{r}_{ll}), \quad \left\langle E_{ll}^{(12)}(\mathbf{r}_{ll}) \right\rangle = 0 \tag{A1.11}$$

Simple estimates of the magnitude of the interaction energy and the corresponding force between two loops, respectively, are obtained by ignoring the vector and tensor character of the quantities in eqs. (A1.8 - A1.10). Assuming that loops (1) and (2) contain *n* and *m* SIAs, meaning $Q^{(1,2)} \approx (n,m)\Omega$, and representing C_{11} and C_{44} simply by μ, we write

$$|E_{ll}(r_{ll})| \sim mn\mu\Omega^2/4\pi r_{ll}^3 \text{ and } |F_{ll}(r_{dl})| \sim 3mn\mu\Omega^2/4\pi r_{ll}^4. \tag{A1.12}$$

These estimates are used in section 3.3.

The detailed evaluation of eq. (A1.8) for given loop orientations is rather involved. Fortunately, with the 6 equivalent loop glide directions **g** along <110> considered here, only 3 independent combinations need to be analysed: glide directions parallel, perpendicular and 60° to each other. Using for **P** eq. (A1.9), for **Q** eq. (A1.1) and for G_{ik} eq. (A1.10), eq. (A1.8) may be explicitly evaluated in the form

$$\begin{aligned} 4\pi r_{ll}^3(1-\nu)E_{ll}^{(1,2)}(\mathbf{r}_{ll})/(mn\mu\Omega^2) = &-2\nu\left\{2-3(\mathbf{g}_1\mathbf{e})^2-3(\mathbf{g}_2\mathbf{e})^2\right\} \\ &-2(1-2\nu)\left\{(\mathbf{g}_1\mathbf{g}_2)^2-3(\mathbf{g}_1\mathbf{g}_2)(\mathbf{g}_1\mathbf{e})(\mathbf{g}_2\mathbf{e})\right\} \\ &+\left\{1-3[(\mathbf{g}_1\mathbf{e})^2+(\mathbf{g}_2\mathbf{e})^2+2(\mathbf{g}_1\mathbf{g}_2)(\mathbf{g}_1\mathbf{e})(\mathbf{g}_2\mathbf{e})]+15(\mathbf{g}_1\mathbf{e})^2(\mathbf{g}_2\mathbf{e})^2\right\} \end{aligned} \quad , \qquad \text{(A1.13)}$$

where **e** is a unit vector in the direction of the separation vector $\mathbf{r}_{ll}$, i.e. $\mathbf{e} = \mathbf{r}_{ll}/r_{ll}$. Equation (A1.13) confirms that $E_{ll}^{(12)}$ is symmetric with respect to the 2 loops and that its directional average vanishes; it is written such that the 3 terms at its right hand side represent mono-, di- and quadrupole terms whose directional averages vanish separately.

For a further evaluation of eq. (A1.13), it is useful to count the coordinates of the loops along their glide path, s_1 and s_2, from the point of closest approach where there separation vector is assumed to be $\mathbf{r}_0$ with a unit vector $\mathbf{n} = (\mathbf{g}_1\times\mathbf{g}_2)/|\mathbf{g}_1\times\mathbf{g}_2|$ With this reference point, the position vectors of the two loops, $\mathbf{r}_1$ and $\mathbf{r}_2$, and their distance, r_{ll}, may be written as

$$\mathbf{r}_1 = \mathbf{r}_0/2 + \mathbf{g}_1 s_1 \,,\ \mathbf{r}_2 = -\mathbf{r}_0/2 + \mathbf{g}_2 s_2 \,,\ \ r_{ll} = \sqrt{r_0^2 + s_1^2 + s_2^2 - 2(\mathbf{g}_1\mathbf{g}_2)s_1 s_2} \qquad \text{(A1.14)}$$

The interaction according to eq. (A1.13) has an extreme value (maximum attractive for $\nu > 1/4$) at the point of closest approach, $\mathbf{r}_{ll} = \mathbf{r}_0$, $s_1 = s_2 = 0$, where $\mathbf{g}_1\mathbf{e} = \mathbf{g}_2\mathbf{e} = 0$ such that eq. (A1.13) yields

$$4\pi r_0^3 E_{ll}^{(1,2)}(\mathbf{r}_0)/(mn\mu\Omega^2) = 1 - 4\nu - 2(1-2\nu)(\mathbf{g}_1\mathbf{g}_2)^2 \,. \qquad \text{(A1.15)}$$

According to eq. (A1.15), the strength of the maximum attractive interaction as a function of the relative loop orientation is -1, -2ν, $-4\nu+1$ for 0°, 60°, 90° configurations, respectively (-1, 0, $+1$, for $\nu = 0$; -1, $-2/3$, $-1/3$, for $\nu = 1/3$ (Cu); -1, -1, -1 for $\nu = ½$). These numbers show that the estimates given by eq. (A1.12) are indeed representative.

In figure (A1.3), equipotential lines calculated on the basis of eq. (A1.13) in conjunction with eq. (A1.14) are plotted for the three different (non-equivalent) combinations of loop configurations as a function of the loop coordinates s_1 and s_2. According to fig. (A1.3a), two equivalent loops with the same Burgers vector have to overcome an energy barrier to reach one of their two energy minima. According to fig. (A1.4b,c), on the other hand, two loops of different configuration reach their minimum at closest approach down hill (through 1 of the 4 valleys) from any point in the 2D loop-loop space.

The interaction of a loop, say of loop (1), with an isotropic defect such as a SFT (dilatation centre) is obtained from eq. (A1.13) by averaging over the directions of the other loop (2). Using $\langle g_i g_j \rangle = \delta_{ij}/3$ we get

$$4\pi r_{ll}^3(1-\nu)E_{ll}^{(1,2)}(\mathbf{r}_{ll})/(mn\mu\Omega^2) = -2(1+\nu)\left\{1/3-(\mathbf{g}_1\mathbf{e})^2\right\} \qquad \text{(A1.16)}$$

It should be noticed here that SFTs are characterised by a negative relaxation volume (- $m\Omega$ for well developed SFTs).

A1.3 Interaction between a dislocation and two loops

In a loop cloud decorating a dislocation, loops interact with each other as well as with the dislocation. The strength of the loop-loop interaction relative to the loop-dislocation interaction is crucial for the evolution of dislocation decoration and the associated yield and flow stresses.

The importance of the loop-loop interaction relative to the loop-dislocation interaction increases with decreasing loop-loop distance compared to the loop-dislocation distance. The correct scaling behaviour and a quantitative estimate for the transition from loop-dislocation to loop-loop dominance in the interaction of a loop containing n SIAs with a dislocation and with a loop containing m SIAs is obtained by equating the estimates for the (maximum) loop-dislocation and loop-loop forces as given by eqs. (A1.6) and (A1.12), yielding for loop-loop distance of this transition, r_{ll}^* ,

$$r_{ll}^{*2} \approx 1.23\sqrt{m}br_{dl} \,. \tag{A1.17}$$

According to eq. (A1.17), the transition from loop-dislocation to loop-loop dominance occurs when the loop-loop distance is approximately equal to the geometrical average of the two other length scales: loop diameter $\sim\sqrt{m}b$ and dislocation-loop distance r_{dl}.

In a rigorous treatment, the energy of each loop in the presence of the other loop and the dislocation must be analysed in detail. The appropriate loop coordinates for such an analysis are the minimum distances of the loops from the dislocation, $r_{\mathrm{d1,2}}$, and between the loops, r_{12}, and the distances, $s_{\mathrm{d1,2}}$ and $s_{1,2}$, from these points of closest approach, as sketched in fig. A1.4. With these coordinates, the energy of the two loops may be written as

$$E_{1,2} = E_{\mathrm{d1,2}}(r_{\mathrm{d1,2}}, s_{\mathrm{d1,2}}) + E_{1,2}(r_{12}, s_1, s_2) \,. \tag{A1.18}$$

An analytical analysis is possible (and useful) only when the distance between the loops is small compared to their distance to the dislocation, $r_{12} << r_{\mathrm{d1,2}}$ such that the field of the dislocation may be expanded about the central point of the loop pair, (x,y). In this case, the 1st partial derivatives of the dislocation-loop interaction energy with respect to $s_{1,2}$ (and analogously the 2nd derivatives) may be written as

$$\partial E_{d1,2}/\partial s_1 = (\partial E_{d1,2}/\partial x)(\partial x/\partial s_1) + (\partial E_{d1,2}/\partial y)(\partial y/\partial s_1); \quad \partial E_{d1,2}/\partial s_2 = \quad ... \tag{A1.19}$$

where the derivatives with respect to (x,y) are to be taken at (x,y). Hence, in this approximation, there are totally five coordinates including s_1, s_2 representing the degrees of freedom of the mobile loops, and x, y, r_{12} representing geometrical parameters. For the most important case of an aligned loop gliding in x-direction (loop 1), where $\partial x/\partial s_1 = 1$ and $\partial y/\partial s_1 = 0$ = 0, eq. (A1.19) simplifies to $\partial E_{d1}/\partial s_1 = (\partial E_{d1,2}/\partial x)$ and $\partial^2 E_{d1}/\partial s_1^2 = (\partial^2 E_{d1,2}/\partial x^2)$.

Two neighbouring loops form a stable pair far away from the dislocation as well as in the stress field of a dislocation, depending on their distance and position with respect to the dislocation. Generally, the force balance conditions $\partial E_{1,2}/\partial s_{1,2} = 0$ in conjunction with the stability conditions $\partial^2 E_{1,2}/\partial s_{1,2}^2 > 0$

$$\partial E_{1,2}/\partial s_{1,2} = 0, \;\; \partial^2 E_{1,2}/\partial s_{1,2}^2 > 0 \tag{A1.20}$$

define the stable region in the x, y, r_{12} parameter space. At given r_{12} and y, for instance, an aligned loop gliding in x-direction (loop 1) and a non-aligned loop gliding in y-direction (loop 2) forming a bound (stable) pair around x = 0 (see fig. A1.4) will remain bound for all x when even the strongest force exerted by the dislocation on loop 1 cannot overcome the force keeping the

loops together. In this case, the boundary between instability in some range of x and stability at all x is defined by the balance of the maximum forces (in x-direction) between the dislocation and loop 1 and between loop 1 and 2, i.e. by

$$\partial E_{d1}/\partial x + \partial E_{12}/\partial s_1 = 0, \quad \partial^2 E_{d1,2}/\partial x^2 = 0, \quad \partial E_{12}/\partial s_1 = 0. \tag{A1.21}$$

A fully analytical evaluation of eq. (A1.21) is possible but rather involved. The treatment is even more involved for other loop-loop combinations than the ones shown in fig. A1.4. The degree of freedom is reduced to s_1 and the procedure becomes much simpler for the important case of the interaction of an aligned loop containing n SIAs with an immobile isotropic cluster containing m SIAs (or a SFT containing m vacancies) as described by eq. (A1.16), for instance in the stress field of an edge dislocation. In this case, the maximum loop-dislocation force (according to table A1) and the maximum loop-cluster force following from eq. (A1.16), respectively, are

$$F_{dl}^{\max} = \frac{0.55}{1-\nu}\frac{n\mu\Omega b}{2\pi y^2}, \; F_{cl}^{\max} = -1.93\frac{1+\nu}{1-\nu}\frac{mn\mu\Omega^2}{6\pi r_{cl}^4} \tag{A1.22}$$

$F_{dl}^{\max} + F_{cl}^{\max} = 0$ yields for $\nu = 1/3$

$$r_{cl}^{*2} \approx 1.25\sqrt{m}by \tag{A1.23}$$

in good agreement with the estimate given by eq. (A1.17). In the following section, this relation is used to define a cross section for the blocking of an aligned loop by a matrix cluster.

A2. Kinetics of Dislocation Decoration with Loops

In the present work, decoration of dislocations by loops is considered to occur in an imaginary 2D space of decoration. In this description, real or apparent fluxes of clusters from the matrix to the decorated area due to cluster diffusion or due to the motion of the dislocation represent cluster sources in the 2D space. The probability for the occurrence of reactions of clusters, already present there, with clusters arriving from the matrix is quantified by appropriate reaction cross sections.

A2.1 Reaction cross sections

The main reactions to be considered are (1) cluster coalescence of loops of equal configuration, (2) alignment of two loops of different configuration, particularly the alignment of a non-aligned in the close vicinity of a aligned loop, (3) immobilisation (blocking) of a loop of a certain configuration by a close interaction without direct contact with a loop of another configuration or with an immobile cluster such as a SFT, and (4) (partial) annihilation of a (SIA) loop with a SFTs. The cross sections for these coalescence, alignment, blocking, annihilation reactions are denoted by s_{co}, s_{al}, s_{bl}, and s_{an}, respectively.

Coalescence of two loops requires that their glide prisms at least touch each other. For two circular loops, (1) and (2), this means that the distance between their centres is smaller than the sum of their radii, $d_{ll} \le r_1 + r_2$. Accordingly, the cross section for coalescence may be described by

$$s_{co} = \pi (r_1 + r_2)^2. \tag{A2.1}$$

For the present purposes, it is useful to express the sizes by the number of SIAs per loop, i.e. $\pi r_{1,2}^2 = n_{1,2}A_0$ where $A_0 \approx b^2$ ($A_0 = \sqrt{3}b^2/4$ in FCC) is the atomic unit area per SIA in a loop, such that eq. (A2.1) may be written in the form

$$s_{co} = (\sqrt{n_1} + \sqrt{n_2})^2 A_0, \qquad \text{(A2.2)}$$

According to eq. (A2.2), $n_{1,2}A_0 < s_{co} < 4\, n_{1,2}A_0$.

A change of the Burgers vector of a loop to an energetically more favourable configuration in the stress field of a dislocation can only be expected to occur when primary loops come very close to the dislocation. Consequently, it is reasonable to assume that alignment of larger loops requires, as coalescence, direct contact of the loops involved, meaning that the corresponding cross sections have the same values as for coalescence, eqs. (A2.1) and (A2.2),

$$s_{al}(n_1,n_2) = s_{co}(n_1,n_2). \qquad \text{(A2.3)}$$

A necessary condition for the blocking of a loop by another loop of different configuration or by a SFT is that the distance is smaller than a critical value as defined by eq. (A1.23). The critical cross section corresponding to eq. (A1.23) is

$$s^* = \pi r_{cl}^{*2} \approx 4\sqrt{m}by \qquad \text{(A2.4)}$$

This cross section increases with increasing distance of the cluster pair from the dislocation. The blocking of an aligned loop by a non-aligned loop requires in addition that no direct contact occurs which would result in alignment is possible, meaning

$$s_{bl} = s^* - s_{al}\ . \qquad \text{(A2.5)}$$

Under deformation, a loop following a moving dislocation may encounter a SFT. Mutual (partial) annihilation requires that a segment of the loop cuts the SFT. Loops developing under deformation may be expected to be considerably larger than SFTs, $d_l >> d_{SFT}$ (about 10 nm compared to 2.5 nm). In this case the cross section for annihilation may be approximated by

$$s_{an} \approx \pi\, d_l\, d_{SFT}. \qquad \text{(A2.6)}$$

Since, for $d_{SFT} << d_l$, s_{an} is significantly smaller than the other relevant cross sections s_{co}, s_{al}, s_{bl}, and since, in addition, annihilation will be only partial, this reaction is neglected in estimating the degree of decoration and its effect on hardening.

A2.2 A simple coalescence model

The evolution of loop size distributions in the 2D space of decoration by fluxes of clusters from the matrix can be treated by the standard procedures developed for 3D. For the present purpose of estimating decoration and hardening, only the fraction of the 2D region occupied by loops (coverage), loop densities, and some average loop size are needed. To illustrate a procedure for deriving these 3 main quantities, we assume that only aligned loops containing m SIAs arrive with flux density J from the matrix in the 2D space of decoration where possible reactions with existing loops, containing n SIAs on the average, are restricted to coalescence. The probability for the occurrence of coalescence is quantified by the size dependent cross sections $s_{co}(n)$.

Coalescence does not affect the increase in the coverage α due to the flux of aligned loops, but reduces the increase in the 2D number density N compared to the increase without coalescence.

Consequently, the evolution of α, N and the average number of SIAs per loop in the 2D space, n, may be described by

$$\mathrm{d}\alpha/\mathrm{d}t = mA_0J\,, \tag{A2.7a}$$

$$\mathrm{d}N/\mathrm{d}t = [1 - s_{co}(m,n)N]\,J\,, \tag{A2.7b}$$

$$nA_0N = \alpha\,. \tag{A2.7c}$$

According to eq. (A2.7a), the time dependence of α is determined by that of mJ in this simple model

$$\alpha = A_0 \int mJ\mathrm{d}t\,. \tag{A2.8}$$

For constant m and J, α increases linearly with time.

Eliminating J from eq. (A2.7a,b), expressing $s_{co}(m, n)$ by eq. (A2.2) and introducing the number of loops per area of incoming loop as normalised 2D number density $N^* = mA_0N$ and the number of incoming to existing loops as normalised loop size, n/m, the following set of equations is obtained for these two quantities

$$dN^*/d\alpha = 1-(1+\sqrt{\alpha/N^*})N^* \tag{A2.9a}$$

$$n/m = \alpha/N^* \tag{A2.9b}$$

The solution of eq. (A2.9a) subject to the initial condition $N^*(\alpha= 0) = 0$ is obtained by numerical integration. The results for N^* and n/m, as functions of α are shown in fig. A2.1. For small α, both N^* and n/m increase linearly with α. When, at $\alpha \approx 0.4$, n/m exceeds about 2.5, a newly arriving loop begins to coalesce on the average with more than 1 existing loop, resulting in a decrease of N^* and an acceleration in the increase of n/m . At the limit $\alpha = 1$, N^* reaches very small and n/m very large values, indicating a state close to percolation. Note that, in a distribution of loop sizes, n would have the meaning of the first moment of the number of SIAs per loop.

A2.3 A kinetic model for the evolution of dislocation decoration under deformation

In the more general case of dislocation decoration under deformation, apparent drift fluxes of matrix clusters of different sizes, including loops of different Burgers vectors and SFTs, would have to be considered to contribute to the evolution of decoration. For the present purpose, it is sufficient to distinguish apparent fluxes of "representative" aligned and non-aligned matrix loops, $J_{l+,l-}$, and SFTs, J_{SFT}, containing averages numbers $m_i^{(l+,l-)}$ and $m_v^{(SFT)}$ of SIAs and vacancies, and the corresponding single defect fluxes, $j_i^{(l+,l-)}$, and j_v, respectively. The relations between these fluxes and the number densities of loops and SFTs, $N_l^{(m)}$ and $N_{SFT}^{(m)}$, and the concentrations of SIAs and vacancies contained in them, $c_i^{(ml)}$ and $c_v^{(SFT)}$, are, respectively,

$$\begin{aligned} &J_{l+,l-} = v_d \chi_{+,-} M_l\,,\; J_{SFT} = v_d M_{SFT}\,, \\ &j_i^{(l+,l-)} = m_{l+,l-} J_{l+,l-} = v_d \chi_{+,-} c_i^{(ml)}/\Omega, \quad j_v = m_{SFT} J_{SFT} = v_d c_v^{(SFT)}/\Omega \end{aligned} \tag{A2.10}$$

Here $\chi_{+,-}$ are the fractions of aligned and non-aligned loops and

$$v_d = \dot{\varepsilon} / b\rho \qquad \text{(A2.11)}$$

is the (average) dislocation velocity.

The following three types of reactions of aligned loop accompanying dislocations with matrix clusters have to be considered.

(a) Incorporation of aligned matrix loops and agglomeration with existing loops:

The effects of this reaction on the evolution of decoration have been discussed in the preceding subsection. It does not affect the increase in the coverage α_+ resulting from the flux of aligned matrix loops, $j_i^{(l+)}$, but it reduces the increase in the 2D number density N_+ compared to that without this reaction. Without other reactions, the temporal evolution of α_+ and N_+, would follow the rate equations

$$d\alpha_+/dt = \chi_+ j_i^{(ml)} A_0 \,,\; dN_+/dt = \chi_+ (1 - s_{co} N_+) J_{ml} \,, \qquad \text{(A2.12a)}$$

where s_{co} denotes the cross section for agglomeration (coalescence).

(b) Agglomeration with non-aligned matrix loops and reaction with SFTs associated with alignment and partial annihilation, respectively:

These reactions result in changes of α_+ (increase or decrease), respectively, but do not affect N_+. Their contributions to the temporal change of α_+ are determined by the fluxes of SIAs and vacancies to the fraction of the decorated area where they are operative, $s_{al,an}N_+ = s_{al,an}\alpha_+/n_+A_0$, and accordingly given by

$$\begin{aligned} (d\alpha_+/dt)|_{al,an} &= \chi_- s_{al} N_+ A_0 j_i^{(ml)} - s_{an} N_+ A_0 j_v^{(SFT)} \\ &= \chi_- (s_{al}/n_+)\alpha_+ j_i^{(ml)} - (s_{an}/n_+)\alpha_+ j_v^{(SFT)} \end{aligned} \qquad \text{(A2.12b)}$$

(c) blocking by non-aligned loops or SFTs:

Blocking reactions reduce N_+, and, by this, also $\alpha_+ = n_+ N_+ A_0$. Their contributions to the temporal change of α_+ and N_+ are

$$\begin{aligned} dN_+/dt|_{bl} &= -\chi_- s_{bl}^{(ml)} N_+ J_{ml} - s_{bl}^{(SFT)} N_+ J_{SFT} \\ d\alpha_+/dt|_{bl} &= -\chi_- s_{bl}^{(ml)} \alpha_+ j_i^{(ml)}/m_i^{(ml)} - s_{bl}^{(SFT)} \alpha_+ j_v^{(SFT)}/m_v^{(SFT)} \end{aligned} \qquad \text{(A2.12c)}$$

Note that the contributions of reactions (b) and (c) to $d\alpha_+/dt$ depend on the average sizes of the decorating loops, n_+, and the matrix clusters, $m_{l,SFT}$, respectively.

In describing decoration under deformation, the expansion of the space of decoration upon dislocation length increase associated with an effective thinning of α_+ and N_+ has to be taken into account. The term describing this may be derived in the following way. Consider, for instance, the total number of aligned loops involved in the decoration of dislocations of total length L over a width d_{dc} within a volume V, which is given by $N_+ L d_{dc} = N_+ \rho V d_{dc}$. Without loop reactions, the temporal change of this number, $(dN_+\rho/dt)Vd_{dc}$ must be equal to the total flux of aligned loops to this stripe, $J_{ml+}Ld_{dc} = \chi_+ J_{ml}\rho V d_{dc}$ yielding $(dN_+\rho/dt) = \chi_+ J_{ml}\rho$ or, after devision by ρ, $(dN_+/dt) + N_+(d\rho/dt)/\rho = \chi_+ J_{ml}$. An analogous relation is obtained for α_+. Accordingly, the relation between

the temporal evolutions of α_+ and N_+ with and without thinning is

$$d(\alpha_+, N_+)/dt\,|_{with} = d(\alpha_+, N_+)/dt\,|_{without} - (\dot{\rho}/\rho)\,(\alpha_+, N_+) \qquad \text{(A.2.13)}$$

The description of the thinning effect by the second term at the r.h.s. of eq. (A.2.13) appears reasonable and could have been guessed without derivation: the factor $\dot{\rho}/\rho$ in this term represents the relative volume increase of the decorated space due to the increase in the dislocation density.

The complete rate equations are obtained by adding the source terms and the reaction terms as given by eqs. (A2.12a,b,c) and (A.2.13). Using eqs. (A2.10) (with $\Omega \approx b^3$, $A_0 \approx b^2$) and (A2.11) to express the fluxes in eqs. (A2.12a,b,c) by the corresponding defect concentrations, and changing from time to strain by $d/dt = \dot{\varepsilon} d/d\varepsilon$, we may write the rate equations for α_+ and N_+ in the form

$$\begin{aligned} d(b^2\rho\alpha_+)/d\varepsilon = {} & \chi_+ c_i^{(ml)} + [\chi_-(s_{al}/(n_+b^2) - s_{bl}^{(ml)}/(m_l b^2)]c_i^{(ml)}\alpha_+ \\ & - [s_{an}/(n_+b^2) + s_{bl}^{(SFT)}/(m_{SFT}b^2)]c_v^{(SFT)}\alpha_+ \end{aligned} \qquad \text{(A2.14a)}$$

$$\begin{aligned} d(b^2\rho N_+)/d\varepsilon = {} & \chi_+ c_i^{(ml)}/(m_l b^2) \\ & - [(s_{co} + s_{bl}^{(ml)})/(m_l b^2)]c_i^{(ml)} N_+ - [s_{bl}^{(SFT)}/(m_{SFT}b^2)]c_v^{(SFT)} N_+ \end{aligned} \qquad \text{(A2.14b)}$$

where ρ, $c_{i,v}^{ml,SFT}$ and $m_{\mathrm{l,SFT}}$ are functions of the variable ε or dose D ($D = D_0 + (\varepsilon/\varepsilon')D$ with $\varepsilon' = d\varepsilon/dD$, respectively.

Equations (A2.14a,b) are subject to appropriate initial conditions for $\varepsilon = 0$. The average number of SIAs per loop in the decorated area follows from the solutions of eqs. (A2.14a,b) as

$$n_+ = \alpha_+/(N_+ b^2) \qquad \text{(A2.14c)}$$

A2.4 Solutions of the rate equations

The rate equations (A2.14a,b) represent inhomogeneous, linear ordinary 1st order differential equations for α_+ and N_+ as functions of the main independent variable strain ε or dose $D = D_0 + \varepsilon/\varepsilon'$ with $\varepsilon' = d\varepsilon/dD$, and parameters including the distance from the dislocation contained in $s^* \approx 4m^{1/2}by$ as the spatial variable.

In discussing solutions of eqs. (A2.14a,b), it is sufficient to consider α_+ described by eq. (A2.14a) since the solution for eq. (A2.14ab) is analogous. The form of the left hand side of eq. (A2.14a) suggests to introduce the new variable $w = b^2\rho(\alpha_+, N_+)$. Assuming equal SIA and vacancy accumulation in the matrix, $c_v^{SFT} = c_i^{ml} = c$, eq. (A2.14a) may be written in the form

$$d(w)/d\varepsilon = \chi_+ c_i^{(ml)} + S c_{i,v}^{(mcl)} w/(b^2\rho)\,, \qquad \text{(A2.15)}$$

where S represents the square brackets at the r.h.s. of eq. (A2.14a). Equation (A2.14b) for N_+ has the same form but with another meaning of S. Note that $c_i^{(ml)}$ and $S c_{i,v}^{(mcl)}/\rho$ are are functions of ε or D.

The solution of eq. (A2.15), subject to the initial conditions at $\varepsilon = 0$ (or $D = D_0$), are obtained by the standard method: first solution of the homogeneous equations; then variation of the constant of that solution. The resulting complete solution contains integrals over the functions involved which, in general, however, can not be expressed in terms of well known functions.

A simplification allowing a closed form analytical representation is obtained by assuming transient build-up evolution for both the matrix clusters and the dislocations, for matrix clusters linear build-up at constant cluster sizes, for dislocations build-up according to (eq. (4.18a))

$$\begin{aligned} &c_{i,v}^{ml,SFT} = c'D, \quad dm_{i,v}^{ml,SFT}/dD = 0; \\ &d\rho/d\varepsilon = \beta\rho^{1/2}/b \rightarrow b^2\rho = (b\rho_0^{1/2} + \beta\varepsilon/2) = (\beta\varepsilon'/2)(D_1 - D_0 + D)^2 \end{aligned}, \tag{A2.16}$$

where $D_1 = 2b\rho_0^{1/2}/\beta\varepsilon'$. Introducing the new independent variable $\tau = D/(D_1 - D_0)$ and the parameter products $P = \chi_+\varepsilon' c'(D_1 - D_0)$ and $Q = 4\chi_- Sc'/\beta^2\varepsilon'$, eq. (A2.15) assumes the form

$$dw/d\tau = Pt + Qw\tau/(1+\tau)^2 \tag{A2.17}$$

The solution of eq. (A2.17) subject to $w(t = t_0) = w_0$ is

$$w(\tau) = w_0\left(\frac{1+\tau}{1+\tau_0}\right)^Q \exp\left\{-Q\frac{\tau - \tau_0}{(1+\tau_0)(1+\tau)}\right\} + P(1+\tau)^Q\left[\exp\{Q/(1+\tau)\}\right]I \tag{A2.18}$$

with

$$I = \int_{\tau_0}^{\tau} dz \frac{z}{(1+z)^Q}\exp\{-Q/(1+z)\} \tag{A2.19a}$$

With the substitution $z = Q/(\zeta - 1)$ the integral (A2.19a) assumes the form

$$I = -\int_{Q/(1+\tau)}^{Q/(1+\tau_0)} d\zeta\, Q^{1-Q}(\zeta - Q)\zeta^{Q-3}\exp(-\zeta) \tag{A2.19b}$$

This form shows that the integral can be expressed in terms of 4 exponential integrals which may be written as incomplete Gamma-functions

$$\begin{aligned} I = Q^{1-Q}\{&\Gamma[Q-2, Q/(1+\tau)] - \Gamma[Q-2, Q/(1+\tau_0)] \\ &- \Gamma[Q-1, Q/(1+\tau)] + \Gamma[Q-1, Q/(1+\tau_0)]\} \end{aligned}. \tag{A2.20}$$

A3. Contribution of Dislocation Decoration to the Yield Stress

In this work, it is assumed that the forces required to move well separated aligned loops with a dislocation are negligible compared to the forces on the dislocation exerted by aligned loops blocked by loops of different configuration. An upper bound estimate of the yield stress is obtained by assuming that each blocked aligned loop contributes with its maximum possible force on the dislocation depending on the distance from the dislocation. It is useful to first consider the case of low coverage and then to extend this consideration to the general case.

A3.1. Limiting case of low coverage

For low coverage (and/or small distance of loops from the dislocation), the probability for a certain aligned loop to be blocked by the close interaction with a loop of different configuration is $s_{bl}(y)pN$ where p (=5/6 and ½ for edge and screw dislocations, respectively) is the fraction of loops of different configuration and N is the total 2D number density of loops in the range of the loop considered. Consequently, the average contribution of such a loop to the maximum force on the dislocation is $s_{bl}(y)pNF^{max}(y)$, and the contribution of all loop pairs in an area $\Delta y\Delta z$ is $s_{bl}(y)pN^2F^{max}(y)\Delta y\Delta z$. An upper bound estimate for the total maximum force of the blocked loops is obtained by assuming, that all blocked loops contribute with the maximum possible force depending on the distance y to the dislocation:

$$F_{d,dc}^{max} = p\int dydz\, N^2 s_{bl} F_{dl}^{max}(y) \quad . \tag{A3.1}$$

The integration has to be performed over the region where $s_{bl}(y) = s^* - s_{al}, \geq 0$ and N is finite ($y \leq d_{dc}$). With $s^* = s^{*\prime} n^{1/2} by$ and $s_{al} = s_{al}' nb^2$ where $s^{*\prime} \approx 4$ and $s_{al}' \approx 1$ to 4, the lower integration limit may be expressed by $y_1 = (s_{al}'/s^{*\prime})\, n^{1/2} b$. Using $nNb^2 \approx \alpha$ (assumed to be constant over the decorated area of width d_{dc}), and $F_{dl}^{max} = f\, n\mu b^4/2\pi y^2$ where f is a factor accounting for the strength of the maximum interaction between a general dislocation and an aligned loop (see table A1), eq. (A3.1) may be written as

$$F_{d,dc}^{max} = (pf/2\pi)\mu\alpha^2 b(s^{*\prime}/\sqrt{n}\Delta z\, I \ , \tag{A3.2a}$$

$$I = \int_{y_1}^{d_{dc}} dy(1/y - y_1/y^2) = \ln(d_{dc}/y_1) - 1 + y_1/d_{dc} \tag{A3.2b}$$

At yielding, the maximum force between the loop ensemble and the dislocation given by eq. (A3.2a) is balanced by the force on the dislocation due to the shear stress $\tilde{\sigma}_y$ acting on it, i.e. $F_{d,dc}^{max} = \tilde{\sigma}_y b\Delta z$. According to this condition, the shear stress for yielding may be written explicitly as

$$\tilde{\sigma}_y = (pf/2\pi)\mu\alpha^2 (s^{*\prime}/\sqrt{n})\left\{\ln[(s^{*\prime}/s_{al}')d_{dc}/\sqrt{n}b] - 1 + (s_{al}'/s^{*\prime})\sqrt{n}b/d_{dc}\right\}, \tag{A3.3}$$

where the last term in the curly bracket can be neglected for realistically large d_{dc}.

According to eq. (A3.3), the yield stress $\tilde{\sigma}$ would increase logarithmically with the width of decoration d_{dc}. This is, however, unrealistic since the quantity $pNs_{bl}(y)$ introduced above for the probability of blocking becomes formally larger than 1, $pNs_{bl}(y) > 1$, for

$y/b > y^*/b \approx \{\sqrt{n}/(s^{*\prime} p\alpha)\}(1 + s_{al}' p\alpha)$, i.e. for the conditions of interest where loop blocking contributes significantly to the yield stress. In this case, $y > y^*$, the probability for the occurrence of more than 1 non-aligned loop in the blocking range of an aligned loop becomes significant.

A3.2. General case

The probability of a certain aligned loop **not** to be permanently blocked by the close interaction with a loop of different configuration decreases exponentially with increasing loop density as $\exp(-s_{bl}(y)pN)$. Correspondingly, the probability of an aligned loop to be blocked by at least 1 loop, i.e. 1 or more other loops, is given by $1- \exp(-s_{bl}(y))$. Consequently, for the more general case, eq. (A3.1) has to be modified as

$$F_{d,dc}^{\max} = N\Delta z \int dy\{1 - \exp(-s_{bl}\, pN)\} F_{dl}^{\max}(y)\,. \tag{A3.4}$$

For $pN \to 0$, eq. (A3.4) converges to the limiting case given by eq. (A3.1). With the same substitutions as used in the preceding subsection, eq. (A3.4) may be written as

$$F_{d,dc}^{\max} = (f/2\pi)\mu\alpha b^2 \Delta z\, I\ , \tag{A3.5a}$$

$$I = \int_{y_1}^{d_{dc}} \frac{dy}{y^2}\{1 - \exp[-(y - y_1)/y_2]\}\,, \tag{A3.5b}$$

where $y_2 = \sqrt{n}b/(ps^{*\prime}\alpha)$. In contrast to eq. (A3.2b), the integral given by eq. (A3.5b) converges for $d_{dc} \to \infty$. The latter limit is indeed a good approximation of the integral for $d_{dc} >> y_1$. For this case, partial integration of eq. (A3.5b) yields

$$I(d_{dc} \to \infty) = y_2^{-1} \exp(y_1/y_2) \int_{y_1}^{\infty} \frac{dy}{y} \exp(-y/y_2) = y_2^{-1} \exp(a)\,\mathrm{Ei}(a)\,. \tag{A3.5c}$$

Here $a = y_1/y_2 = ps_{al}'\alpha$ and Ei(a) is the standard exponential integral of the variable a with

$$\mathrm{Ei}(a) = \int_a^{\infty} \frac{da}{a} \exp(-a)$$

with the limiting behaviour

$$\mathrm{Ei}(a \to 0) \to -\ln(a) - \gamma; \quad \mathrm{Ei}(a \to \infty) \to \exp(-a)/a$$

where $\gamma = 0.5772$ is Euler's constant.

Using eq. (A3.5c) for the integral in eq. (A3.5a) and assuming force balance at yielding we obtain for the shear yield stress

$$\tilde{\sigma} = (pf/2\pi)\mu\alpha^2 (s^{*\prime}/\sqrt{n}) \exp(a)\,\mathrm{Ei}(a) \tag{A3.6a}$$

with the limiting behaviour

$$\tilde{\sigma}(a \to 0) \to (pf/2\pi)\mu\alpha^2 (s^{*\prime}/\sqrt{n})[-\ln(ps_{al}'\alpha) - \gamma] \tag{A3.6b}$$

$$\tilde{\sigma}(a \to \infty) \to (f/2\pi)\mu\alpha (s^{*\prime}/s_{al}')/\sqrt{n}) \tag{A3.6c}$$

The factor in front of the curly bracket in eq. (A3.6b) is the same as in eq. (A3.3) but the logarithm inside the bracket is different and, most importantly, it does no longer contain the width of the decorated region d_{dc}. On the other hand, the form of eq. (A3.6a) together with eqs. (A3.6b) is similar to eq. (5.4) of the main text, except that the magnitude of yield stress according to eq. (A3.5a) is, as expected for an upper bound estimate, larger than according to eq, (5.4).

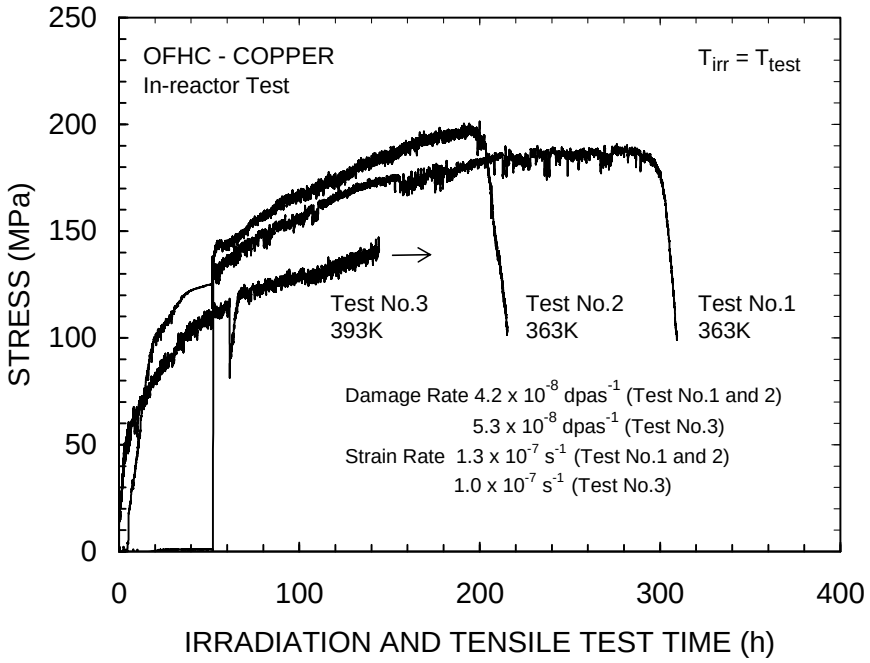

Fig. 2.1: Continuously measured stress response as a function of irradiation and tensile test time during the in-reactor tensile tests. Note that the specimens in the Test No. 1, 2, 3 received different levels of pre-loading displacement dose before the actual tensile test was activated and the specimens started experiencing applied stress. As a result, different amounts of irradiation-induced defects and their clusters accumulated during the pre-yield period in the absence of dislocation generation (fig.3 in [4]).

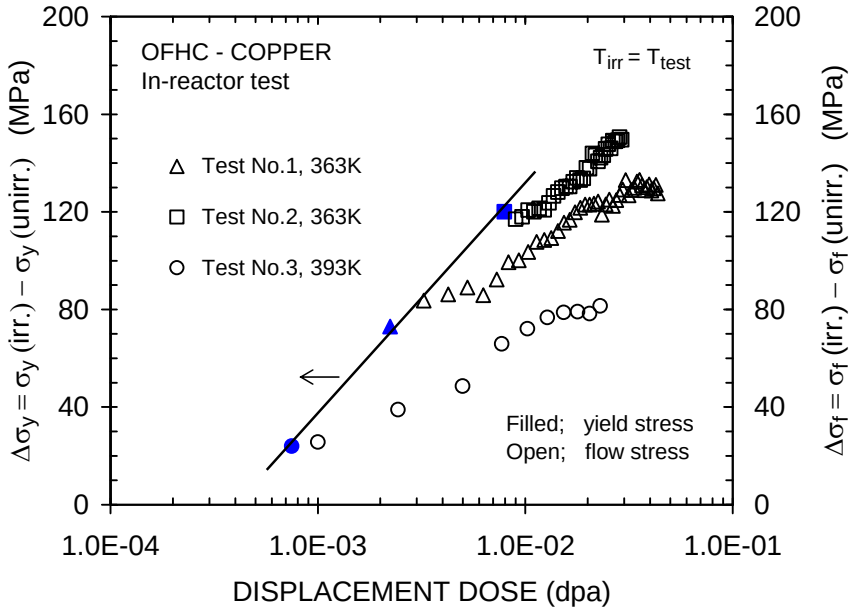

Fig. 2.2a: Irradiation induced increase in yield stress, $\Delta\sigma_y$, and flow stress, $\Delta\sigma_f$, as a function of displacement dose level for the in-reactor tensile tests at 363 and 393K. The following features are worth noting: (a) the increase in the yield stress with dose is faster than that of the flow stress, (b) the rate of flow stress increase tends to saturate at a certain dose level particularly when the pre-yield dose level is low (e.g. Test No. 1 and 3) and (c) the magnitude of the increase in the flow stress decreases substantially with decreasing the pre-yield dose level (fig. 7 in [4].

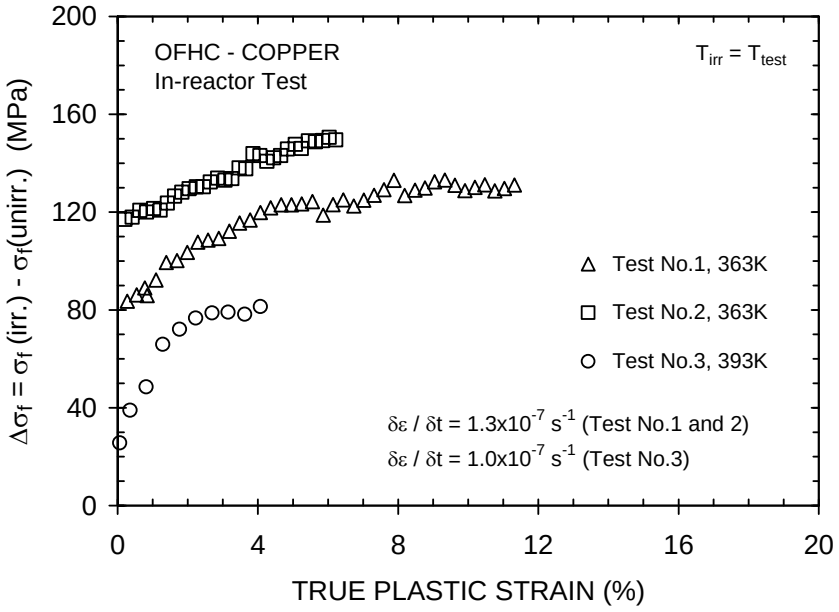

Fig. 2.2b: Increase in flow stress, $\Delta\sigma_f$, as a function of true plastic strain for in-reactor tests at 363 and 393K. Note that while the increase in the flow stress, $\Delta\sigma_f$, decreases with strain, the magnitude of the increase in the flow stress (at a given strain/dose level) increases with increasing level of pre-yield displacement dose. Furthermore, the increase in the flow stress beyond a certain strain level (i.e. dose) decreases with increasing strain (dose) and then tends to saturate (e.g. Test No. 1 and 3) (fig. 8 in [4]).

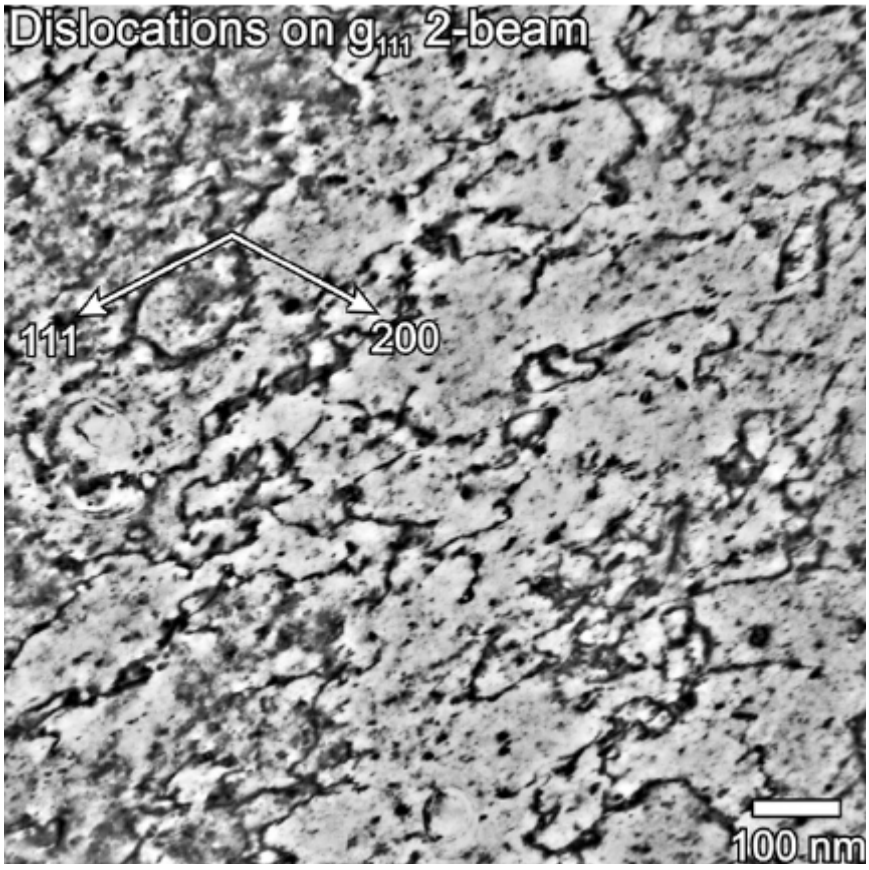

Fig. 2.3: An example of the dislocation microstructure in the in-reactor deformed specimen in the Test No. 1 at 363K. Note the homogeneous nature of spatial distribution of deformation induced decorated dislocations and an almost complete lack of dislocation segregation in the form of dislocation walls (fig. 18 in [4]).

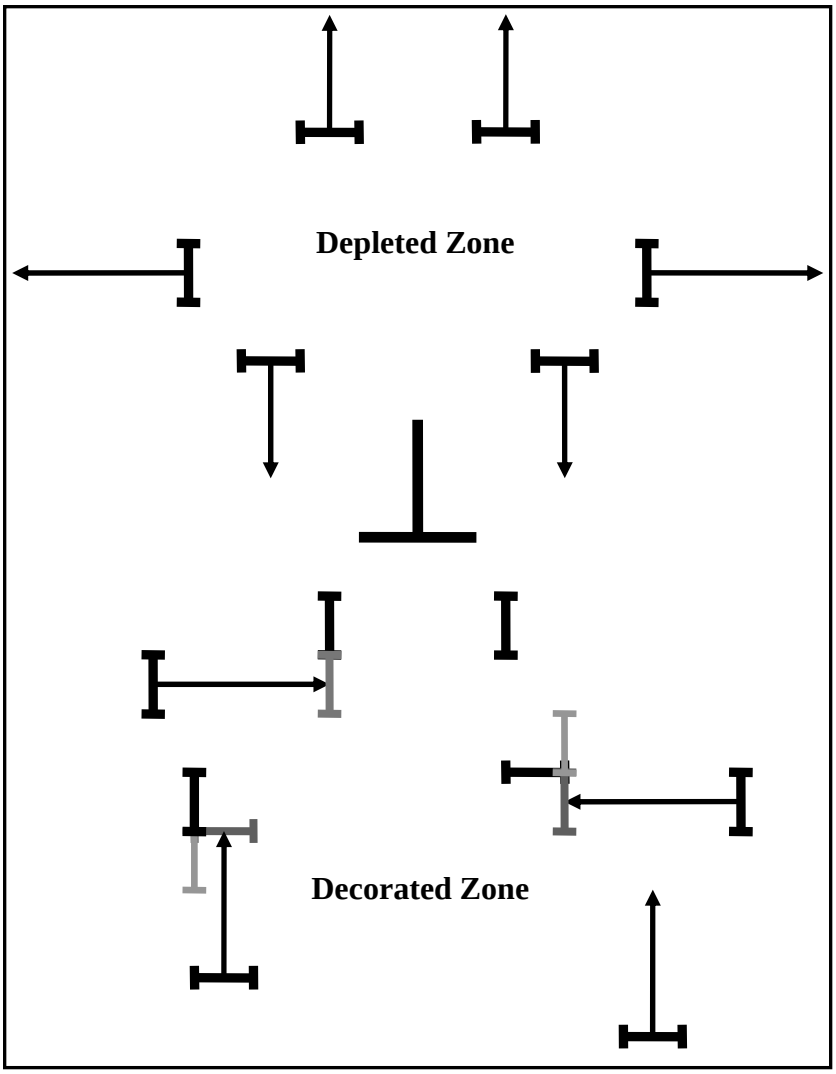

Fig. 2.4: Schematic illustration of dislocation decoration during pre-yield irradiation: primary cascade induced glissile SIA loops with 2 different 1D diffusion directions (indicated by arrows), aligned and non-aligned with an edge dislocation, are repulsed at the compressive side where they leave a depleted zone and attracted at the dilated side where they accumulate. Possible reactions in the decorated zone: agglomeration of 2 aligned (or 2 “non-aligned”) loops and agglomeration of a non-aligned with an aligned loop with subsequent alignment; present stage: black and fat lines; intermediate stage: medium thick and medium grey lines, final stage: thin and light grey lines.

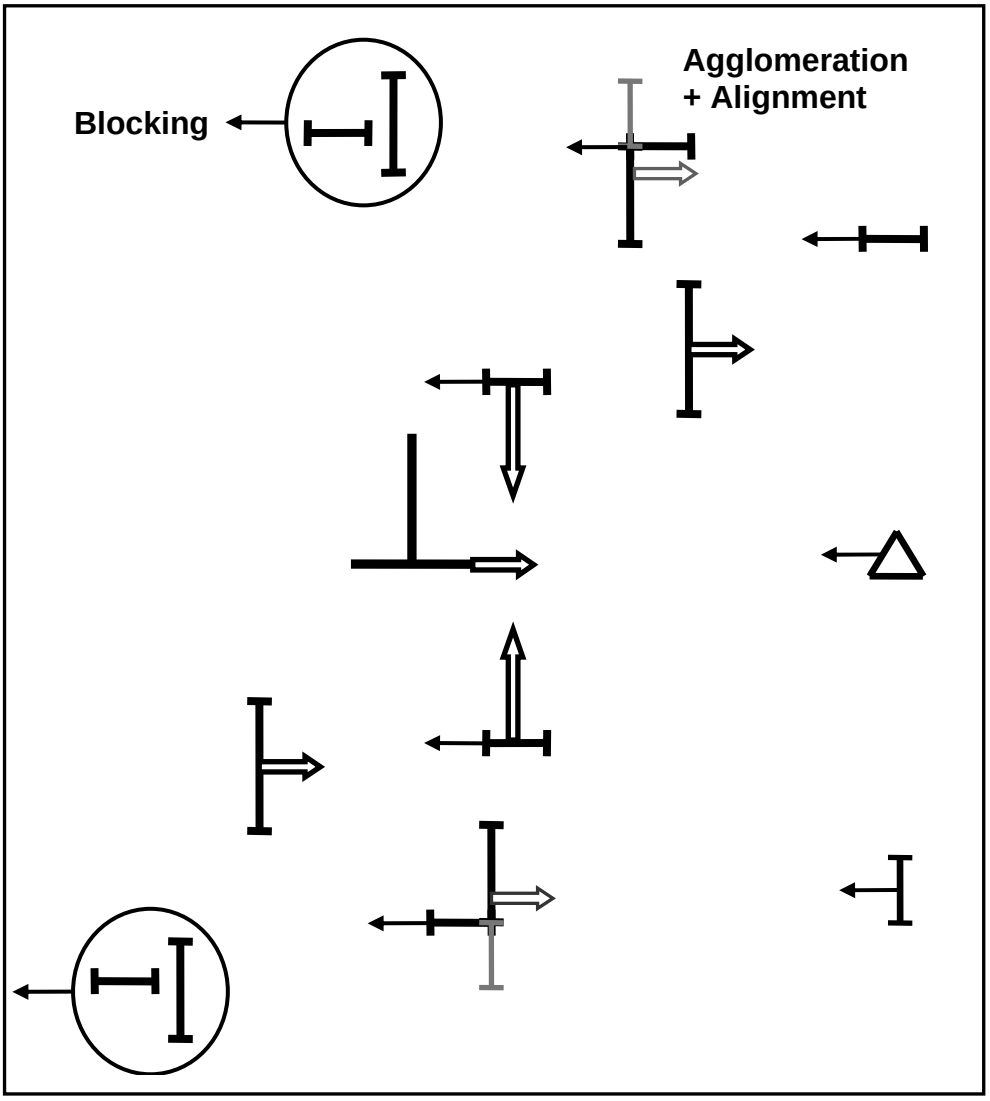

Fig. 2.5: Schematic illustration of dislocation decoration during deformation. An edge dislocation and a crowd of aligned loops, pushed and pulled at the compressive and dilated (upper and lower) side, respectively, move together and "see" by this an apparent drift flux of matrix clusters (loops and SFTs) with whom they reacts (double arrows: motion relative to matrix; normal arrow: motion relative to dislocation). Possible reactions are: attraction and absorption of non-aligned loops (middle region), agglomeration of 2 aligned loops (not shown), agglomeration of a non-aligned with an aligned loop with subsequent alignment and incorporation into the loop cloud (thin and light grey lines and double arrows: final stage), partial recombination of loops with SFTs (not shown), blocking and removal of an aligned loop by its interaction with a non-aligned loop (or SFT), particularly in the outer region (encircled).

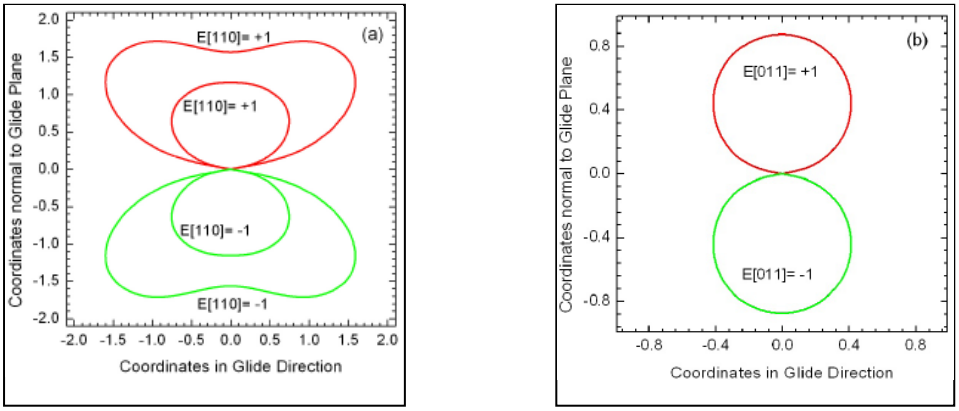

Fig. 3.1: Energy of the interaction between a dislocation with [110]/2 Burgers vector (BV) and a loop with BV parallel to the $(1\,\bar{1}\,1)$-glide plane of the dislocation as a function of their mutual distance: lines of equal energy (equi-potential lines) in a plane perpendicular to the dislocation line, with x and y coordinates in glide direction and normal to the glide plane, respectively; energy and distance in units of $n\mu\Omega/2\pi$ and b, respectively, Poisson's ratio $\nu = 1/3$; red lines: E = +1 (repulsive interaction), E = -1 (attractive interaction) (a) edge dislocation with [110] loops (outer lines) and $[011]/[10\,\bar{1}]$ loops (inner lines), (b) screw dislocation with a [011] loop ($E_{[10\bar{1}]} = - E_{[011]}$). Equi-potential lines for other energy values are obtained by the scaling $E \propto 1/r_{dl}$.

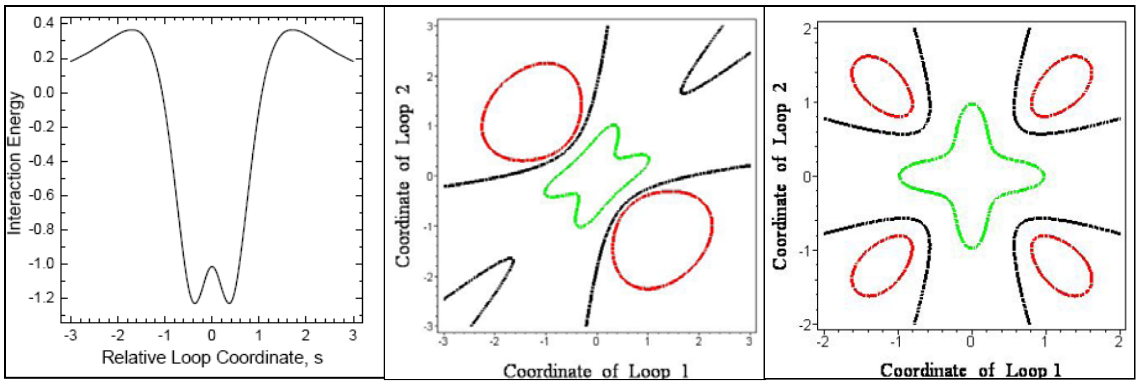

(a) (b) (c)

Fig. 3.2: Interaction energies of two loops (in units of $mn\mu\Omega/4\pi$) along their glide paths as a function of their coordinates s_1 and s_2 measured from their points of closest approach (all length scales in units of b); (a) 2 parallel loops, (b) 2 loops with 60° inclination, (c) 2 loops with 90° inclination. Equi-potential lines for other energy values are obtained by the scaling $E \propto 1/r_{dd}^3$.

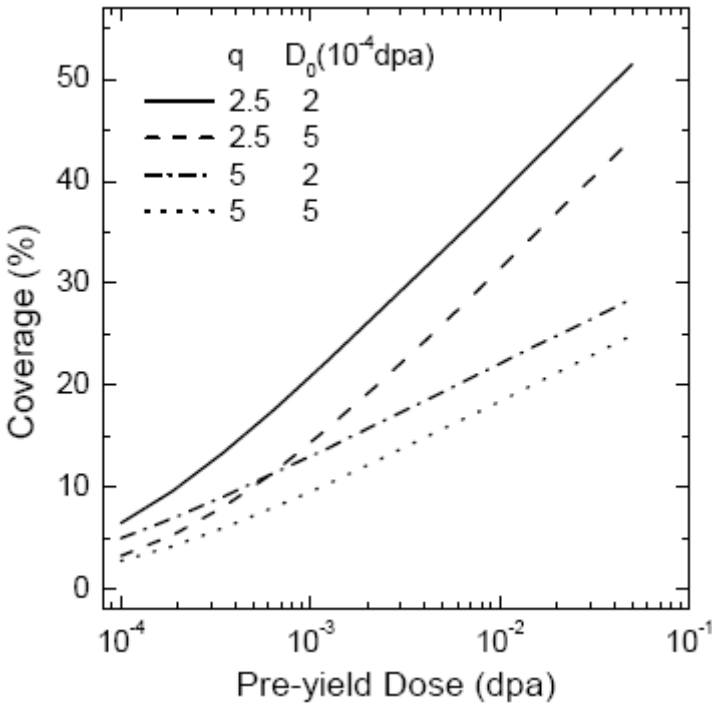

Fig. 4.1: Coverage vs pre-yield dose according to eq. (4.9) for $\alpha_0 = 0.2$ and the pairs of q, D_0 values q = 2.5, $D_0 = 2x10^{-4}$ (full line); q = 2.5, $D_0 = 5x10^{-4}$ (dashed line); q = 5, $D_0 = 2x10^{-4}$ (dashed-dotted line); q = 5, $D_0 = 5x10^{-4}$ (dotted line).

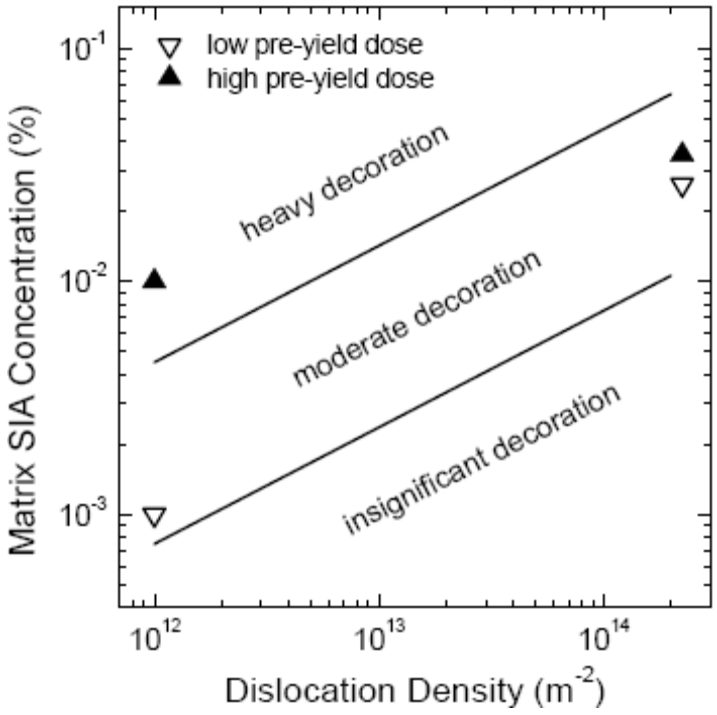

Fig. 4.2: Sketch of the range of "moderate decoration", 5% < α < 30%, in the parameter plane of dislocation density, ρ, and SIA concentration accumulated in matrix loops, $c_i^{(ml)}$, according to eq. (4.20). Values of $c_i^{(ml)}$ (≈ 1% of dpa) and ρ (10^{12} … $2x10^{14}$ dpa) expected for low and high pre-yield dose (10^{-3} and 10^{-2} dpa) at the beginning and towards the end of deformation of the IRTs (strain 0 and 5%), respectively. For low and high pre-yield dose, the estimated positions of the IRTs considered here move from the lower and somewhat above the upper boundary to the middle of the range. Above the upper boundary, realised by higher dose rates and/or lower strain rates, heavy decoration as in PITs is expected to occur, whereas below the lower boundary, realised for higher strain rates and/or lower dose rate, decoration is expected to be insignificant.

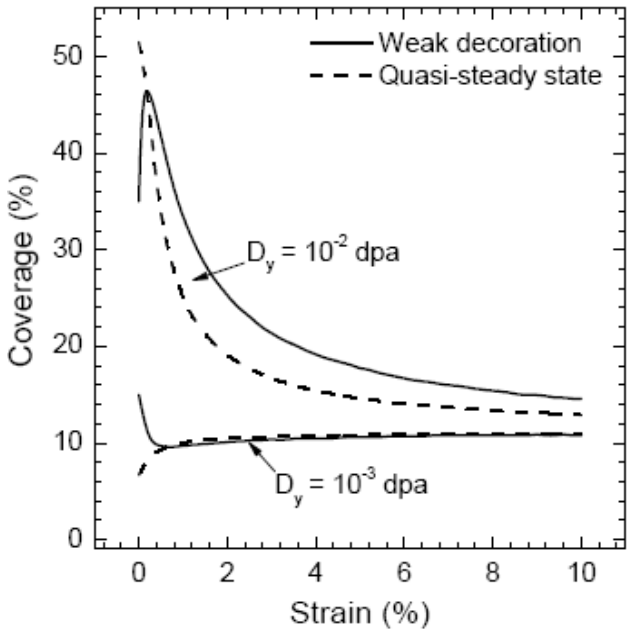

Fig. 4.3: Evolution of decoration during deformation: coverage vs. strain for low and high pre-yield doses according to eq. (4.19a) (weak decoration). Dashed lines are for the corresponding quasi-steady state approximation according to eq. (4.19b). For low and high pre-yield dose, D_y = 10^{-3} dpa, and D_y = 10^{-2} dpa, α_y = 15% and α_y = 35% is assumed, respectively. Main parameters used in eq. (4.19a,b) in conjunction with eq. (4.18a): $\chi_+ = 1/4$, $c_i^{(ml)} = 0.01D = 0.005\varepsilon$, $\beta = 0.15$, $\rho_0 = 10^{12}/\mathrm{m}^2$. Effect of dislocation sweeping on matrix clusters is neglected.

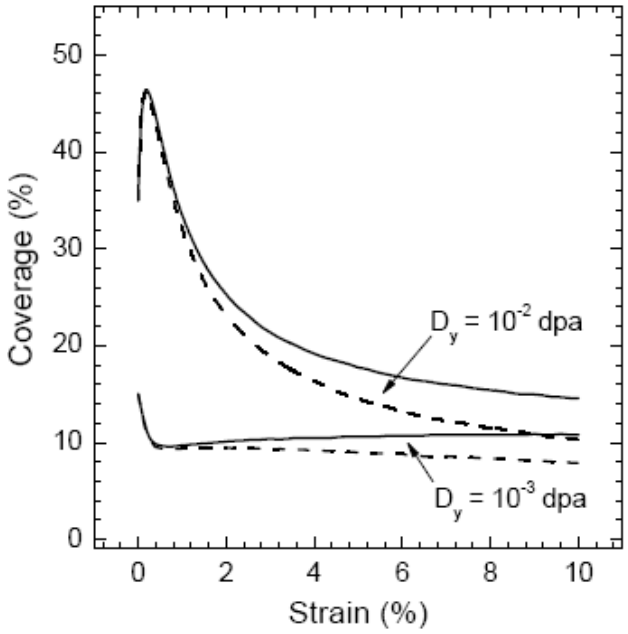

Fig. 4.4: Effect of dislocation sweeping on the evolution of decoration during deformation according to eq. (4.22). Full lines without (as in fig. 4.3), dashed lines with sweeping effect. The sweeping effect decreases with increasing coverage. Accordingly, for low and high dose, D_y = 10^{-3} dpa and D_y = 10^{-2} dpa, characteristic strains for the sweeping effect $\varepsilon_{i,v}^{(sw)}$ = 10% and 20% are assumed, respectively (see discussion in the paragraph after eq. (4.22)).

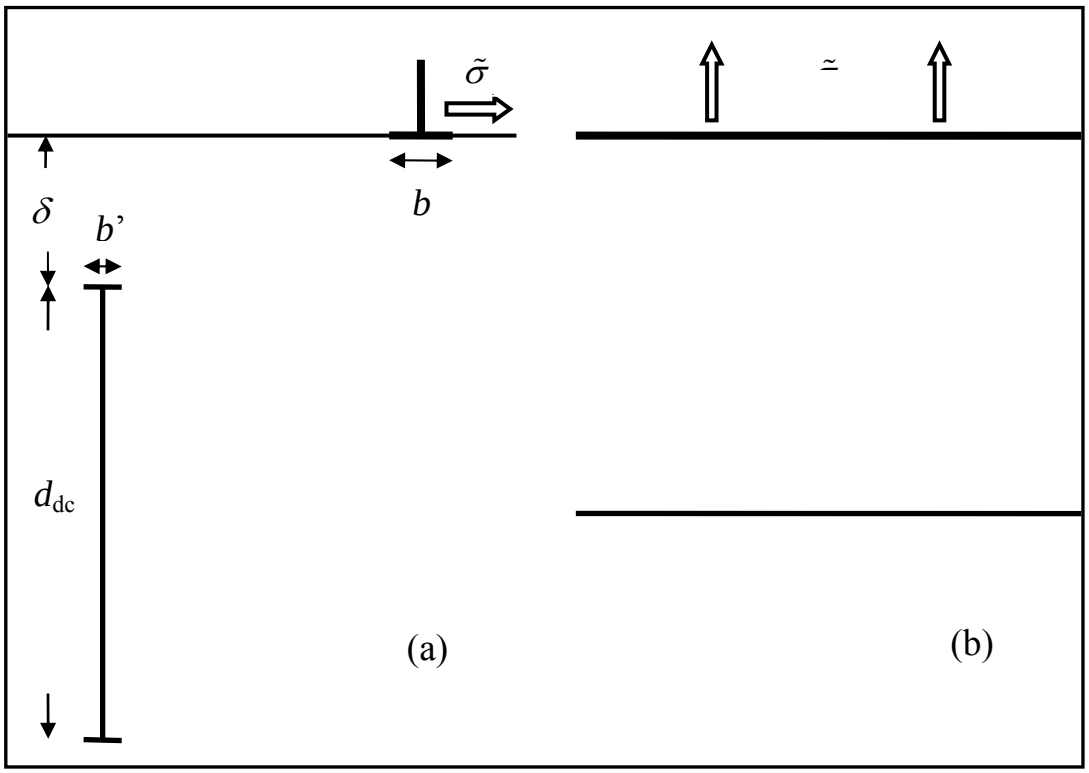

Fig. 5.1: Schematic illustration of the contribution of decoration to the yield stress: unlocking of a dislocation of Burgers vector b from a loop distribution of coverage α and width d_{dc} by a shear stress $\tilde{\sigma}$; loop distribution approximated by a sessile dislocation dipole of effective Burgers vector $b' = \alpha b$ and width d_{dc} separated from the glide plane of the dislocation by a stand-off distance δ; (a) cross section, (b) projection on glide plane.

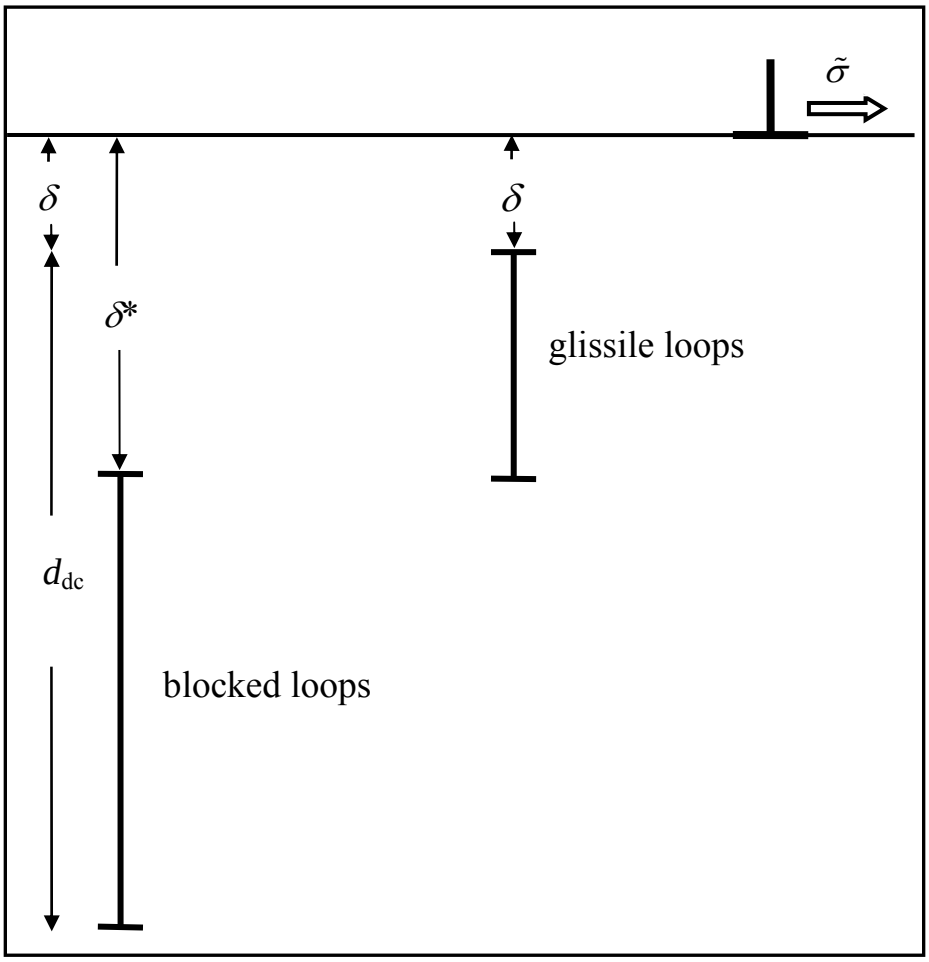

Fig. 5.2: Schematic illustration of the different contributions of the inner and outer region of decoration to the yield stress: in the inner region, loops can glide since mutual blocking is negligible; in the outer region, loops are immobilised by mutual blocking. The yield stress is assumed to be controlled by unlocking of the dislocation from the outer region. The loop distributions in the inner and outer regions are approximated by glissile and sessile dislocation dipoles (of total width d_{dc}) separated from the glide plane of the dislocation by distances δ and δ^*, respectively.

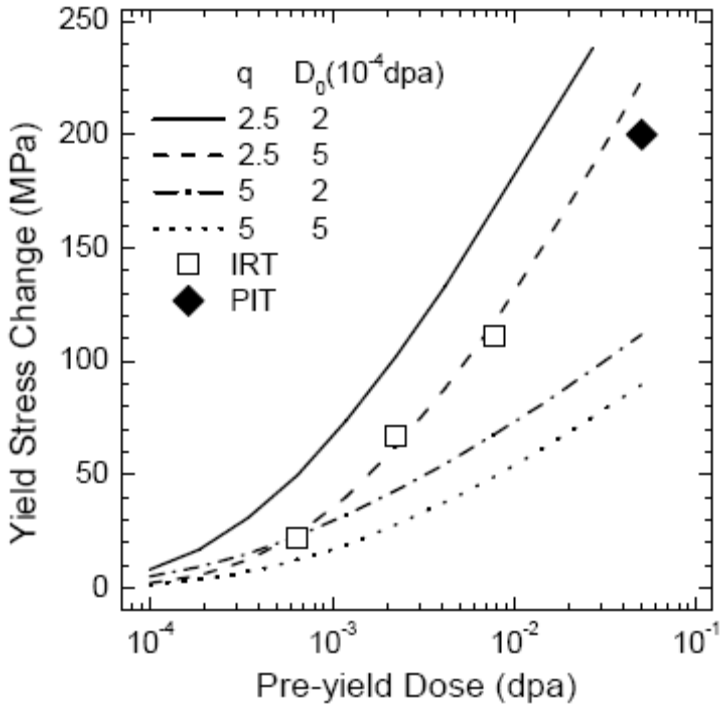

Fig. 5.3: Contributions of blocking of members of loop clouds decorating dislocations to the yield stress as a function of dose according to eq. (5.4a) for $\alpha_0 = 0.2$, $k = 0.1$, $n = 100$, $s^* = 4\sqrt{n}$ by, $s_{al} = 3nb^2$. Squares and diamond: experimental values for IRTs and a PIT, respectively.

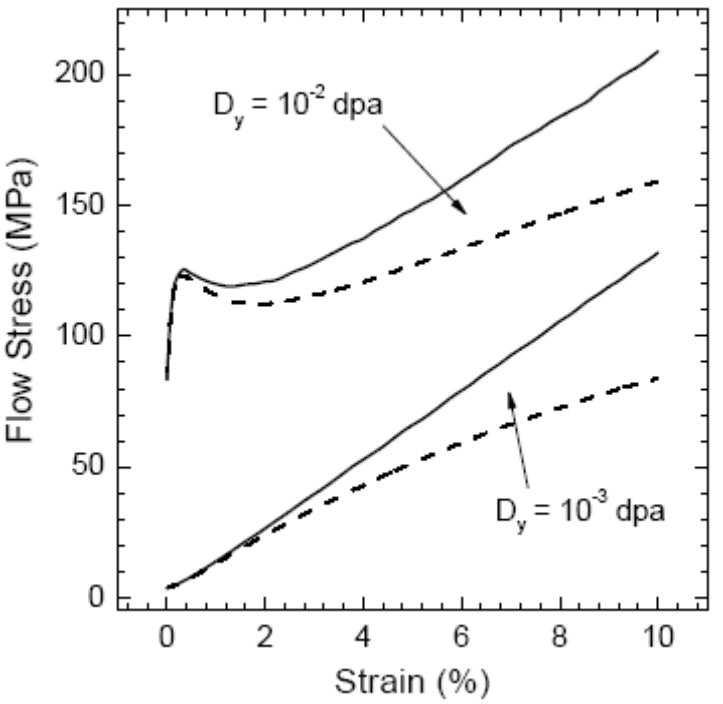

Fig. 5.4: Contributions of blocking of members of loop clouds by matrix clusters to the flow stress as a function of true strain according to eq. (5.6) for $d_{dc} = 80b$, $m_{SFT} = 70$, $m_l = 150$ and decoration parameters as in figs. 4.3 and 4.4 ($\chi_+ = 1/4$, $c_i^{(ml)} = 0.01D = 0.005\varepsilon$, $\beta = 0.15$, $\rho_0 = 10^{12}/m^2$). Full/ dashed lines: effect of dislocation sweeping on matrix clusters neglected/ included.

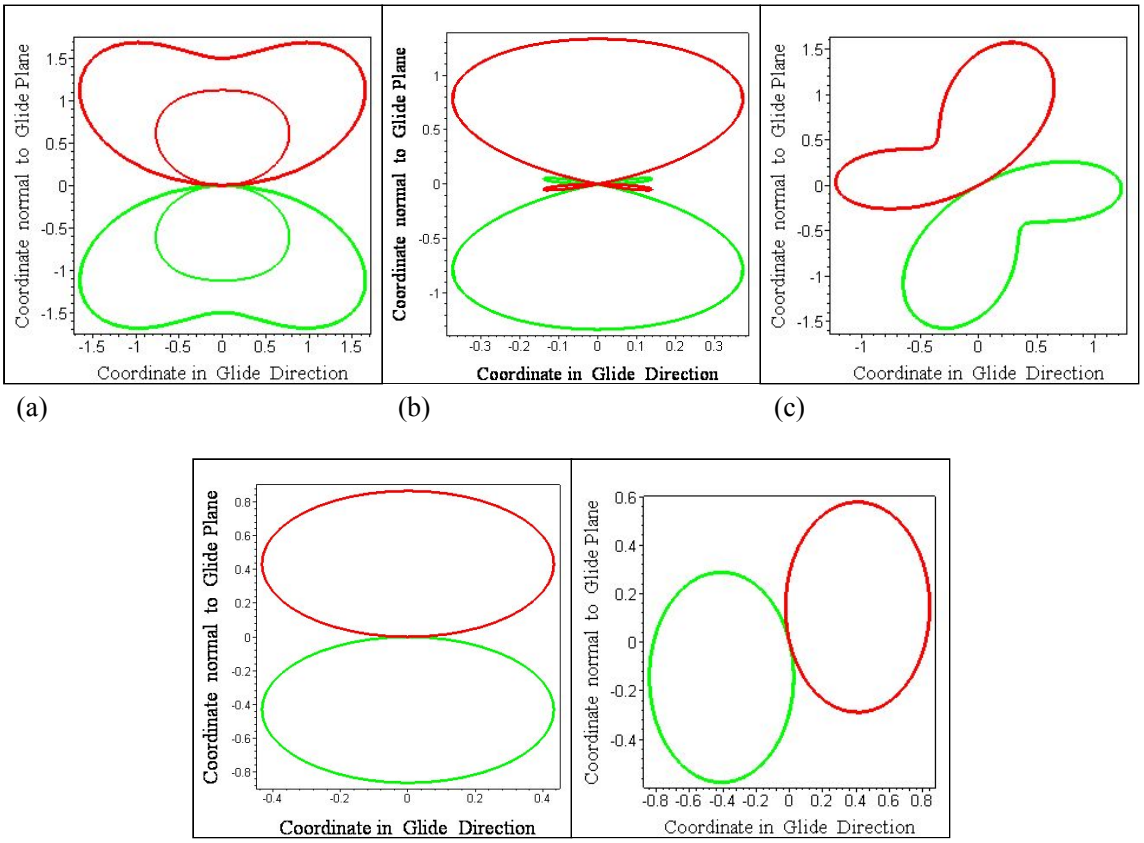

Fig. A1.1: Energy of the interaction between a loop and dislocation with [110]/2 Burgers vector and $(1\,\bar{1}\,1)$-glide plane as a function of their mutual distance: lines of equal energy (equipotential lines) in a plane perpendicular to the dislocation line; energy and distance in units of $n\mu\Omega/2\pi$ and b, respectively, Poisson's ratio $\nu = 1/3$; (a) [110] and $[011]/[10\,\bar{1}]$ loops parallel to glide plane of edge dislocation, (b) $[1\,\bar{1}\,0]$ loops with BV perpendicular to BV of edge dislocation, (c) [101] loops with BV oblique to glide plane of edge dislocation (for $[01\,\bar{1}]$-loops $E[01\,\bar{1}](x) = E[101](-x)$), (d) [011] loops parallel to glide plane of screw dislocation (for $[10\,\bar{1}]$-loops $E[10\,\bar{1}] = -E[011]$), (e) [101] loops with BV oblique to glide plane of screw dislocation (for $[01\,\bar{1}]$-loops $E[01\,\bar{1}](x) = -E[101](-x)$). Note that (e) corresponds to a rotation of (d) around the screw dislocation by the angle of 70° between two glide planes.

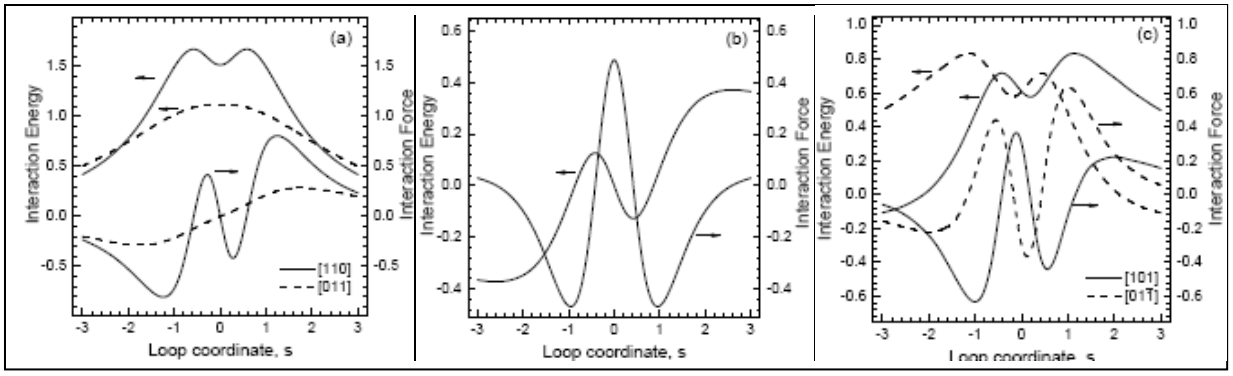

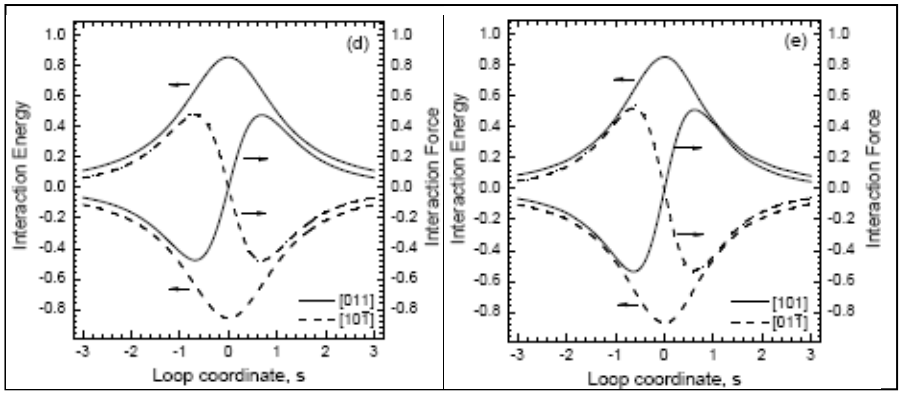

Fig. A1.2: Interaction energies and the corresponding forces acting on a loop passing a dislocation with [110]/2 Burgers vector at unit minimum distance as a function of the loop coordinate s; energy, force and loop coordinate in units of $n\mu\Omega/2\pi$, $n\mu\Omega/2\pi b$, and b, respectively, Poisson's ratio $\nu = 1/3$; (a) [110] and [011]/ $[10\bar{1}]$ loops passing edge dislocation, (b) $[1\bar{1}0]$ loops passing edge dislocation, (c) [101] and $[01\bar{1}]$ loops passing edge dislocation ($E[01\bar{1}](s) = E[101](-s)$, $F[01\bar{1}](s) = - F[101](-s)$), (d) [011] and $[10\bar{1}]$ loops passing screw dislocation ($E[10\bar{1}](s) = - E[011](-s)$, $F[10\bar{1}]_{[10\bar{1}]}(s) = - F[011](-s)$), (e) [101] and $[01\bar{1}]$ loops passing screw dislocation ($E[01\bar{1}](s) = - E[101](-s)$, $F[01\bar{1}]$ $(s) = - F[101](-s)$). Since (e) follows from (d) by a rotation, the curves in (e) and (d) are equal.

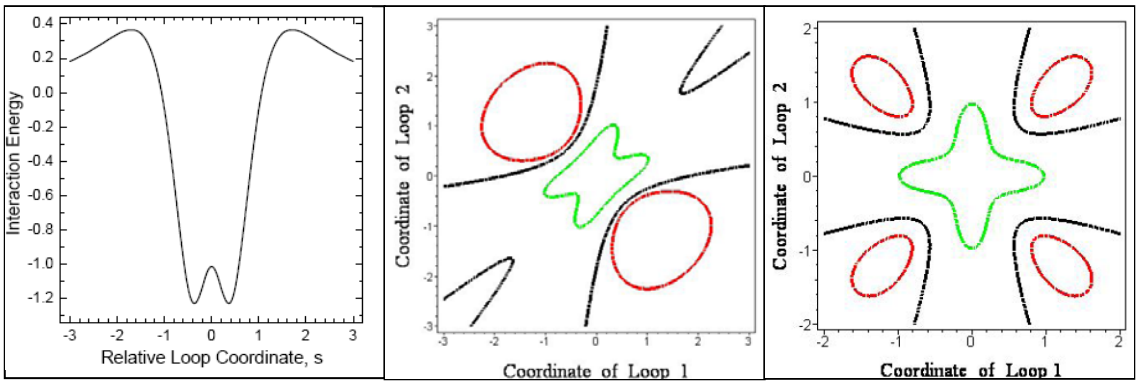

(a) (b) (c)

Fig. A1.3: Interaction energies of two loops in units of $mn\mu\Omega/4\pi$ as a function of their mutual distance in units of b measured from the point of closest approach (a) 2 parallel loops, (b) 2 loops with 60° inclination, (c) 2 loops with 90° inclination.

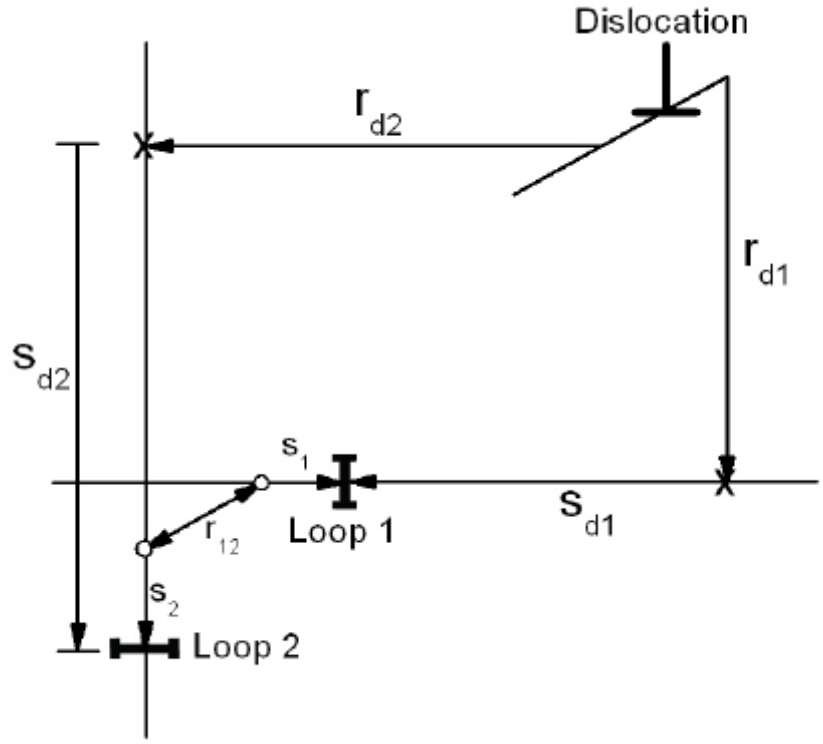

Fig. A1.4: Geometry used to describe the interaction of two loops 1and 2 in the field of a dislocation. Horizontal and vertical straight lines: glide paths of loops 1 and 2; small circles: points of closest approach of the loop paths; r_{12}: distance between these points; s_1 and s_2: actual distance of the loops from these points; small crosses: points of closest approach of the loop paths to the dislocation line; r_{d1} and r_{d2}: distances of these points from the dislocation line; s_{d1}, s_{d2}: actual distances of the loops from these points. Oblique lines are meant to be perpendicular to the drawing plane (perspective view).

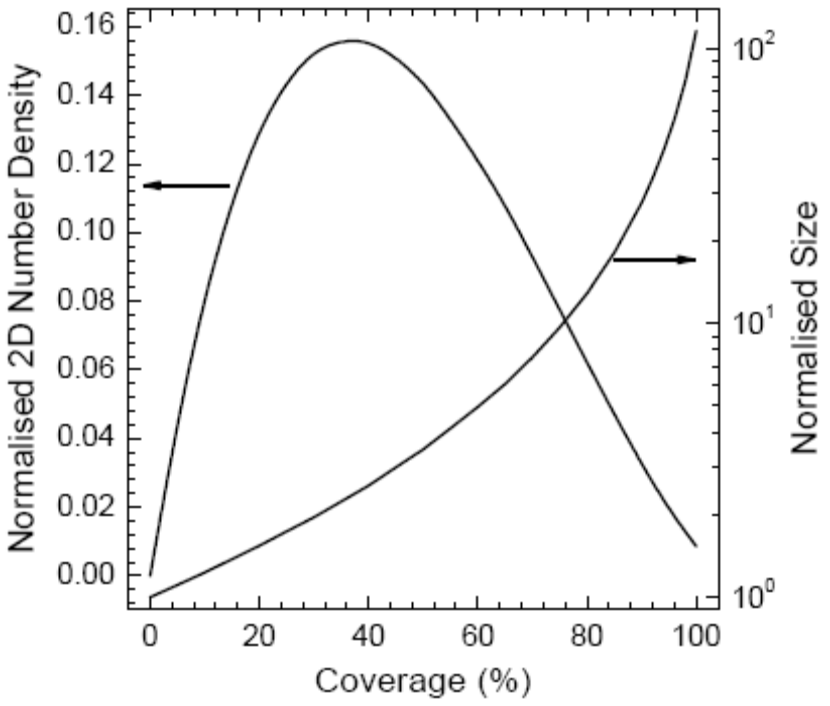

Figure A2.1: Simple coalescence model for the evolution of loops in the 2D space of decoration: normalised 2D number density, $N^* = mA_0N$ (number of loops per area of incoming loop) and normalised loop size, n/m (number of incoming to existing loops) as functions of coverage α. At the limit $\alpha = 100\%$, N^* reaches a state close to percolation.

Risø's research is aimed at solving concrete problems in the society.

Research targets are set through continuous dialogue with business, the political system and researchers.

The effects of our research are sustainable energy supply and new technology for the health sector.